TAMPEREEN TEKNILLINEN YLIOPISTO
TAMPERE UNIVERSITY OF TECHNOLOGY

JUKKA LAPPALAINEN

SIMULATION MODEL FOR HYDROTHERMAL LIQUEFACTION REACTIONS

Master of Science Thesis

Examiner: TUT Industry Professor
Tero Joronen
Examiner and topic approved by the
Faculty Council of the Faculty of Natural Sciences on 3.1.2018

ABSTRACT

JUKKA LAPPALAINEN: Simulation model for hydrothermal liquefaction reactions
Tampere University of technology
Master of Science Thesis, 75 pages, 11 Appendix pages
May 2018
Master's Degree Programme in Environmental and Energy Engineering
Major: Energy and Biorefining Engineering
Examiner: TUT Industry Professor Tero Joronen
Keywords: hydrothermal liquefaction, supercritical water, simulation model, thermochemical conversion technology, renewable transport fuel

Lately the production of biofuels from renewable sources has aroused interest due to the decreasing number of fossil fuels and preventing the climate change. Especially the replacement of fossil transportation fuels by renewable ones is important, since the use of energy of the traffic sector corresponded to 22.5% of total energy consumption in the European Union in 2015. There are several different process technologies to produce renewable transport fuels from biomass, such as production of biodiesel by NExBTL technology. One of the most promising technology under development is hydrothermal liquefaction, where biomass is converted into liquid biofuel in hot pressurized water.

The aim of this thesis was to study the possibility to develop a simulation model for hydrothermal liquefaction of lignocellulosic biomass. The interest of creating the simulation model is that the simulation model will be used as reactor scaling tool in the future. The objectives of the thesis were both to study existing research focusing on both reactions in the supercritical water and existing hydrothermal liquefaction simulation models, and to create a simulation model for modelling the hydrothermal liquefaction reactions. The simulation model will be tested and validated in the future when hydrothermal liquefaction pilot facility is completed.

The work included literature research, creating the simulation model and simulating a case study. The literature research focused on both finding the reaction pathways and kinetics in supercritical water related to lignin, hemicellulose and cellulose, and studies that included creation of simulation model. The process layout of the simulation model came from the test facility, which was under construction during the study. The other needed information for the simulation, such as reactions and reaction kinetics, was gathered in the literature research. There were couple of different reaction pathways and kinetics used, before the most suitable one was found. Finally, the simulation model was linked with Excel spreadsheet that works as user interface for the model.

The outcome of the study were the simulation model for hydrothermal liquefaction of biomass and case study results. The case study showed that treating Norway spruce by using hydrothermal liquefaction can produce biocrude with good energy and mass efficiency. The results of recoveries of mass and energy were 30 % and 63 % when using 15 minutes residence time. However, the comparison of simulation model results with other studies results showed that the model predicts both biocrude yield and gas yields too low while the char yield is too high. The results showed that the model needs developing before it is suitable for calculation tool for scaling the reactor into desired scale.

TIIVISTELMÄ

JUKKA LAPPALAINEN: Biomassan hydrotermisen nesteytyksen simulointimalli
Tampereen teknillinen yliopisto
Diplomityö, 75 sivua, 11 liitesivua
Toukokuu 2018
Ympäristö- ja energiatekniikan diplomi-insinöörin tutkinto-ohjelma
Pääaine: Energia- ja biojalostustekniikka
Tarkastaja: TUT Industry Professor Tero Joronen
Avainsanat: hydroterminen nesteytys, superkriittinen vesi, simulaatiomalli, termokemiallinen konversiotekniikka, uusiutuva liikennepolttoaine

Viime aikoina biopolttoaineiden tuottaminen uusiutuvista lähteistä on herättänyt kiinnostusta johtuen fossiilisten polttoaineiden vähentymisestä ja ilmastonmuutoksen hillitsemisen takia. Erityisesti fossiilisten liikennepolttoaineiden korvaaminen uusituvilla on tärkeää, sillä esimerkiksi Euroopan unionin alueella liikennesektorin energiantarve vastasi 22.5 % kokonaisenergian kulutuksesta vuonna 2015. Tällä hetkellä on olemassa useita eri prosesseja biopolttoaineiden tuottamiseen, kuten biodieselin tuottaminen NExBTL –prosessin avulla. Tällä hetkellä yksi lupaavimmista kehitteillä olevista teknologioista on hydroterminen nesteytys, jossa biomassaa nesteytetään korkeassa paineessa ja lämpötilassa veden läsnä ollessa.

Tämän työn tarkoituksena oli tutkia mahdollisuutta tehdä simulointimalli, jolla pystytään simuloimaan lignoselluloosa –pohjaisen biomassan hydrotermistä nesteytystä. Yksi tämän työn intresseistä oli se, että simulointimallia voitaisiin käyttää reaktorin skaalaustyökaluna tulevaisuudessa. Tämän työn tavoitteet olivat sekä tutkimuksien etsiminen, joissa käsitellään biomassan reaktioita superkriittisessä vedessä ja olemassa olevia malleja näiden mallintamiseen, että biomassan hydrotermisen nesteyttämisen simulointimallin luominen. Mallin testaaminen ja validointi tullaan tekemään hydrotermisen nesteytysreaktorin valmistuessa.

Työ sisälsi lopulta kirjallisuusselvityksen, simulointimallin luomisen ja tapaustutkimuksen simuloinnin. Kirjallisuusselvitys keskittyi etsimään sekä biomassan hajoamisen keskeiset reaktiomekanismit superkriittisessä vedessä että olemassa olevia simulointimalleja hydrotermiselle nesteytykselle. Simulointimallin prosessikaavio perustuu rakenteilla olevaan reaktoriin. Reaktioiden mallintamisessa testattiin useampaa eri reaktioväylä- ja reaktiokinetiikkamallia ennen kuin parhaiten sopiva malli löydettiin. Lopuksi, simulointimalli yhdistettiin Excel –tiedostoon, joka toimii mallin käyttöliittymänä.

Työn tuloksena saatiin biomassan hydrotermisen nesteytyksen simulointimalli ja tapaustutkimuksen tulokset. Tapaustutkimus osoitti, että kuusen hydrotermisellä nesteytyksellä voidaan tuottaa bioöljyä hyvällä hyötysuhteella. Massan ja energian talteenoton hyötysuhteeksi saatiin 30 % ja 63 % käytettäessä 15 minuutin vipyaikaa. Malllin tuloksien ja kokeellisten tuloksien perusteella havaittiin, että malli ennustaa sekä bioöljyn ja kaasun tuoton liian pieneksi, kun taas muodostuvan koksin saannon liian suureksi. Tuloksien perusteella voitiin päätellä, että malli vaatii sekä kehittämistä että validoinnin ennen kuin se soveltuu reaktorin skaalaustyökaluksi.

PREFACE

This Thesis was made in the Laboratory of Chemistry and Bioengineering at the Tampere University of Technology from September 2017 to April 2018. I would like to thank my supervisors, Industry Professor Tero Joronen and Professor Jukka Konttinen, for possibility to study this interesting subject and directing this thesis. I would also like to thank University Lecturer Henrik Tolvanen for giving advice on how to improve this thesis. Thanks to this thesis, I have had the opportunity to study he simulation of chemical processes with Aspen Plus software, which I have experienced to be useful skill in the modern labor market.

Lastly, I want to thank my family and friends who have supported me during my studies.

Tampere, 21.5.2018

Jukka Lappalainen

CONTENTS

1. INTRODUCTION 1
1.1 Background of the work 1
1.2 Research questions of the work 3
1.3 Objectives of the work 4
1.4 Research methods 4
1.5 Structure of the work 4
2. UPGRADING LIGNOCELLULOSIC BIOMASS 5
2.1 Biomass 6
2.2 Thermochemical conversion technologies 10
2.2.1 Torrefaction 10
2.2.2 Pyrolysis 11
2.2.3 Gasification 13
2.2.4 Hydrothermal treatment 15
3. HYDROTHERMAL LIQUEFACTION IN SUPERCRITICAL WATER 18
3.1 Supercritical fluids 18
3.2 Properties of water at elevated temperature and pressure 19
3.3 Effects of process variables 21
3.3.1 Effects of biomass and its properties 21
3.3.2 Effects of process conditions 23
3.3.3 Effects of catalyst materials, solvents and reducing gases 25
3.4 Reaction pathways of the hydrothermal liquefaction 28
3.4.1 Cellulose 29
3.4.2 Hemicellulose 34
3.4.3 Lignin 35
3.4.4 Other reactions in supercritical water 37
3.4.5 Reaction kinetic parameters 38
3.5 Products of the hydrothermal liquefaction process 38
3.6 The scalability of hydrothermal liquefaction process 41
4. CALCULATION THEORY 43
4.1 Soave-Redlich-Kwong Equation-of-State 43
4.2 Predictive Soave-Redlich-Kwong Equation of state method 45
4.3 UNIFAC method 46
4.4 Relationship between departure functions and Equation-of-State 48
4.5 Reaction kinetics in plug flow reactor 49
5. HYDROTHERMAL LIQUEFACTION PILOT FACILITY 52
5.1 Pretreatment of biomass 53
5.2 Pressurizing the slurry 53
5.3 Heat exchangers 54
5.4 Hydrothermal liquefaction reactor 54
5.5 Cooling 54

5.6 Depressurizing the product 55
5.7 Extraction of gaseous products 55
6. HYDROTHERMAL LIQUEFACTION REACTION SIMULATION MODEL ..56
6.1 Existing simulation models 56
6.2 Introduction to ASPEN PLUS 59
6.3 Creating simulation model 60
6.4 Model overview 61
6.4.1 Hydrothermal liquefaction reactions 63
6.4.2 Property method 63
6.4.3 Biomass 64
6.5 Model compounds 64
7. SIMULATION MODEL RESULTS AND DISCUSSION 65
7.1 Results of case study 65
7.2 Simulation model results comparison with experimental results 69
7.3 Discussion 71
8. CONCLUSIONS 73
REFERENCES 76

APPENDIX A: STRUCTURES OF HEMICELLULOSE

APPENDIX B: STRUCTURE OF LIGNIN

APPENDIX C: THE PROCESS FLOW CHART

APPENDIX D: STREAM RESULTS OF THE MODEL

APPENDIX F: AN OVERVIEW OF EXISTING HTL MODELS

LIST OF FIGURES

Figure 1 Development of energy consumption and Greenhouse gas (GHG) emissions in the European Union- (The data is adapted from: European Environment Agency 2017; Eurostat 2018; Climate Action Tracker).....2
Figure 2 Different conversion processes of biomass (Adapted from: Demirbaş 2009, p. 262).....6
Figure 3 Van Krevvler diagram (Adapted from Krevelen 1993).....7
Figure 4 Structure of fiber in the plant cell wall (Adapted from Hsu et al. 1980, p. 315-316).....8
Figure 5 Structure of cellulose (Adapted from Bajpai 2016).....9
Figure 6 Main components of lignin (Adapted from Doherty et al. 2011, p. 260).....9
Figure 7 Torrefaction process (Adapted from Dutta & Leon 2011).....11
Figure 8 The basic idea of the integrated pyrolysis plant into CHP plant. (Adapted from Heiskanen 2013, p. 8).....12
Figure 9 Fast Pyrolysis process developed by BTG (BTG).....13
Figure 10 GoBiGas gasifier (Adapted from Karlbrink 2015, pp. 15-18).....14
Figure 11 The phase diagram of water, including areas where different water treatment is mainly performed.....15
Figure 12 The variation of water density when changing the temperature. The ρ-T - functions are produced with Aspen Plus V9 software.....19
Figure 13 Enthalpy change as a function of temperature. The ΔH-T –functions are produced with Aspen Plus V9 software.....21
Figure 14 Cellulose hydrolysis to Cellobiose.....30
Figure 15 Decomposition of cellulose into glucose in supercritical water (Adapted from Kabyemela et al. 1998, p. 359; Kabyemela et al. 1999, p. 359; Sasaki et al. 2002, p. 6644).....31
Figure 16 Decomposition of glucose (Adapted from Kabyemela et al. 1999, p. 2891).....32
Figure 17 Dehydration of fructose to 5-HMF (Adapted from Gomes, F N D C et al. 2015).....32
Figure 18 Degradation of glyceraldehyde (Adapted from Honma & Inomata 2014).....33
Figure 19 Rehydration of 1,6-anhydroglucose (Adapted from Yakaboylu et al. 2015, p. 8102).....33
Figure 20 Decomposition of glycoaldehyde (Adapted from Goodwin & Rorrer 2010, p. 12; Yakaboylu et al. 2015, p. 8102).....33
Figure 21 Decomposition of erythrose (Adapted from Yakaboylu et al. 2015, p. 8102).....33
Figure 22 Decomposition of pyruvaldehyde (Adapted from Aida et al. 2007).....34

Figure 23 Decomposition of xylan (Adapted from Goodwin & Rorrer 2010, p. 8102; Paksung & Matsumura 2015, p. 7606-7609; Yakaboylu et al. 2015, p. 8102-8103; Yakaboylu, Harinck et al. 2015, p. 877). *34*
Figure 24 Decomposition of lignin (Adapted from Yong & Matsumura 2012, p. 11984) *35*
Figure 25 Degradation of lignin (Adapted from Forchheim et al. 2014, p. 988) *36*
Figure 26 Decomposition of guaiacol, catechol and phenol (Adapted from Forchheim et al. 2014, pp. 988 & 992) *37*
Figure 27 Formation of 2-methylcyclopentan-1-one (Adapted from Pedersen et al. 2015, p. 214) *37*
Figure 28 Water-Gas-Shift reaction *38*
Figure 29 Methanation reaction *38*
Figure 30 Key elements of upscaling the reactor to industrial size. (Adapted from Donati & Paludetto 1997, pp. 486-488) *42*
Figure 31 Plug flow reactor *51*
Figure 32 Hydrothermal liquefaction process overview. *52*
Figure 33 the main idea of piston pump *53*
Figure 34 Basic idea of hydrothermal liquefaction reactor *54*
Figure 35 The basic idea of the cooler *55*
Figure 36 Hydrothermal liquefaction integrated with hydrogen plant and hydrotreating (Adapted from Tews et al. 2014, p. 14) *57*
Figure 37 The overall process of combined biogas plant and hydrothermal liquefaction unit (Adapted from Hoffmann et al. 2013, p. 404). *58*
Figure 38 the used procedure to build up the simulation model *60*
Figure 39 Pretreatment of biomass-water slurry *61*
Figure 40 Hydrothermal liquefaction reactor *62*
Figure 41 Cooling and depressurizing the product and vapor-liquid-liquid separation *62*
Figure 42 Model yields of hydrothermal liquefaction of Norway spruce with optimal reactor size. *66*
Figure 43 Biocrude yield as a function of time with four different temperatures *68*
Figure 44 Experimental results of hydrothermal liquefaction of empty fruit bunch and palm kernel shell compared with model results. The empirical data is adapted from Chan et al. (2015, p. 184) *70*

LIST OF SYMBOLS AND ABBREVIATIONS

APR	Aqueous Phase Reforming
BFB	Bubbling Fluidized Bed
CFB	Circulating Fluidized Bed
CFD	Computational Fluid Dynamics
CO_{2eq}	Carbon dioxide equivalent
EoS	Equation-of-State
HTC	Hydrothermal carbonization
HTG	Hydrothermal gasification
HTL	Hydrothermal liquefaction
HTT	Hydrothermal treatment
PFR	Plug Flow Reactor
SRK	Soave-Redlich-Kwong
PSRK	Predictive Soave-Redlich-Kwong

1. INTRODUCTION

The growing need for the energy, the decreasing amount of fossil fuels and the climate change drives humankind to develop new, sustainable, clean sources of energies. Solar power, wind power and geothermal power are emission-free sources of energies, but the distribution of these sources of energy varies depending on the region and both season and time of day. Furthermore, energy transfer from countries with the oversupply of emission-free energy to countries with the need for energy is possible between relatively short distances, because in many countries power grids cannot pass large amounts of energy without major losses (European Commission 2017b).

Energy storage systems are a solution to storing excess emission-free energy and provide the stored energy for users when there is a need for energy. Energy storage systems stores energy as heat energy, mechanical energy, potential energy or chemical energy, but these technologies are expensive and the amount of recovered energy is rather low with relation to the size of storage. For these reasons, there is a need to develop new flexible sources of energy, which does not increase the amount of greenhouse gases. The second possibility is to use carbon-neutral energy sources, where biomass based biofuels are combusted when there is need for energy. The combustion of biofuels produces carbon dioxide, but the same amount of carbon dioxide bounds to growing biomass. Biomass converts into solid, liquid or gaseous biofuel in different processes, such as pyrolysis and hydrothermal treatment processes. The other major questions is that how to cover the energy demand for the transportation system, which mainly basis on fossil fuels. Solution for this is liquid or gaseous biofuels, but this sets requirements for fuel purity and energy content.

This study focus on hydrothermal liquefaction, where the conversion of lignocellulosic biomass happens in water at an elevated pressure and temperature, in this case, in supercritical water. The hydrothermal liquefaction process converts biomass into biocrude, which has high heating value and low oxygen content compared with other biofuels. The product, i.e. biocrude, is possible to use directly as fuel for engine power plants to produce electricity and heat with a very short start-up time. The other solution is to upgrade the biocrude to transport fuel.

1.1 Background of the work

Globally, the total need of energy is enormous, in 2015 the amount reached 577 EJ (EJ = 10^{18} J) and the production generated 32 294 Mt CO_{2eq} (Mt = 10^6 ton CO_{2eq}) of greenhouse gas emissions (IEA 2017, pp. 60-61). In the European Union, the total energy consumption and the produced CO_{2eq} emissions were 68.2 EJ and 4 451 Mt in 2015 (European

Environment Agency 2017; Eurostat 2018). Figure 1 shows that the greenhouse gas emissions and total energy consumption have decreased in the European Union between 2007 and 2015. In last decades, humans have paid attention to environmental consciousness and sustainable development to ensure safe life for future generations. Due this, the European Union has set targets for preventing the climate change and improving the production and usage of energy (European Commission 2016b).

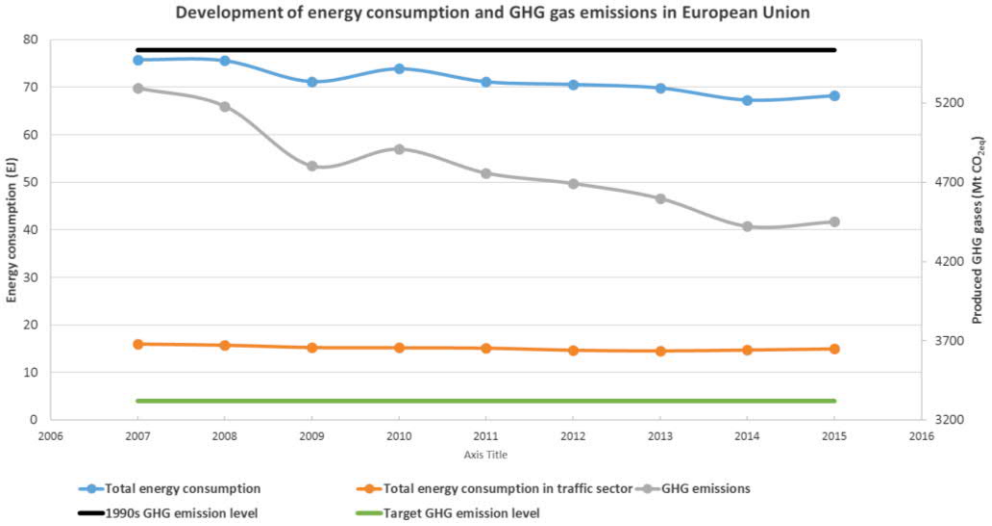

Figure 1 Development of energy consumption and Greenhouse gas (GHG) emissions in the European Union- (The data is adapted from: European Environment Agency 2017; Eurostat 2018; Climate Action Tracker).

The European Union adopted the Paris Agreement in December 2015, which set target to limit the average temperature increase to 2 ˚C (European Commission 2015). Due this, reducing the greenhouse gases are important part of achieving the goal. The target of CO_2 emission reduction is 40 % compared with the 1990s emission levels (European Commission 2015; European Commission 2016a). By 2015, the emission level reached 78% of the 1990 levels, so there is still a lot to be done before reaching the target. Using biomass to produce energy is one way to reduce greenhouse gas emissions if and only if production of biomass takes place in a sustainable way (European Commission 2017a). The total biofuel or biofuel based biofuels energy consumption was 41.31 EJ in the European Union in 2015 and the share of it compared with total energy consumption is 6.05 % (Eurostat 2018). The goal for renewable energy from the whole energy consumption is 20 % in 2020 and 27 % in 2030 (European Commission 2017c).

Traffic is one of the biggest energy user and greenhouse gas producer at the same time in European Union. The energy consumption in transportation sector was 15.37 EJ, i.e. 367.2 million tons of oil equivalent (TOE), in 2015, which corresponds to approximately 22.5 % of total consumption (Eurostat 2018). European Union's program, White Paper 2011, set goals to transportation sector including cut of transport emission by 60 % by 2050 (European Commission 2011). It also includes a target that cars use only renewable fuels in 2050. The share of renewable fuels in the transportation sector was 8.70 % in

European Union in 2015, so there is a huge gap to catch up by 2050 (Eurostat 2018). The electrifying of the whole traffic system is fairly challenging or impossible task, and therefore the replacement of fossil fuels with biofuels is necessary. The production of biofuels occurs via different conversion technologies, such as thermochemical and biochemical conversion technologies, where biomass converts into biogas or biofuel (Demirbaş 2009, p. 262).

Biomass is a source of renewable energy and the biomass growth is 4 000 EJ of solar energy yearly (Hall & Rao 1999, pp. 4-5). Hoogwijk et al. (2005, pp. 234) estimated the global potentials of biomass energy in 2050 and in 2100, where they studied four different future scenarios. The estimated bioenergy potentials ranged between 311 EJ and 657 EJ in 2050. In 2100, the estimated minimum and maximum potentials were 395 EJ and 1115 EJ (Hoogwijk et al. 2005, p. 254). For example, globally the production of woody biomass is around 56 EJ of energy annually, which is around 10 percent of the total energy demand (World Energy Council 2016, p. 4).

The problem when using biomass as fuel is that it has a low energy content and it is not suitable for transport vehicles in a solid phase. The hydrothermal liquefaction is one of the most promising way to convert biomass into liquid biofuel, known as biocrude. The biocrude has much higher heating value than biomass and it is in the liquid phase. In this form, biocrude is not suitable for transportation vehicles, but it is possible to use it in engine power plants. It is possible to upgrade the biocrude into the biofuel, for example biogasoline and biodiesel, by using it as feed or as co-feed in a refinery plant.

1.2 Research questions of the work

This study aims to answer following research questions:

- The hydrothermal liquefaction has been studied for several decades. However, the knowledge of the existing reaction pathways and kinetics are limited. How well the current knowledge can be applied to the Aspen Plus simulation software?
- Are there enough data related to the reaction pathways and kinetics of the hydrothermal liquefaction process available?”
- Does the simulation model give reasonable calculation results?
- Which issues should take account for when scaling the reactor from pilot plant size to industrial plant size?

The first question relates to Aspen Plus simulation software and its capability to use the available reaction data, i.e. what has to be done to make data suitable for the model. The second question means the availability of data of possible reactions and reaction kinetics in the supercritical water. It is impossible to create the simulation model, if there are not enough data related to the reaction pathway and the reaction kinetics. The third question

is important when estimating the usability of the model. If the model is not enough accurate, it is not suitable for simulating the hydrothermal liquefaction reactions. Lastly, the research focus on answering to last question by studying the leading principles of upscaling the chemical reactor.

1.3 Objectives of the work

The main objective of the study is to create a simulation model to simulate the reactions in hydrothermal liquefaction reactor. The simulation model calculates the products of the reactor and the energy need to make the reactions possible under various reactor conditions. The second objective of the study is to gather data from reaction pathways and reaction kinetics of treating biomass in supercritical water. The third objective is to estimate the accuracy of the model by comparing the model's results and experimental results with each other. The fourth objective is to make a case study with Norway spruce to study the optimum reactor size to obtain high biocrude yield. The last objective is to study the scaling of chemical reactor from a pilot plant size to an industrial plant size.

1.4 Research methods

This work research method divides into literary research, creating a simulation model for calculating hydrothermal liquefaction process with Aspen Plus -program and estimating the accuracy of the results by comparing the results of the model with the experimental results. The literary research includes the investigating of earlier studies focusing on reaction pathways and kinetics in supercritical water, finding studies including experimental hydrothermal liquefaction results and looking for reports focusing on creating hydrothermal liquefaction models. The creating of the simulation model contains building of the process and creating Excel spreadsheet connected with Aspen Plus simulation model. To estimate the accuracy of the simulation, the study includes a comparison study between experimental hydrothermal liquefaction results and simulation model results with the same feed and the same reaction conditions.

1.5 Structure of the work

The chapters 1-4 contain the results of literature research. The chapter 5 presents hydrothermal liquefaction facility, which is under construction at Tampere University of Technology during this thesis. The chapter 6 demonstrate the simulation tool developed during this thesis. The chapter 7 includes the results of validation and case study. The chapter 8 concludes results of this thesis.

2. UPGRADING LIGNOCELLULOSIC BIOMASS

Biomass is an abundant source of energy, and is available nearly everywhere in the world (McKendry 2002a, p. 38). The problem with biomass as a source of energy is that it has a low heating value due to the high contents of oxygen and moisture (Demirbaş 2001, p. 1363; McKendry 2002a, p. 43). The other problem is that using biomass directly as fuel for vehicles is not possible. The main interest of this study focus on converting lignocellulosic biomass into liquid biofuel, in this case known as biocrude.

The biofuels divides into four different categories: first-generation, second-generation, third-generation and fourth-generation biofuels (Singh et al. 2011, p. 1349). Dividing biofuels into different generation depends on both method used to produce biofuel and the used raw material in production. The production of first-generation biofuels, such as biodiesel, ethanol, and biogas, takes place from edible biomass, like wheat, corn or rapeseed. The manufacturing methods for first-generation biofuels are, for example, fermentation of wheat or separating oil from turnip rapeseed by compression and transesterification (Singh et al. 2011). The feedstock of second-generation biofuels are mostly non-edible biomass, like wood, or food waste, which is not suitable for consumption (Singh et al. 2011). The second-generation biofuel manufacturing processes include lignocellulosic biomass processing. Lignocellulosic biomass is hard to decompose, because the lignin content of biomass (Singh et al. 2011). The third-generation biofuels basis on algae with ability to bind carbon dioxide and to convert it into biomass with good efficiency (Singh et al. 2011; Aro 2016). The fourth-generation biofuels use sunlight and electricity as source of biofuels (Aro 2016).

There are several conversion process technologies to convert biomass into biofuel (Figure 2), such as thermochemical conversion, electrochemical conversion, indirect liquefaction and biochemical conversion and physical extraction. The direct combustion releases the energy content of biomass as heat or by transforming heat into electricity. An example of the existing conversion technology is NExBTL technology, where waste material and vegetable oils are converted into biodiesel (Neste Oil Plc).

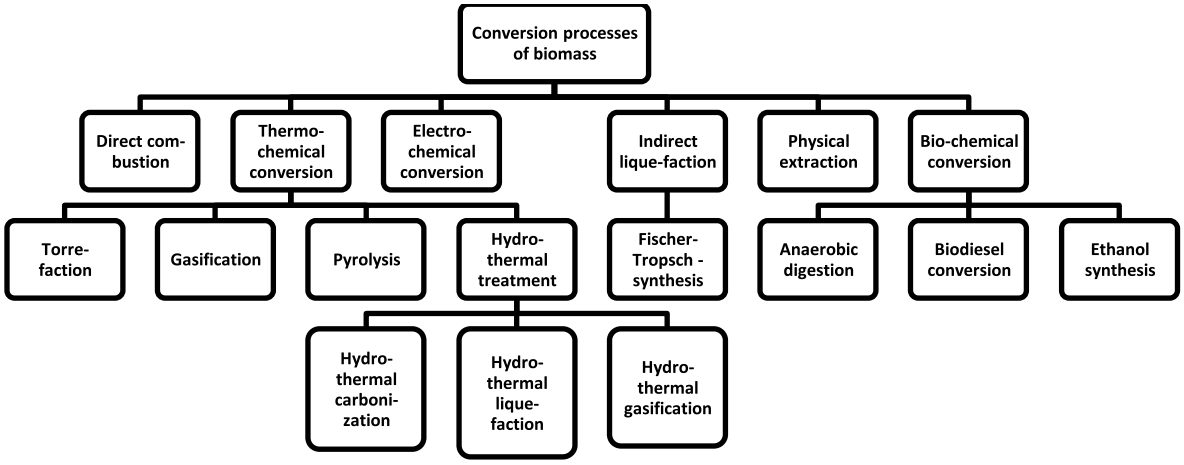

Figure 2 Different conversion processes of biomass (Adapted from: Demirbaş 2009, p. 262).

One promising way to upgrade lignocellulosic biomass into biofuel is to use thermo- or biochemical conversion techniques (Demirbaş 2001, pp. 1368-1377), whereby the resulting fuel is classified as the second-generation biofuel. Thermochemical conversion techniques include torrefaction, pyrolysis, liquefaction, gasification and hydrothermal treatment methods. Biochemical conversion techniques divide into anaerobic digestion and microbial fermentation (Demirbaş 2009, p. 262). This chapter focus on both biomass and its properties, and thermochemical conversion techniques used to convert biomass into biofuels.

2.1 Biomass

Living organisms produces biomass used as source of energy or biochemical (Anikeev & Fan 2014, p. 89). Biomass sources are, for example, wood, food residues, plants and agricultural waste. Plant based biomass forms when plant produces biomass via photosynthesis, where water, carbon dioxide and sunlight react to form carbohydrates (McKendry 2002a). The biomass properties depends on the biomass type. Table 1 includes typical properties of wood, peel, and peat. It also includes coal properties for comparison. When comparing coal and wood with each other, it is notable that the lower heating value (LHV) of wood (19.5 MJ/kg) is much lower than lower heating value of coal (28.7 MJ/kg). This is due to high contents of oxygen and moisture in biomass. In addition, a significant proportion of hydrocarbons in the biomass are volatile hydrocarbons.

Table 1 Properties of different fuels (Adapted from Alen et al. 2002, p. 137).

	Wood	*Peel*	*Peat*	*Coal*
Moisture (%)	30-45	40-65	40-55	10
Ash (dry wt-%)	0.4-0.5	2-3	4-7	14
Volatile (dry wt-%)	84-88	70-80	65-70	29.5
C (dry wt-%)	48-50	51-66	50.7	76-87
H (dry wt-%)	6-6.5	5.9-8.4	5-6.5	3.5-5
N (dry wt-%)	0.5-2.3	0.3-0.8	1-2.7	0.8-1.2
O (dry wt-%)	38-42	24.3-40.2	30-40	2.8-11.3
S (dry wt-%)	0.05	0.05	<0.2	<0.5
Cl (dry wt-%)	<0.01	<0.01-0.03	0.03	<0.1
HHV (MJ/kg)	21	20	21.6	29.6
LHV (MJ/kg)	19.5	20.4	20.4	28.7

Van Krevvler diagram shows different solid fuels by theirs O/C and H/C atomic ratios (Figure 3). When the O/C ratio decreases and H/C ratio increases, the heating value of studied compound increases. Biomass consists of a significant amount of oxygen compared with coal and anthracite, which causes the low heating value of biomass. de Caprariis et al (2017) tested various biomasses in the HTL reactor using different reactor temperatures. When the used temperature of the reactor was 320 ˚C, they achieved biocrude, which O/C and H/C ratios were comparable with coal, lignite and peat.

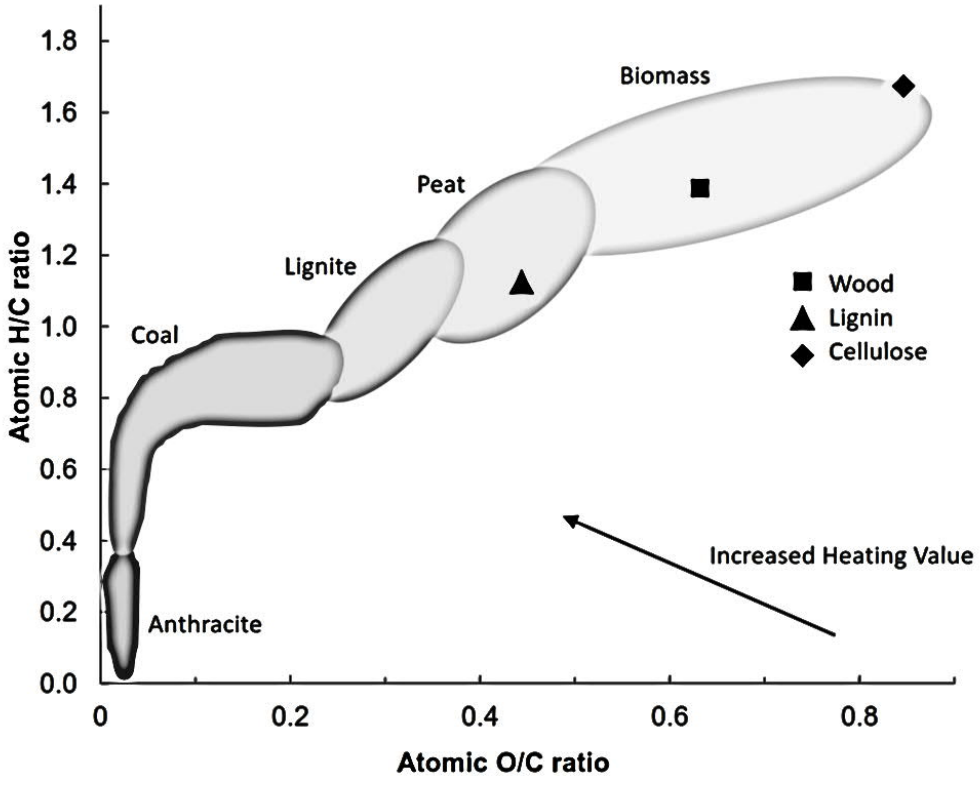

Figure 3 Van Krevvler diagram (Adapted from Krevelen 1993).

Lignocellulosic biomass includes mostly cellulose, hemicelluloses and lignin, but it also contains small amounts of other components, such as extractives and ash (Bajpai 2016, pp. 7-10). The amounts of these components depend on the biomass and the studied part of biomass shown in Table 2. The cellulose is the most common component found in the lignocellulosic biomasses, but the lignin content is significant high in some cases. For example, the walnut shell contains over 50 wt-% lignin from its mass (Demirbaş 2001, p. 48; Bajpai 2016, p. 8; de Caprariis et al. 2017, p. 620).

Table 2 Composition of different biomasses.

	Cellu-lose wt-%	***Hemi-cellulose*** wt-%	***Lignin*** wt-%	***Extrac-tives*** wt-%	***Reference***
Hardwood	40 - 55	24 - 40	18 - 25	-	(Demirbaş 2001, p. 48)
Hardwood	27 - 35	27 - 35	16 - 24	2-8	(Bajpai 2016, p. 8)
Softwood	45 - 50	25 - 50	25 - 35	-	(Demirbaş 2001, p. 48)
Wheat straw	30	50	15	-	(Demirbaş 2001, p. 48)
Corn cobs	45	35	15	-	(Demirbaş 2001, p. 48)
Walnut shell	23.3	20.4	53.5	2.8	(de Caprariis et al. 2017, p. 620)

Lignocellulosic-derived biomass consists of plant cells, where cell wall surrounds the cell. The cell wall contains lignocellulosic fibers built of hemicellulose, cellulose and lignin shown in Figure 4 (Crocker & Andrews 2010, p. 13).

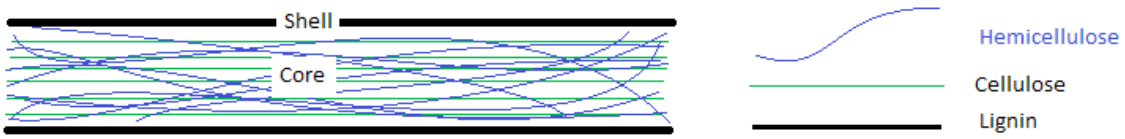

Figure 4 Structure of fiber in the plant cell wall (Adapted from Hsu et al. 1980, p. 315-316).

Cell walls mainly contains cellulose making it a significant part of biomass (Demirbaş 2001, p. 7). Cellulose builds up from β-glucopyranose –units linked to each other by (β-(1->4))-linkage (H. Chen 2014, p. 29; NIIR Project Consultancy Services 2015, p. 32). The chains are linear and consist of hundreds even thousands linked β-glucopyranose –units (Figure 5) (H. Chen 2014, p. 29-30). (β-(1->4))-linkage and hydrogen bond makes cellulose difficult to break down into smaller monomers (NIIR Project Consultancy Services 2015).

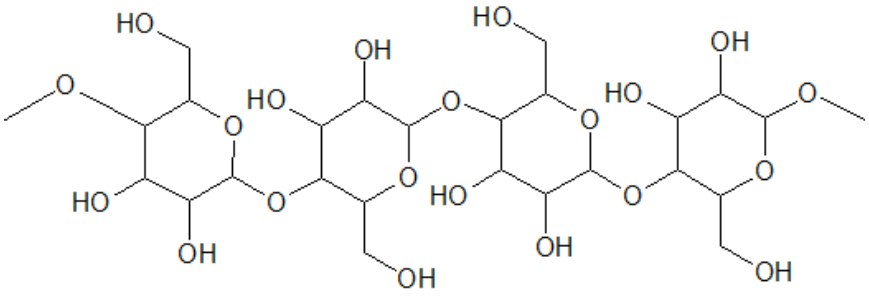

Figure 5 Structure of cellulose (Adapted from Bajpai 2016).

Hemicellulose is the second most common compound found in the cell plans of plants. Unlike cellulose, hemicellulose does not have a certain structure but it exist in a number of different structures (Ebringerová et al. 2005, p. 2, 4-5). Hemicellulose divides into four class by its structure, xylans, mannans, β-glucans and xyloglucans, shown in Appendix A (Ebringerová et al. 2005, p. 4-5). Hemicellulose, like cellulose, chains into polysaccharides, but the chains are shorter and, in some cases, branched (Mussatto 2016, p. 172). Hemicellulose decomposes easier than cellulose, because of shorter and partly branched chains. Furthermore, linkages between monosaccharides of hemicellulose are not as strong as linkages between monosaccharides of cellulose (Mussatto 2016, p. 172).

Lignin is the third most compound founds on cell walls of plants. The structure of lignin varies depending on source on biomass. Appendix B represents the suggested structures of lignin in softwood and in hardwood. Lignin mainly builds up from hydroxycinnamyl alcohols, sinapyl alcohol, coniferyl alcohol and p-coumaryl alcohol (Figure 6), whose incidence in structure depends on the source of biomass (Vanholme et al. 2010; Crocker & Andrews 2010, p. 14). These alcohols links to each other in various different ways, such as β-O-4 –link. The amorphous structure of lignin makes it resistant to mechanical and chemical treatment (Crocker & Andrews 2010, p. 14).

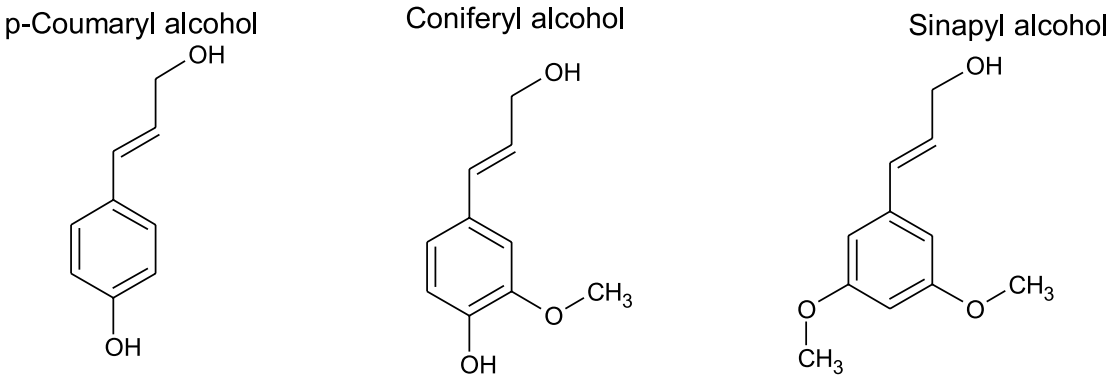

Figure 6 Main components of lignin (Adapted from Doherty et al. 2011, p. 260).

The degradation of cellulose, hemicellulose and lignin differs from each other, because cellulose and hemicellulose breaks down easily using, e.g. acid hydrolysis, while breaking down the structure of lignin needs significantly harsher processing (Crocker & Andrews 2010, pp. 13-14). When studying the fibers in the cell walls of lignocellulosic biomass, the lignin locates in the outermost part of fiber (Figure 4) (Crocker & Andrews 2010, p. 14). For this reason, lignocellulosic biomass is resistant to most treatment technologies, such as fermentation (Crocker & Andrews 2010, pp. 14-15). There are several technologies to degrade the lignocellulosic biomass, such as pyrolysis and hydrothermal liquefaction.

2.2 Thermochemical conversion technologies

Thermochemical conversion technologies use high temperature for converting biomass into desired product. The reactions take place in a reaction medium, which can be, for example, air, inert gas or water. Thermochemical conversion technologies include torrefaction, gasification, pyrolysis and hydrothermal treatment. The hydrothermal treatment divides into hydrothermal carbonization, hydrothermal liquefaction and hydrothermal gasification. Torrefaction, gasification and pyrolysis mainly occur under inert gas, whereas hydrothermal treatment happens in the presence of water or other reaction medium, such as ethanol.

2.2.1 Torrefaction

Torrefaction, known also as mild pyrolysis, is a thermochemical process, where wet biomass converts into torrefied charcoal-like fuel, i.e. biochar, with high energy density and low moisture content (W. Chen et al. 2015; Tran et al. 2016, p. 409). When using biomass as a fuel, the problem is the low calorific fuel due to high moisture, volatile matter and oxygen contents (Dutta & Leon 2011). For these reasons, it has a low energy density. Torrefaction process aims at improve calorific value and energy density (W. Chen et al. 2015). Biomass is hygroscopic (i.e. absorbs moisture) before torrefaction process, whereas torrefied biomass is hydrophobic (i.e. resists water), resulting in better preservability (Dutta & Leon 2011; W. Chen et al. 2015). Furthermore, biomass is heterogeneous, for which reason the quality of the same biomass varies greatly. Torrefaction process homogenizes biomass leading to the more stable and cleaner combustion of torrefied fuel.

Torrefaction process occurs at temperatures between 200 ˚C and 300 ˚C in the presence of inert gas, such as nitrogen (Figure 7) (W. Chen et al. 2015). There are three different kind of torrefaction process: light, mild and severe torrefaction; light torrefaction process occurs at temperatures between 200 – 235 ˚C, mild torrefaction between 235 – 275 ˚C and severe torrefaction between 275 - 300 ˚C (W. Chen & Kuo 2011, p. 804; W. Chen et al. 2015). Hemicellulose, extractives and volatile organic compounds (VOCs) volatilize

at temperatures between 200 and 300 ˚C while cellulose and lignin remain almost completely in the residue of biomass (Tran et al. 2016, p. 409). Products of the torrefaction process are in liquid, gaseous, and solid forms (Basu 2013, p. 100). Liquid products are water, organics, such as alcohols and furans, and lipids, like waxes and terpenes. Solid products include biochar and sugar. Gaseous product consists of CO, CO_2, CH_4 and other hydrocarbons. The energy density of biochar is around 70 % better compared to the original energy density of biomass (Dutta & Leon 2011). Furthermore, about 90 % of energy content of biomass remains in biochar (Dutta & Leon 2011).

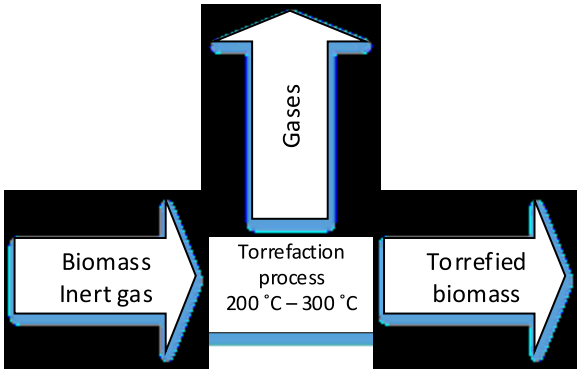

Figure 7 Torrefaction process (Adapted from Dutta & Leon 2011)

There are numerous of companies offering solutions of a different kind for torrefaction process, such as BTG torrefaction process (BTG). In the BTG torrefaction process, a screw conveyor drives biomass through the process. The torrefaction of biomass occurs with hot inert gas produced. The inert gas comes from combustible gases produced from torrefaction in the combustor. An electric heater brings additional heat energy to process, if the heat energy from the combustion of torrefaction gases is not enough. Finally, the torrefied biomass cools down in the cooler and goes into product tank. Flashtor® technology is a torrefaction process using several torrefaction reactors to optimize the torrefaction process (Blackwood Technology). The required heat energy comes from burning torgas, i.e. torrefaction gases, from the process. There is a torrefaction plant in Duiven proved the Flashtor® technology working at the industrial scale.

2.2.2 Pyrolysis

The basic idea of a pyrolysis process is similar with the torrefaction process, but the pyrolysis process occurs at higher temperature and the desired product from the pyrolysis process is either pyrolysis oil, gas or char (Yaman 2004, p. 652). However, the pyrolysis oil is the most interesting product from the pyrolysis process. The pyrolysis has high fuel-to-feed efficiency up to 95.5 % and the conversion efficiency of biomass to pyrolysis oil is even 70 % (Demirbaş 2001, p. 1370). The properties of pyrolysis oil depend on the raw material and the process conditions. The lower heating value is between 14 – 18 MJ/kg

due to high oxygen and water content (Oasmaa & Czernik 1999, p. 915). The other essential properties of pyrolysis oil are poor stability, non-homogenous and low pH value (Oasmaa & Czernik 1999, pp. 915-916; Gollakota et al. 2016, pp. 1547-1548).

The pyrolysis process occurs in the presence of inert gas at the temperatures of 377 ˚C - 527 ˚C and pressures of 0.1 – 0.5 MPa (Demirbaş 2001, p. 1370). The pyrolysis process types divides into two main types: slow and fast pyrolysis (Brownsort 2009, p. 3). The fast pyrolysis name is due to a high heating rate while keeping the residence time as short as possible. The process occurs at the temperature near of 500 ˚C and the desired product is pyrolysis oil in most cases. The slow pyrolysis process produces charcoal or biochar with lower heating rate and longer residence time compared with the fast pyrolysis. Typically, the slow pyrolysis process takes place at the temperature of 400 ˚C.

Fortum Corporation has built a fast pyrolysis demo plant integrated into the combined heat and power (CHP) plant (Fortum). Valmet has designed and supplied the demo plant. The production of pyrolysis oil is around 50 000 tons a year. The pyrolysis oil replaces fossil fuels in district heat plants or in the steam production plants. Figure 8 shows the basic idea of the process used in the demonstration plant. The heat required in the fast pyrolysis process comes from a hot bed material used in the bubbling fluidized bed (BFB), which is the boiler used in the CHP plant to burn the biomass. The biomass fed into the pyrolysis process dries and volatile part of biomass evaporates. Next, the gaseous product from the pyrolysis process goes into a condenser. The non-condensable gases flow into BFB to be burned and the condensable product, i.e. pyrolysis oil, goes into product tank.

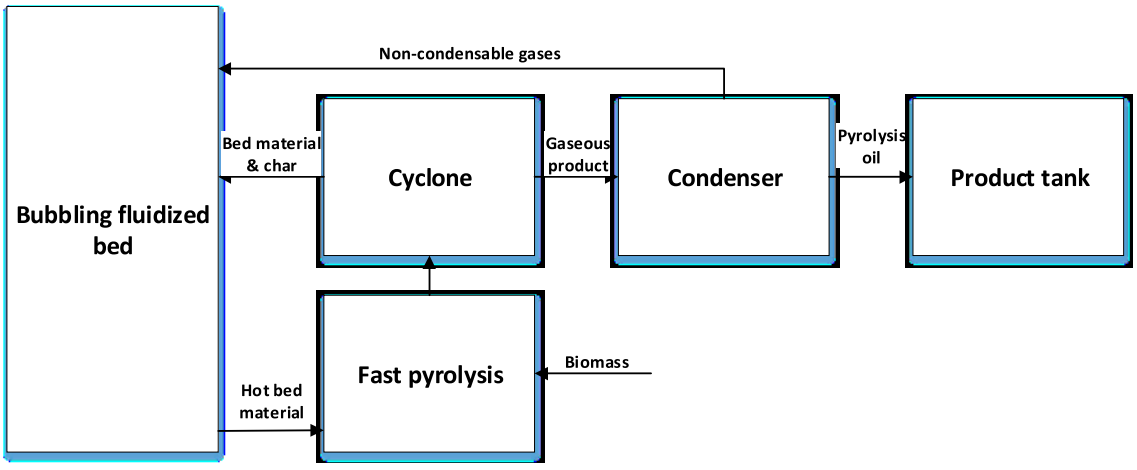

Figure 8 The basic idea of the integrated pyrolysis plant into CHP plant. (Adapted from Heiskanen 2013, p. 8)

Biomass Technology Group has developed a fast pyrolysis process using a rotating cone reactor as a pyrolysis reactor (Figure 9) (BTG). The formed char in the pyrolysis reactor flows into BFB with sand. The heat required for the pyrolysis comes from hot bed material from the BFB. The heating of the bed material occurs via burning the char in the BFB.

The produced gases in the pyrolysis reactor go into a condenser, where the condensable oil is collected and the non-condensable gases go into afterburner.

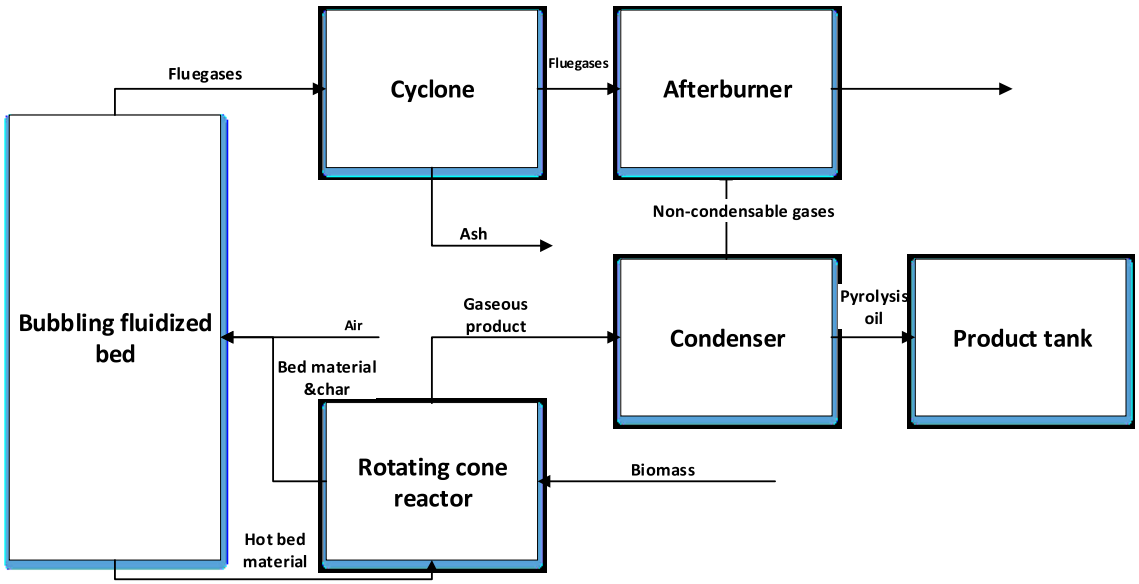

Figure 9 Fast Pyrolysis process developed by BTG (BTG)

2.2.3 Gasification

Gasification is a thermochemical process, where the gasification of fuel, such as biomass, occurs under elevated temperature and a low oxygen content (Warnecke 2000). The oxygen is received from air or even pure oxygen can be used as a gasification medium (McKendry 2002b). In some cases, the gasification medium is steam or H_2 (McKendry 2002b). The temperature of gasification is between 800 ˚C and 1800 ˚C depending on the properties of feedstock (Higman & van der Burgt 2008, p.11). Mainly the melting point of ash of feedstock defines the maximum temperature of the process. Products of gasification are gaseous products, such as CO, CO_2, H_2, H_2O and gaseous hydrocarbons, ash and condensing gases, such as tars and hydrocarbons (Puig-Arnavat et al. 2010). Furthermore, small amount of char will remain in gasification products. Depending on gasification medium, the calorific value of product gas varies between 4 – 40 MJ/Nm^3 (McKendry 2002b). Gasification with air produces product gas, which calorific value is between 4 and 6 MJ/Nm^3 while with pure oxygen or steam leads to product gas with calorific value between 12 and 18 MJ/Nm^3. Gasification with hydrogen can produce product gas, which calorific value is up to 40 MJ/Nm^3.

The gasification process of biomass includes biomass drying, pyrolysis reactions, oxidation reactions and reduction reactions (Susastriawan & Saptoadi 2017). In the drying zone, the moisture content is vaporized at temperatures between 100 and 200 ˚C (Puig-Arnavat et al. 2010). In the pyrolysis zone, volatile content of biomass volatilizes at tem-

peratures between 200 and 700 ˚C. A part of char oxidizes in the oxidation zone at temperatures between 800 and 1400 ˚C. The oxidation of char is either partial oxidation into CO or total oxidation into CO_2. Char also reacts with CO_2 (the Bouduard reaction), H_2O (the water-Gas reaction) and H_2 (the methanation reaction) producing CO, H_2, CH_4 in the reduction zone (Forchheim et al. 2014, p.12-13; Susastriawan & Saptoadi 2017). Furthermore, both the water-gas shift, and the steam methane reforming reactions take place in reduction zone. Gasification reactors divide into three main types: fixed bed, fluidized bed and indirect gasifier (Belgiorno et al. 2003). Fixed bed gasifier subdivides into updraft and downdraft gasifiers and fluidized bed gasifier into bubbling and circulating gasifiers.

GoBiGas is a working gasifier plant in Gothenburg based on a combination of a circulating fluidized bed and a bubbling fluidized bed (GoBiGas). Valmet Corporation has designed and supplied the technology. The plant can produce biogas around 6900 Nm^3/h (20 MW) and is capable to transforming energy content from biomass into biogas up to 65 % while the overall energy efficiency is over 90 %. The GoBiGas gasification plant uses a dual fluidized bed to convert wet residues into biogas (Figure 10). The gasifier type is a bubbling fluidized bed, where endothermic gasification reactions occur and the energy needed for reactions comes from hot bed material (Karlbrink 2015, pp. 15-18). The warming up of the bed material occurs via burning the char coming from the gasifier. After the gasifier, the syngas goes into cooling and cleaning sectors, where the syngas cools down and impurities are removed. After cleaning, the product gas goes into methanation process. The combustible gases from cleaning and a combustion chamber are combusted in the afterburner and particles from cleaning goes into the combustion chamber.

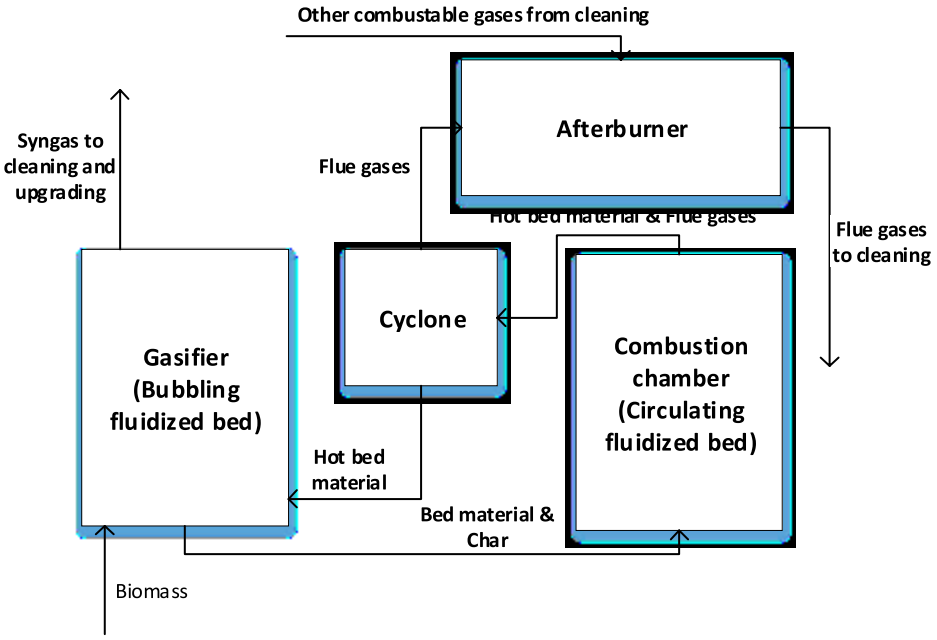

Figure 10 GoBiGas gasifier (Adapted from Karlbrink 2015, pp. 15-18)

2.2.4 Hydrothermal treatment

Hydrothermal treatment (HTT) includes thermochemical processes, whose reactions occur in hot pressurized water. Producing energy carrier with higher heat value than biomass itself is one of the biggest interests when hydrothermal treatment processes are used. Hydrothermal treatment divides into three or four different techniques: hydrothermal carbonization (HTC), hydrothermal liquefaction (HTL), aqueous phase reforming (APR) and hydrothermal gasification (HTG), which depends on conditions in the reactor (Hrnčič et al. 2016).

Hydrothermal carbonization typically takes place at temperatures below 250 ˚C and pressure of 2.4 MPa (Child 2014, p.17; Elliott et al. 2015a), but even higher temperatures and pressures are used, up to temperature of 350 ˚C and pressure of 10 MPa. (Hoekman et al. 2011, p. 114). The main product of the hydrothermal carbonization is hydrochar (Elliott et al. 2015a). Hydrothermal liquefaction takes place near the critical point of water with the temperature between 250 and 374 ˚C (Elliott et al. 2015a). However, it is possible to use temperatures higher than 374 ˚C for hydrothermal liquefaction, but in these cases, the used residence time is shorter than under the supercritical point of water. Pressure of the hydrothermal liquefaction is between 2 – 400 bar (Elliott et al. 2015a). The product of the hydrothermal liquefaction is biocrude and it is possible to upgrade the biocrude into biofuel such as biogasoline and biodiesel. Hydrothermal gasification happens at temperature and pressure above the critical point (374 ˚C and 22.1 MPa) and main products of the hydrothermal gasification are CO_2, CO, H_2 and CH_4 (Toor et al. 2011; Elliott et al. 2015a). In summary, there are no well-defined temperature and pressure ranges for hydrothermal processes, but Figure 11 represents typical regions of HTC, HTL and HTG.

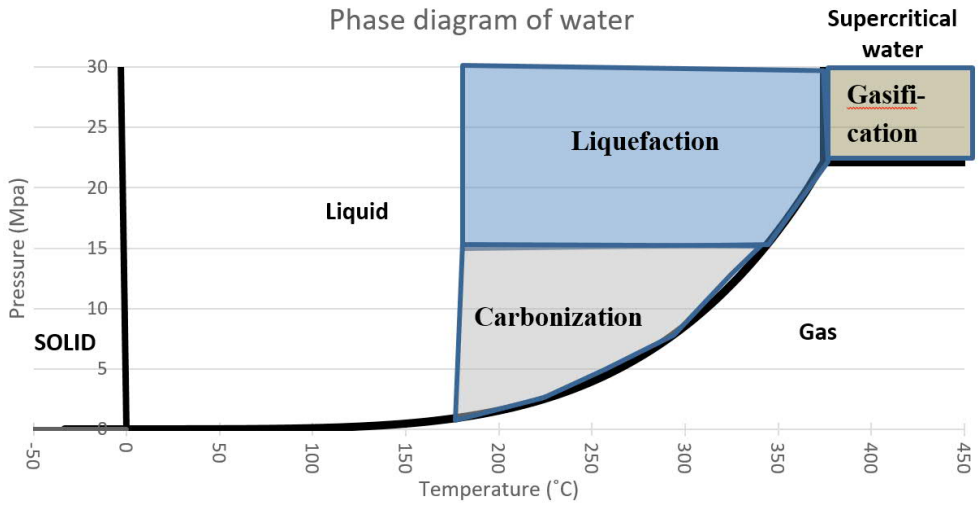

Figure 11 The phase diagram of water, including areas where different water treatment is mainly performed

Benefits of using hydrothermal treatment processes are that wet feedstock goes directly into the process and due this, there is no need for an energy-intensive drying process and the temperatures of hydrothermal processes are relatively low (Elliott 2011). When comparing biocrude produced in HTL with pyro-oil produced in pyrolysis reactor, the biocrude contains more energy than the production of it needs while producing pyro-oil consumes more energy than pyro-oil contains (Jena & Das 2011, p. 5481). Moreover, heating value of biocrude varies between 30 and 36 MJ/kg while the heating value of pyro-oil is between 20 and 25 MJ/kg (Kruse & Dahmen 2015, p. 37). This is mainly due to lower contents of oxygen and moisture in the biocrude (Xiu & Shahbazi 2012, p. 4409). Overall, the quality of biocrude is better in comparison with pyro-oil making it more suitable for upgrading to other products, such as transportation fuels (Xiu & Shahbazi 2012, p. 4407).

Hydrothermal carbonization

HTC produces a hydrochar from biomass. The hydrochar is significantly homogenous compared with biomass, even if the biomass used to produce the hydrochar comes from different sources (Hoekman et al. 2011, p. 8). Furthermore, the hydrochar has better heating value compared with biomass (Hoekman et al. 2011, p. 8). They conclude that hydrochar and a low rank coal have similar fuel properties. HTC happens when biomass reacts with water at low temperature (180 ˚C - 350 ˚C) and autogenous pressure, which can be even 2.4 MPa (Hoekman et al. 2011; Child 2014, p.17). However, in some cases HTC occurs under higher pressures up to 10 MPa (Hoekman et al. 2011). HTC process also produces gases, water-soluble products and water (Hoekman et al. 2011, p. 3-4).

HTC includes several main reactions from biomass to hydrochar that are hydrolysis, dehydration, decarboxylation, condensation, polymerization and aromatization (Child 2014, p. 21). Feedstock and process conditions have significant influence on the quality of hydrochar; when the temperature and pressure increase, the char yield decreases (Child 2014, p. 29). The HTC decreases oxygen and hydrogen contents similarly improving the heating value of the hydrochar (Child 2014). However, there are little difference between hydrochar produced from different kind of biomasses (Berge et al. 2011, pp. 5699-5700; Child 2014, s. 21-22, 29).

Hydrothermal liquefaction

HTL converts biomass into biocrude and other chemical components with good efficiency (Elliott 2011, p.205). Process inputs are, for example, manure, algae, digested anaerobic sludge, wood residues and black liquor from pulp process (Vardon et al. 2011; Nazari et al. 2015). HTL process occurs, when water that is in sub- or supercritical condition is reacted with biomass. The critical point of water is at pressure of 22.1 MPa and temperature of 374 °C (Figure 11). Water has properties of both the gas-like and liquid-

like phase and the density of water varies between densities of these phases in the supercritical conditions. Water acts as both solvent and reactant in supercritical conditions, which allows the dissolution of organic compounds from biomass in water (Elliott 2011, p. 204; Berni et al. 2014). The chapter 3 focus on the background of HTL.

Aqueous-phase reforming

APR enables hydrogen production from oxygenated hydrocarbons dissolved in the water (Cortright et al. 2002, p. 964). APR takes place in the presence of water and catalyst material at temperatures between 215 ˚C and 265 ˚C (Davda et al. 2005, pp. 172-173; Kruse 2009, p. 391). The APR technology can also be categorized as a gasification technique, but the APR occurs at much lower temperature compared with catalyzed near-critical gasification and supercritical gasification.

Hydrothermal gasification

HTG occurs under near-critical water or supercritical water, where the condition of the system enhances gasification reactions. Catalyzed near-critical HTG takes place near critical or slightly critical water and the main product is methane (Peterson et al. 2008). The supercritical HTG occurs above the supercritical point of water producing mainly hydrogen (Elliott 2011, pp. 221-222). The both hydrogen and carbon dioxide yield rise while the methane yield decreases simultaneously when the temperature of the system increases under supercritical conditions (Lu et al. 2007, pp. 238-239). When comparing HTG with traditional gasification, the HTG is able to treat wet biomass with good efficiency (Schmieder et al. 2000, p. 146). The salt and nutrition separation is possible during the HTG enabling the recovery of expensive inorganic compounds (Schubert et al. 2010, p. 100-111; Reimer et al. 2016, pp. 114-120).

3. HYDROTHERMAL LIQUEFACTION IN SUPERCRITICAL WATER

Hydrothermal liquefaction is a thermochemical conversion technique, where the input material, such as biomass, decomposes in the liquid reaction medium at elevated pressure and temperature. The hydrothermal liquefaction reactions take place under sub- or supercritical conditions, where the properties of reaction medium is suitable to decompose the input material. The water as reaction medium is an interesting option, because it also works as reactant, catalyst and solvent at the same time in sub- and supercritical water conditions (Jindal & Jha 2015, p. 10). The reactions in water depends on the reaction temperature and the pressure, because the subcritical water enhances ionic reactions while supercritical water enhances free radical reactions (He et al. 2014, pp. 1129-1130). This is due to water properties, for example dielectric constant and ionic product, which varies a lot when reaction conditions change from subcritical conditions to supercritical conditions.

3.1 Supercritical fluids

The fluid is in supercritical state when the temperature and the pressure of fluid exceed the critical point of fluid (Brunner 2010, p. 3). In supercritical state, the fluid is neither in gaseous phase nor in liquid phase, but the properties of fluid varies between these phases. For example, the density of supercritical fluid is between the density of liquid and gaseous (Brunner 2010, p. 3). Table 3 includes supercritical properties of several chemical compounds, such as water and methane.

Table 3 Supercritical properties of some fluids

Supercritical fluid	Pc (MPa)	ρc (kg/m3)	Tc (K)	Reference
Methane	4.6	162.0	190.6	(NIST 2017b)
Ethane	4.9	193.6	305.3	(NIST 2017a)
CO_2	7.4	468.0	304.2	(Suehiro et al. 1996, p. 1157)
Ethanol	6.3	273.2	514.7	(Bazaev et al. 2007, p. 216)
H_2O	22.1	322.0	647.0	(Bermejo & Cocero 2006; Brunner 2010, p. 323; NIST 2017c)

The critical point of fluid depends on the intermolecular attractive forces (Chemistry LibreTexts). When the kinetic energy of molecules has grown so big that the intermolecular attractive forces power cannot keep it anymore together, the system is above the supercritical point. This leads to phenomena that the supercritical point of chemical compound is higher with chemical compounds having stronger intermolecular forces.

3.2 Properties of water at elevated temperature and pressure

Water is a polar chemical compound in normal pressure and temperature, which means that it works as solvent for polar compounds and different salts, but it cannot dissolve non-polar compounds (Kruse & Dahmen 2015). However, when temperature and pressure increase near to supercritical point (374 ˚C and 22.1 MPa), the polarity of water decreases drastically. This is due to the decreased density of water due to increased temperature movement as the temperature rises (Matubayasi et al. 1997). Therefore, there are fewer hydrogen bonds between water molecules and they are more unstable compared with lower temperature. Furthermore, decreasing density of water leads to lower static dielectric constant, which affect to polarity of water by decreasing it (Tsou et al. 1986, p. 3860). Dielectric constant is 80 at ambient conditions and about 12 at 250 bar and 375 ˚C (Creager 2007, p. 64). Polar solvents dissolve organic compounds, such as cellulose, when the dielectric constant is between 2 and 30 (Gallina et al. 2017, p. 130-131).

Figure 12 presents water density in the function of temperature with different pressures. Water density decreases drastically when the temperature exceeds the evaporation point of water at subcritical conditions. However, the evaporating point of water disappears when water pressure rises above the critical point (22.1 MPa). In that case, increasing temperature over the critical point does not vaporize the water, but the water phase settles between the liquid and gas phase. Because of this, the density drop is not as drastically as at subcritical conditions when temperature increases over the critical point. Increasing the pressure reduces the pressure drop under supercritical conditions when increasing the temperature.

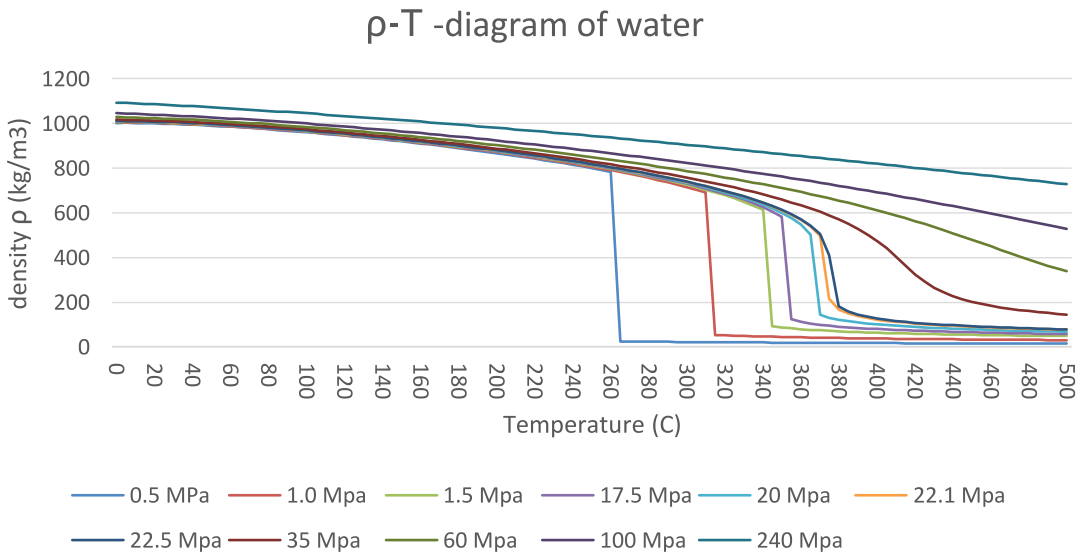

Figure 12 The variation of water density when changing the temperature. The ρ-T -functions are produced with Aspen Plus V9 software.

One of the most important feature of water is the autoionization of water, where, by simplifying, the two water molecules are divided into the hydrogen ion and the hydroxide ion (Halstead & Masters 2010, pp. 193):

$$2H_2O \leftrightarrows H_3O^+ + OH^- \quad (3.1)$$

The ion product of water is calculated by equation 3.2:

$$K_W = a_{OH^-} a_{H_3O^+}, \quad (3.2)$$

where a_{OH^-} is the activity of hydroxide ion and $a_{H_3O^+}$ is the activity of hydronium ion (Halstead & Masters 2010, p. 193). The ion product of water is 10^{-14} at ambient conditions at the temperature of 25 ˚C and the pressure of 101.3 kPa (Möller et al. 2011). The endothermic nature of the dissociation reaction drives the dissociation of water into ionic products ($[H^+]$ and $[OH^-]$ when increasing the temperature of the system. At a temperature of 300 ˚C, the ion product of water is higher than at ambient conditions (Halstead & Masters 2010, p. 193; Möller et al. 2011). Increasing temperature above 300 ˚C, the ionic product starts to decrease and the decreasing of the ionic product is significant above the supercritical point of water (Möller et al. 2011). The ion product is lower in supercritical conditions at temperatures above around 400 ˚C than in ambient circumstances, in which case conditions prefer non-ionic reactions, i.e. free radical reactions (Möller et al. 2011; Gallina et al. 2017, p. 130-131). The variations of ion product lead to situation, where subcritical hydrothermal liquefaction reactions are predominantly ionic reactions whereas near- and supercritical reactions are mainly free radical reactions. However, increasing the pressure slightly enhances ionic reactions in supercritical reactions (Möller et al. 2011). For instance, the density, the dielectric constant, and the ion product of water at the temperature of 400 ˚C and the pressure of 25 MPa are 170 kg/m^3, 2.4 and 3.6x10^{-20} mol^2/dm^2 (Sasaki et al. 2002, p. 6646). When chancing pressure to 40 MPa while keeping the temperature at the same these same properties change into are 520 kg/m^3, 2.4 and 3.6x10^{-13} mol^2/dm^2 (Sasaki et al. 2002, p. 6646).

The other properties of water change similarly when the temperature of water increases. For example, the viscosity drops drastically when increasing the temperature (Pioro & Mokry 2011, pp. 579-581). This leads to improved mass transfer properties (Möller et al. 2011). Figure 13 shows the value of enthalpy as a function of temperature. Below the critical point, the enthalpy increases significantly at the evaporating point. There is still a significant enthalpy increment above the supercritical point, but the enthalpy increment decreases as the pressure increases. The thermal conductivity of water decreases while increasing the temperature of water, but there is a local maximum at supercritical point (Cheng & Schulenberg 2001, p. 7).

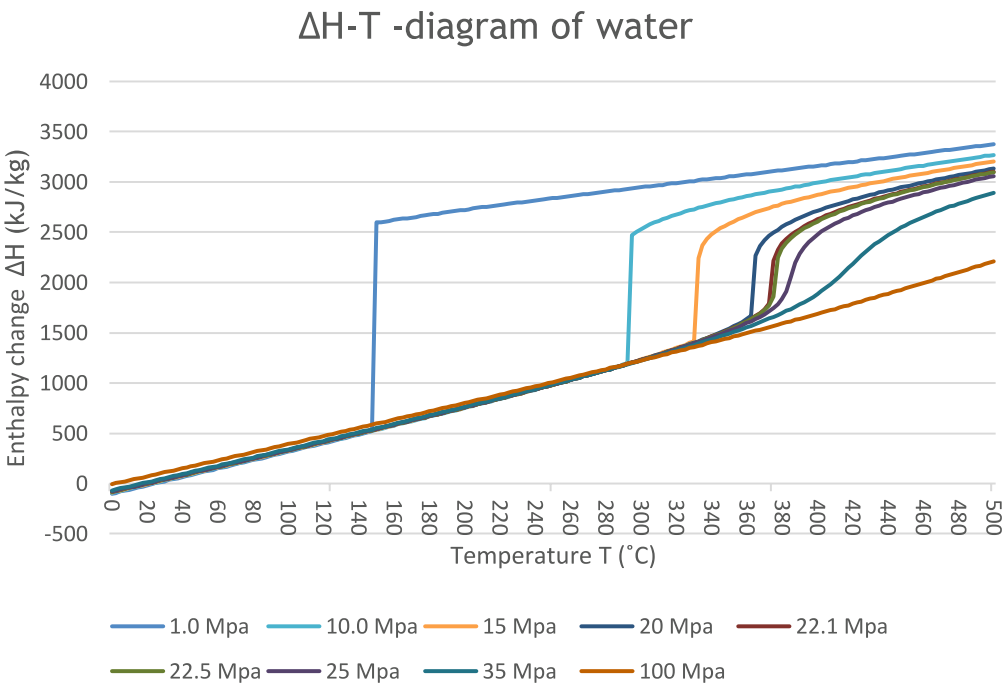

Figure 13 Enthalpy change as a function of temperature. The ΔH-T –functions are produced with Aspen Plus V9 software.

The changes in the properties of water lead to that subcritical water is capable of dissolve polar components, but in near-critical and supercritical water, it has ability to dissolve organic compounds (Elliott 2011, p. 204; Tolonen 2016, p. 13). In the subcritical water, the high ionic product enables ionic reactions, but the ionic product decreases drastically in the near-critical and supercritical favoring radical reactions (Kruse 2009, p. 417). Overall, the properties of water changes drastically when temperature and pressure of water increases near to critical point of water. Furthermore, there are significant changes with properties of the water in supercritical water when the temperature stays constant and pressure changes.

3.3 Effects of process variables

Changing the process conditions has a significant effect on hydrothermal liquefaction process. This chapter focus on studying experimental results related to the hydrothermal liquefaction, such as the type of the feedstock, the process conditions and using catalyst materials and solvents to enhance the process.

3.3.1 Effects of biomass and its properties

The biomass has a significant effect on the product achieved from the process, because the contents of different compounds changes between different biomasses. The particle size of biomass has a slight effect on the liquefaction, mainly to the pumpability of the

biomass slurry. The ratio of biomass to water influences on the yield of the process by decreasing the biocrude yield when the ratio of biomass to water increases. It has an effect on the pumpability of the slurry.

Biomass type

Biomass feedstock type affects on the hydrothermal liquefaction process, because the biomass source influences on the biocrude properties. Especially, contents of lignin, cellulose and hemicellulose vary between different kinds of biomasses. Zhong and Wei (2004, pp. 1733-1737) noticed that increasing lignin content decreases heavy biocrude yield. Furthermore, increasing the lignin content increased the solid residue yield at the same time. They assumed that lignin decomposes and forms free phenoxyl radicals that condensate or repolymerize to the solid residue in subcritical water. Bhaskar et al. (2008, p. 2238-2242) observed the same thing that the higher lignin content the lower biocrude yield in subcritical zone without catalyst. They noticed that higher contents of hemicellulose and cellulose enhanced the acetic acid yield and higher content of lignin increased the content of phenolic derivatives in biocrude. However, de Caprariis et al. (2017, pp. 620-624) come to as an opposite result that increasing lignin content increased the biocrude yield. They made the experiments with three different biomasses, where the lignin content varied from 12.0 wt-% to 53.5 wt-% at the temperatures between 240 ˚C and 320 ˚C. The biocrude yield was over 25 wt-% with biomass including 53.5 wt-% at the temperature of 320 ˚C.

Biomass particle size

The biomass particle size in the slurry can have effect on the pumpability of the slurry and the dissolution of the particles. Moreover, the grinding of biomass into small particles is an energy intensive process (Nunes et al. 2017, p. 136). For this reason, unnecessary grinding decreases the profitability of the hydrothermal process. Elliot et al. (1989, pp. 23-24) noticed that when increasing the particle size above 0.125 inches (around 0.32 cm), the slurry transformed unpumpable. Zhang et al. (2009, p. 21) tested hydrothermal liquefaction of grassland perennials, which contained a mixture of 18 perennial herbaceous grassland species. They made experimental tests with three different particle size that were 1 inch long particles or spherical with the radius of 0.5 mm and 2 mm. The batch tests were carried out with 10 minutes residence time and at the temperatures of 350 ˚C and 374 ˚C. The results showed that grinding the particles to smaller did not significantly affect the yield of biocrude. However, the test with the smallest particle size let the highest yield of solid residue.

The ratio of biomass to water

Qu et al. (2003, pp. 601-603) made an experimental test with Cunninghamia lanceolate in subcritical conditions (280 ˚C -360 ˚C), where they changed the ratio of biomass to water. They discovered that increasing the ratio of biomass/water decreases the heavy

biocrude yield when using 10 minutes residence time. Zhu et al. (2018, pp. 1-15) conducted experimental tests with barley straw in a hydrothermal liquefaction reactor. They experimented with how different process variables, such as the biomass/water ratio, catalysts, affect biocrude yield. The highest biocrude yield was achieved with the biomass/ratio of 14.5 wt-% - 17 wt-%. However, increasing the biomass/water ratio above 17 wt-% decreased the biocrude yield.

3.3.2 Effects of process conditions

The process conditions affect the hydrothermal liquefaction, because the properties of water change considerably when changing the pressure and the temperature of the system from subcritical conditions to supercritical conditions. This chapter focuses on studying experimental results related to the effects of temperature, the density of the water, residence time and both heating and cooling rate to the hydrothermal liquefaction reactions.

Temperature

The temperature of a process has a significant effect on the reactions, which occurs in the hydrothermal liquefaction reactor. Qu et al. (2003, pp. 600-605) made experimental tests with Cunninghamia lanceolate in a non-catalytic hydrothermal liquefaction reactor at temperatures of 280 ˚C to 360 ˚C and a reaction times of 10, 20 and 30 minutes. Zhong and Wei (2004, pp. 1735-1736) continued these tests and tested four different woody biomasses in hydrothermal liquefaction reactor with and without catalyst and the reaction time of 10 minutes. On the grounds of these tests (Qu et al. 2003, pp. 600-605; Zhong & Wei 2004, pp. 1735-1736), the hydrothermal liquefaction process achieved the highest heavy biocrude yield in the temperature range of 300 ˚C – 340 ˚C. At the same time, yields of solid residue and dissolved hydrocarbons in the water decreased when the heavy biocrude yield increased. They noticed a connection between lignin content of biomass and the optimal temperature for heavy biocrude yield; the higher lignin content increased the required temperature to achieve the optimal biocrude yield.

Zhang et al. (2009, p. 20) carried out experiments with grassland perennials. The condition of experiment varied from 300 ˚C to 450 ˚C and the pressure varied depending on the temperature from 10 to 35 MPa. They discovered that increasing the temperature above the critical point of water decreased the liquid product yield while gaseous product yield increased. The solid residue yield decreased when increasing the temperature above the critical point. The gaseous phase contained hydrogen, carbon monoxide, methane and carbon dioxide. The composition of gaseous phase changed while increasing the temperature; yields of hydrogen, carbon monoxide and methane increased meanwhile the yield if methane decreased.

Qian et al. (2007, pp. 197-201) performed experiments with silver birch in sub- and supercritical water using potassium carbonate (K_2CO_3) as a catalyst material. They changed

temperature of the reactor from 280 ˚C to 420 ˚C and achieved the maximum biocrude yield (53.3 %) at the temperature of 380 ˚C.

Water density

The water density varies depending on the temperature and the pressure of the system, which has a significant effect on the reactions in the water, especially near the critical point of water. Sasaki et al. (2008, pp. 1614-1619) studied the effect of water density on the hydrothermal liquefaction of lignin derivatives at temperatures of 350 ˚C and 400 ˚C and pressures of 25 to 40 MPa. They concluded that increasing water density increases the hydrolysis reactions of ethers and C-C bonds between alkylphenols. Sato et al. (2002, pp. 3126-3130) tested dealkylation and rearrangement reactions of 2-isopropylphenol in sub- and supercritical water. They discovered that increasing the density of water under supercritical conditions enhanced dealkylation reaction, but it did not have significant effect on rearrangement reaction.

Residence time

Residence time means the time, which a single molecule spends in the hydrothermal liquefaction reactor. It has a significant effect on the yields of biocrude, gas, solids and water-soluble hydrocarbons and the composition of these streams. Zhang et al. (2009, p. 20) tested hydrothermal liquefaction of biomass with different residence times and at two different temperature (300 ˚C and 374 ˚C). They achieved the highest the biocrude yield after 6 minutes at the temperature of 300 ˚C and after 1 minute at the temperature of 374 ˚C. The maximum yield of biocrude at the temperatures of 300 ˚C and 374 ˚C were 76.8 % and 82.1 %. The increase in residence time resulted in the growth of gaseous and solid products.

Heating rate and cooling rate

Both heating rate and cooling rate means change in temperature per time unit, typically the unit is $^{\circ}Cs^{-1}$ or $^{\circ}Cmin^{-1}$, but the heating rate relates to increase in temperature and the cooling rate relates to decrease of temperature. Zhang et al. (2009, pp. 20-21) completed hydrothermal liquefaction experiments with grassland perennials in sub- and supercritical water. They discovered that rapid heating rate increases the biocrude yield, but does not have an effect on the composition of biocrude. The cooling rate did not have significant effect on the biocrude yield. Tran et al. (2017, p. 219-223) tested different heating rates with raw and torrefied spruce in subcritical water. They achieved the same results as Zhang et al. (2009, pp. 20-21); using the higher heating rate which resulted in the better biocrude yields. The biocrude yield increased from 18.9 wt-% to 35.8 wt-% with heating rates 66 $^{\circ}Cmin^{-1}$ and 376 ˚C min^{-1}. Faeth et al. (2013, pp. 1392 & 1398) tested hydrothermal liquefaction of Nannochloropsis with different heating rates. The results supported observations that the higher heating rate would result in the higher biocrude yield.

3.3.3 Effects of catalyst materials, solvents and reducing gases

The problems with hydrothermal liquefaction, especially in supercritical water, are the high residual content of oxygen in the biocrude and high char formation while using the lignocellulosic biomasses. There are large amount of studies related to the effects of catalyst materials, solvents, and reducing gases on the hydrothermal liquefaction of biomass. This chapter presents a part of those studies.

Catalyst

Catalyst materials used in hydrothermal liquefaction are either homogenous catalysts or heterogeneous catalysts. The difference between homogenous and heterogeneous catalysts is that homogenous catalysts reactions occur in a single phase whereas heterogeneous reactions take place in two or three phases, e.g. the reaction medium is in liquid form and the catalyst is in solid form (Baiker 1999, p. 454). The aim of using catalysts is that they improve the biocrude yield while minimizing the yield of unwanted products, such as solids and water-soluble hydrocarbons.

Qu et al. (2003) tested non-catalytic liquefaction of Cunninghamia lanceolate at temperatures of 280 ˚C – 360 ˚C and the reaction time of 10 minutes. Zhong and Wei (2004, pp. 1735-1736) tested the same biomass with catalyst under the same conditions, but they also tested four different biomasses with and without catalyst. Zhong and Wei used potassium carbonate as a catalyst. They observed that catalyst improved the heavy biocrude yield and decreased the amount of residues in most cases. The improvement of the heavy biocrude yield was over 10 % at its best when using Cunninghamia lanceolate (Chinese spruce) at the temperature of 340 ˚C. However, using the catalyst decreased the heavy biocrude yield in some cases. The catalyst has a significant effect on the residue yield; the residue yield fell by more than half nearly in almost all cases. Hwang et al. (2018, pp. 4-10) studied the effect of a different mass fraction of potassium carbonate (0.0, 0.1, 0.5 and 1.0 wt-%) on hydrothermal liquefaction of woody biomasses (Mongolian oak and larch) in subcritical water at the temperature of 300 ˚C. They reached the highest biofuel yield with both biomasses when the catalyst mass fraction was 0.5 wt-%. The improvement of the biofuel yield compared with non-catalytic hydrothermal liquefaction was from 13.9 wt-% to 25.7 wt-% for the larch and from 18.1 wt-% to 27.7 wt-% for the Mongolian oak. However, increasing the mass fraction 1.0 wt-%, the biocrude yield decreased. The catalyst also improved the higher heating value of biocrude and lowered the amount of oxygen in biocrude.

Zhang et al. (2009, p. 21) made hydrothermal liquefaction experiments with four different catalyst materials and without catalyst material. They used sulfuric acid (H_2SO_4), solid superacid (SO_4^{2-}/ZrO_2-Al_2O_3), sodium hydroxide (NaOH), and solid alkali (CaO-ZrO_2). Batch tests were completed at the temperature of 300 ˚C and the pressure of 10 MPa with the residence time of 10 minutes. They noticed that these catalyst materials did not have

remarkable influence on the biocrude yield. However, the amount of solid residue decreased when using the solid superacid, solid alkali and sodium hydroxide. They concluded that the use of the catalyst was not economical as it had a small impact on the biocrude yield and the high costs of using and recovering the catalyst.

Christensen et al. (2014, p. 159-165) studied ZrO_2 as a catalyst material in the hydrothermal liquefaction reactor operating under subcritical water conditions. They made experiments with ZrO_2 and K_2CO_3, where the half of tests were conducted with both catalyst materials and the rest of with K_2CO_3. The biocrude yield was better in experiments without ZrO_2, but in these cases, the solid residue yield was also higher. However, it is impossible to estimate the effect of ZrO2 on hydrothermal liquefaction in supercritical water without experimental data.

Reactor wall as catalyst

The walls of the reactor can affect hydrothermal liquefaction, as it may act as a catalyst for various reactions. This effect has more influence on hydrothermal liquefaction reactions in a small reactor, since the area of the reactor wall relative to the reactor volume is greater compared with the larger reactors. Christensen et al. (2014, p. 159-165) studied the effect of reactor wall using a gold liner to prevent the effects of reactor wall and compared these results to experiments without the gold liner in subcritical water. The results showed that reactor wall has a small effect on the biocrude yield. The biocrude yield increased from 21.2 wt-% (with the cold liner) to 23.3 wt-% (without the cold liner) when ZrO_2 and K_2CO_3 were used as catalyst materials. Using only the K_2CO_3 as catalyst increased the yield of biocrude from 22.2 wt-% (with cold liner) to 23.8 wt-% without cold liner.

Co-solvent

Using a co-feed in the hydrothermal liquefaction process may have a great effect on reaction. This causes changes in yields of different products and composition of products. The co-solvents are mainly used because of to prevent char formation stabilizing the decomposition reactions of biomass.

Pedersen (2016, p. 116) came in conclusion that adding glycerol as co-feed in the hydrothermal liquefaction of biomass decreases the amount of forming char of reactions under alkaline supercritical water (400 ˚C). Pedersen assumed this was because Glycerol stabilizes lignin degradation as a donor of hydrogen in radical reactions. The yield of forming char was 18.3 % when using pure water as the reaction medium (Pedersen et al. 2015, p. 889). When adding 25 wt-% of glycerol and rest of it water as input, the char formation decreased to 7.41 wt-% (Pedersen et al. 2015, p. 889).

Chumpoo and Prasassarakich (2010, pp. 2075-2077) tested hydrothermal liquefaction of bagasse in ethanol-water solution with three different ethanol concentrations of 50 V-%,

70 V-%, 95 V-% and 100 V-%. They noticed that the biocrude yield increased when increasing the ethanol concentration from 50 V-% to 95 V-%. However, the yield decreased at the ethanol concentration of 100 V-%. They concluded that water works as hydrogen donor helping the decomposition of the bagasse, which causes the decrease of the biocrude yield at the ethanol concentration of 100 V-%. Murti (2017, pp. 26-29) also made experiments with alcohol-water solution, where the water concentration of alcohol to water changed from 0 wt-% to 100 wt-%. The results showed that the biocrude yield increased while increasing the ethanol concentration until the concentration of 60.7 wt-%, where the biocrude yield was 60 wt-%. After this point, the biocrude yield started to decrease and simultaneously the yield of solid residue increased. Cheng et al. (2010, pp. 4662-4667) achieved similar results compared with results from Murti (2017, pp. 26-29); the biocrude yield was at its maximum using 50 wt-% ethanol and the solid residue yield was its minimum. The ethanol yield collapsed while the solid residue yield increased when the solvent was 100 wt-% ethanol. They also tested methanol as the co-solvent resulting in similar results compared with using ethanol as the co-solvent. They concluded that water enhances the hydrolysis reactions in the hydrothermal liquefaction process, and ethanol works as a hydrogen donor in reactions. The solvent type has an effect with the biocrude composition achieved in the liquefaction of biomass. When comparing ethanol with methanol as solvent in the hydrothermal liquefaction, the lignin degrades better when using the ethanol as solvent.

Kim et al. (2014, p. 6430-6437) made experiments with solvents working as a hydrogen donor in the hydrothermal liquefaction of lignin. They made experiments with tetralin, isopropanol and naphthalene. The tetralin and isopropanol work as the hydrogen donor, but the naphthalene does not act as the hydrogen donor. They concluded that the use of the hydrogen donor solvents stabilizes the degradation reactions, preventing char formation in the hydrothermal liquefaction of biomass. It also prevented the decomposition of oxygenated aromatics to smaller components.

Reducing gases

The reducing gas works as electron donor, whereby it has ability to receive an oxygen molecule from oxidizing agent, i.e. oxygenated hydrocarbon in this case (Valle et al. 2017, pp. 4-5). For example, hydrogen and CO gases act as hydrogen donor (Appell et al. 1971, p. 10; Yin et al. 2010, pp. 3659-3660). The reducing gas or hydrogen donor prevents free radicals, especially lignin derivatives, to repolymerize into char (Xu & Etcheverry 2008, p. 340). The reducing gas is assumed to remove oxygen from oxygenated hydrocarbons stabilizing the structure (Yin et al. 2010, p. 3660). The aromatic free radical (Ar^*) stabilizes by hydrogen gas or hydrogen free radical (H^*) shown in equations 3.3 and 3.4. (Xu & Etcheverry 2008, p. 340).

$$Ar^* + H_2 \rightarrow Ar + H^* \quad (3.3)$$

$$Ar^* + H^* \rightarrow Ar \quad (3.4)$$

Appell et al. (1971, p. 10) studied the effect of carbon monoxide gas as reducing gas on the hydrothermal liquefaction. They noticed that increasing the initial pressure of carbon monoxide increased the biocrude yield. Yin et al. (2010, pp. 3659-3660) tested the effects of different reducing and inert gases when treating cattle manure in the subcritical water. The tested gases were CO, H_2, N_2, and air, and temperatures of reaction varied between 290 ˚C and 330 ˚C. CO and H_2 improved the biocrude yield, while air and N_2 did not have significant effect on the biocrude yield. They achieved the best yield of biocrude with CO gas. They assumed that the improved yield was due to Fischer-Tropsch synthesis, which occurs between CO and H_2. The improvement in biocrude yield in the presence of H_2 was due to a hydrogenolysis reaction, where hydrogen gas removes oxygen from oxygenated hydrocarbon.

3.4 Reaction pathways of the hydrothermal liquefaction

The structure of lignocellulosic biomass is very complex making it difficult to decompose into smaller monomers. For this reason, the degradation of biomass takes place via numerous chemical reactions in supercritical water. The main reactions of converting biomass into biofuel in supercritical water are hydrolysis, dehydration, isomerization, tautomerization, retro-aldol condensation and free radical reactions.

Hydrolysis reaction takes place when water reacts with carbohydrates and carbohydrates degrade into smaller carbohydrates (Hart et al. 2002, p. 449). For example, hydrolysis reactions happen when polysaccharide reacts with water. The polysaccharide breaks into oligosaccharides, and oligosaccharides and water reacts further into monosaccharides. Isomerization refers to a reaction where the isomeric form of the chemical compound is changed to another while the chemical composition remains unchanged (Britannica Academic). In this case, the structure changes influence into the properties of chemical compounds (Britannica Academic). In tautomerization reaction, one or more atomic nucleus changes the place in the structure and these two different structures are in equilibrium, such as keto-enol tautomerism (Bell). In dehydration reaction, two chemical compounds react and forms both a new chemical compound and water, such as ethanol reacts with sulfuric acid at 180 ˚C forming ethylene and water (Hart et al. 2002, p. 213; Helmenstine). Aldol condensation reaction takes place when two chemical compounds react both forming a larger chemical compound and eliminating a small compound, such as water (Loudon 2009, pp. 1065-1066). The formed chemical compound is an aldol, because it contains both alcohol and aldehyde functional groups (Hart et al. 2002, p. 274). Retro-aldol condensation is a reverse reaction of the aldol condensation, where C-C bonds are broken forming two smaller substances (Soderber).

The free radical reactions under supercritical water conditions are quite complex and the exact reaction mechanism is unknown. For example, Pedersen (2016, p. 82) proposed that the hydrolysis reaction and radical reactions occur simultaneous as in the reactions below

$$R - R' + H_2O \rightarrow 2\,R - OH \quad (3.5)$$

$$R - O - R' + Heat \rightarrow R = O + R' \bullet \quad (3.6)$$

$$R - R' + Heat \rightarrow R \bullet + R' \bullet \quad (3.7)$$

The cleavage of the hydrocarbon may base on double bond rule, which means that the double bond between carbon atoms strengthens the next single bond, but the next single bond of that weakens. This makes the weakened bond reactive for external effects.

The proposed reactions to cellulose, hemicellulose and lignin are overall reactions in chapters 3.4.1, 3.4.2, 3.4.3 and 3.4.4. In reality, the reactions are significantly more complicated.

3.4.1 Cellulose

The decomposition of cellulose occurs through several stages. The first cellulose decomposes into oligomers, which continue to hydrolyze to glucose and fructose. Reactions of glucose and fructose to products occur via multiple simultaneous reactions. Because of these several different reaction pathways, the final product includes a wide spectrum of various chemical compounds, such as organic acids, aldehydes and ketones.

The first stage of the decomposition of crystallized cellulose takes place when the hydrogen bonds between glucoses break resulting in microcrystalline cellulose (Sasaki et al. 2000, p. 2889). In the near- and supercritical microcrystalline cellulose dissolves into cello-oligosaccharides, which includes cellobiose, cellotriose, cellotetraose and cellopentaose. Cellobiose occurs most abundantly in the product of hydrolysis of crystallized cellulose (Figure 14).

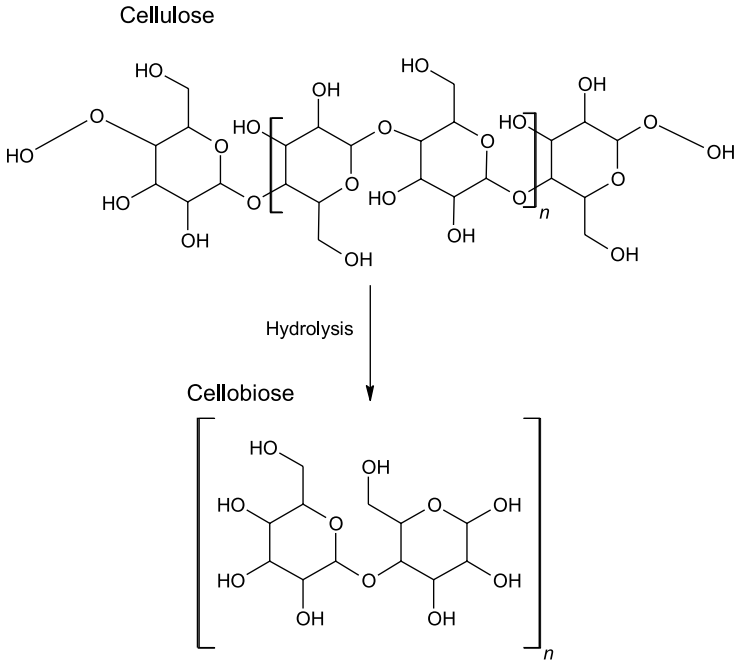

Figure 14 Cellulose hydrolysis to Cellobiose

Sasaki et al. (2000, p. 2886) tested the conversion of cellulose at the pressure of 25 MPa and in different temperatures. At the temperature of 320 ˚C, the conversion of cellulose was 46.8 % with residence time of 1.6 s and 100 % with residence time of 9.9 s at the temperature of 400 ˚C. At the temperature of 350 ˚C, the conversion of lignin achieved 62.2 % with residence time of 0.9 s and the conversion degree of 100 % was reached with residence time of 9.9 s. When the temperature was increased to 400 ˚C, the conversion of cellulose reached 100 % with the time of only 0.05 seconds. Sasaki et al. (2004) explained the difference between the conversion rates of cellulose in the sub- and the supercritical water. In the subcritical water at temperatures below 350 ˚C, the hydrolysis reaction occurs only in the surface region of microcrystalline causing long dissolving time for cellulose. Above the temperature of 350 ˚C, the surface of crystallized cellulose dissolves and recrystallizes back to cellulose II region. The crystallized cellulose II region hydrolyzes easily increasing the conversion rate of cellulose.

Oligosaccharides, in this case cellobiose, decompose into glucose by hydrolysis and into glucosyl-erythrose, glucosyl-glucoaldehyde, glucoaldehyde and erythrose by retro-aldol condensation (Figure 15) (Kabyemela et al. 1999, p. 359; Sasaki et al. 2002, p. 6644). Glucosyl-erythrose and glucosyl-glycoaldehyde hydrolyze further to glucose and other intermediate products (Figure 15).

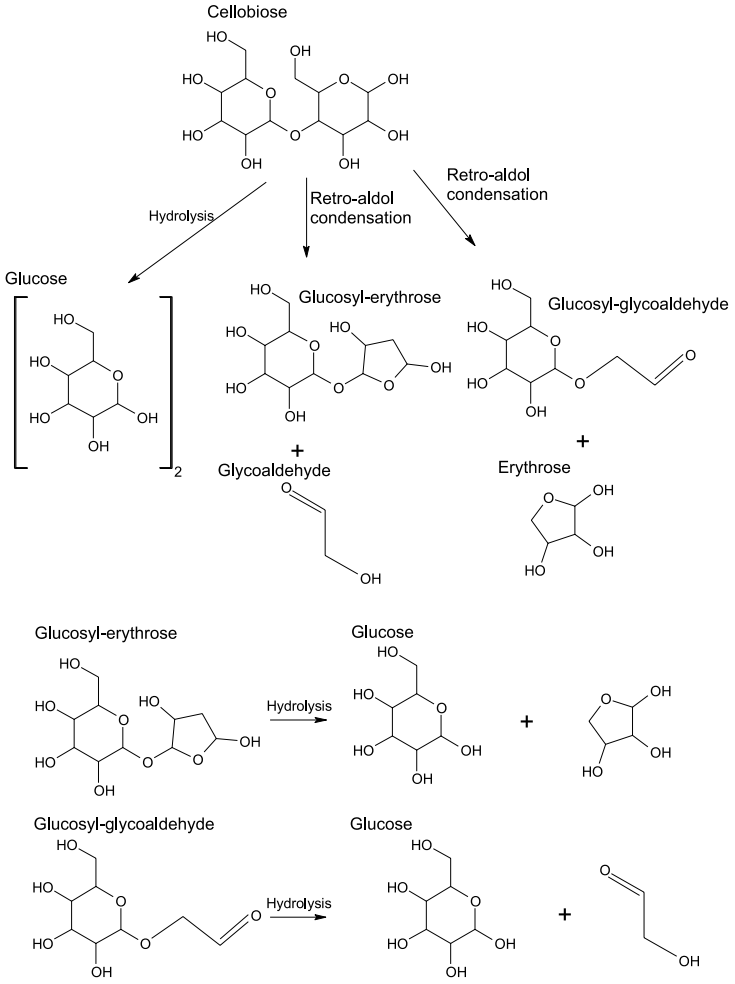

Figure 15 Decomposition of cellulose into glucose in supercritical water (Adapted from Kabyemela et al. 1998, p. 359; Kabyemela et al. 1999, p. 359; Sasaki et al. 2002, p. 6644).

Glucose reacts into products through several simultaneously occurring reactions (Figure 16) (Kabyemela et al. 1999, p. 2891). D-Fructose, both pyranose and furanose, are formed from glucose by tautomerization reactions. The dehydration reaction of glucose produces 1,6-anhydroglucose. Two different reaction pathways form erythrose and glucoaldehyde. On the first pathway glucose tautomerises into an intermediate product, 2,3,4,5,6-pentahydrohexanel, and then erythrose and glucoaldehyde are formed by retro-aldol condensation reaction. In the second pathway glucose tautomerises into (2E)-hex-ene-1,2,3,4,5,6-hexol and then intermediate product breaks to glucoaldehyde and erythrose. The cleavage of intermediate products is based on double bond rule. Glyceraldehyde is also produced in two different reaction pathways. In the first one, glucose tautomerises into (1E)-hex-1-ene-1,2,3,4,5,6-hexol and then breaks into two glyceraldehyde. In the second case, glucose tautomerises into 1,3,4,5,6-pentahydroxyhexan-2-one, which reacts into two glyceraldehyde basing on retro-aldol condensation. Glyceraldehyde tautomerises into dihydroxyacetone or reacts into pyruvaldehyde basing on dehydration.

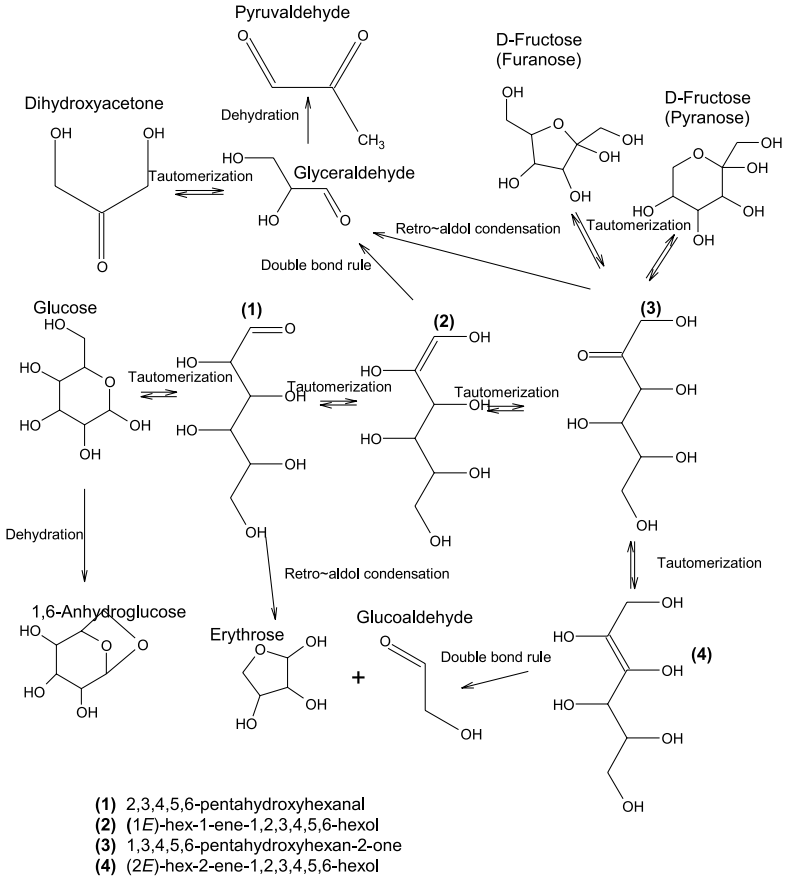

Figure 16 Decomposition of glucose (Adapted from Kabyemela et al. 1999, p. 2891).

D-fructose, i.e. furanose, decomposes into 5-hydroxymethylfurfural (5-HMF) by dehydration (Figure 17) (Danilo Alberto Cantero Sposetti 2014, p. 104-106; Gomes, F N D C et al. 2015). 5-HMF can react into acetic acid and lactic acid by rehydration. However, the yield of 5-HMF depends on the ambient conditions (Aida et al. 2007). Under subcritical conditions, the 5-HMF yield is high, but when increasing the pressure and temperature above the critical point of water, the 5-HMF yield decreases drastically. However, increasing the pressure in the supercritical conditions grows the 5-HMF yield.

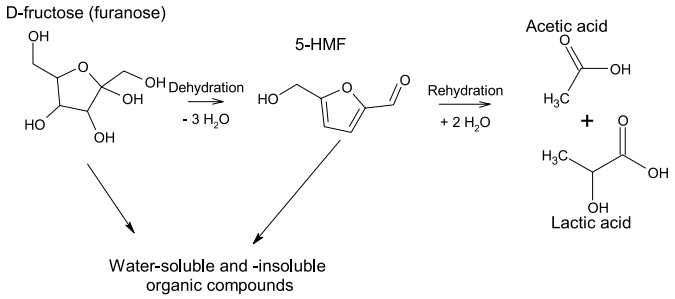

Figure 17 Dehydration of fructose to 5-HMF (Adapted from Gomes, F N D C et al. 2015).

Glyceraldehyde reacts into products by dehydration and retro-aldol reactions (Honma & Inomata 2014). The dehydration reaction of glyceraldehyde produces 2-hydroxyprop-2-

enal, which tautomerises into pyruvaldehyde. Retro-aldol reaction of glyceraldehyde produces formaldehyde and (E)-ethene-1,2-diol. (E)-ethene-1,2-diol further reacts to glycoaldehyde by tautomerization. Honma and Inomata (2014) concluded that hydro-thermal liquefaction conditions favors retro-aldol reactions, where reaction is catalyzed by water.

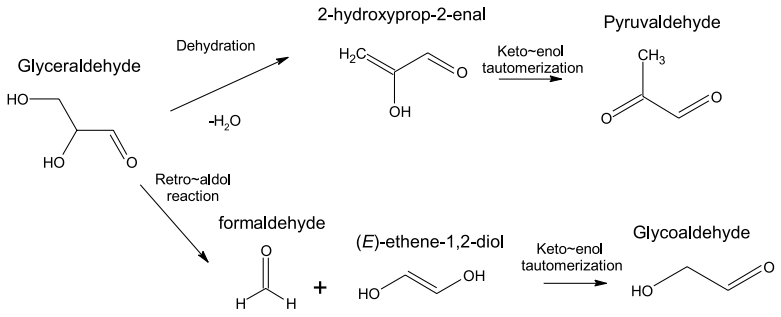

Figure 18 Degradation of glyceraldehyde (Adapted from Honma & Inomata 2014)

Figure 13 represents the supposed reaction from 1,6-anhydroglucose to acetic acid (Yakaboylu, Yapar et al. 2015, p. 8102).

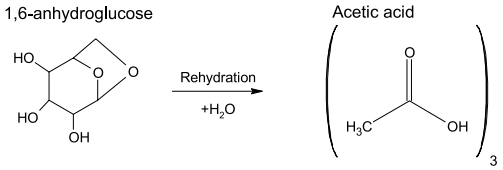

Figure 19 Rehydration of 1,6-anhydroglucose (Adapted from Yakaboylu et al. 2015, p. 8102).

Yakaboylu et al. (2015, p. 8102) supposed that glycoaldehyde decomposes into acetic acid, which is shown in figure 14.

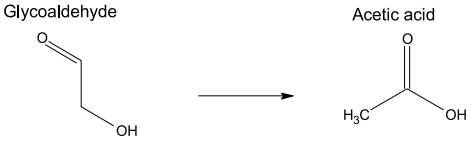

Figure 20 Decomposition of glycoaldehyde (Adapted from Goodwin & Rorrer 2010, p. 12; Yakaboylu et al. 2015, p. 8102).

Erythrose is supposed to decompose into acetic acid (Yakaboylu et al. 2015, p. 8102).

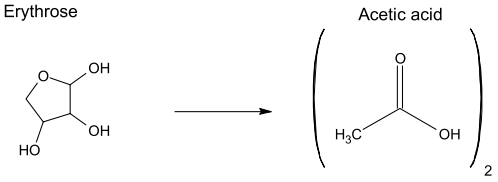

Figure 21 Decomposition of erythrose (Adapted from Yakaboylu et al. 2015, p. 8102).

Figure 16 shows rehydration of pyruvaldehyde to lactic acid (Aida et al. 2007).

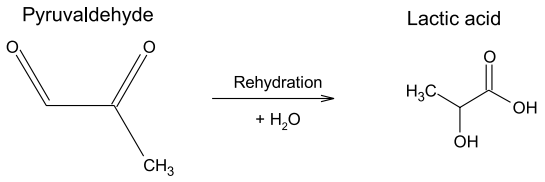

Figure 22 Decomposition of pyruvaldehyde (Adapted from Aida et al. 2007).

3.4.2 Hemicellulose

The decomposition of hemicellulose is more complicated in comparison with the decomposition of cellulose, because of hemicellulose consists of several different chemical compounds. In this case, xylan is used to indicate hemicellulose in supercritical water. Figure 23 presents the supposed decomposition way of xylan into products. The reaction pathway is a combination of several reaction ways which have been obtained from sources Goodwin & Rorrer (2010, p. 8102), Paksung & Matsumura (2015, p. 7606-7609), Yakaboylu et al. (2015a, p. 877) and Yakaboylu et al. (2015b, p. 8102-8103).

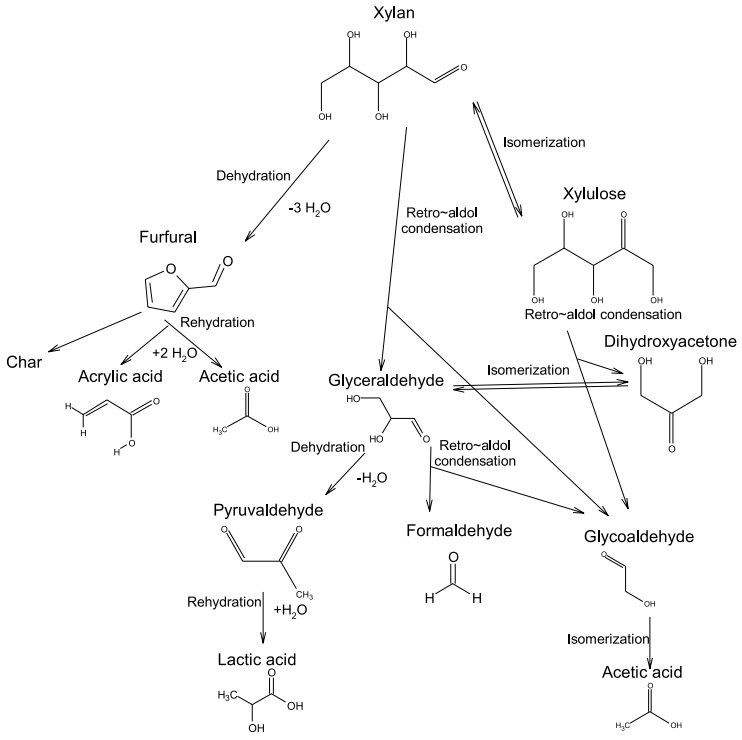

Figure 23 Decomposition of xylan (Adapted from Goodwin & Rorrer 2010, p. 8102; Paksung & Matsumura 2015, p. 7606-7609; Yakaboylu et al. 2015, p. 8102-8103; Yakaboylu, Harinck et al. 2015, p. 877).

3.4.3 Lignin

The structure of lignin (see appendix B) is more complicated compared with the other components in biomass, which is why the decomposition of lignin is more complicated. The degradation of lignin occurs both by hydrolysis reactions and by cleavage of C –C and C – O bonds between aromatic rings (Pedersen & Rosendahl 2015, p. 214). There are couple of proposed reaction pathways, how lignin degrades in supercritical water.

Yong and Matsumura (2012) proposed that the degradation of lignin occurs as shown in Figure 24 below. They tested alkali lignin produced from the Norway spruce. The alkali lignin was treated in a commercial pulp mill. After the commercial pulp mill, the alkali lignin was extracted. Due to processing, the lignin was completely soluble in water at normal ambient conditions. The lignin decomposes into oxygenated aromatic compounds, such as guaiacol, catechol and phenol. Lignin and its derivate decompose into TOC (Total Organic Carbon), which contains hydrocarbons dissolved in water, such as oxygenated aromatic compounds. Oxygenated aromatic compounds can react into aromatic compounds, such as benzene, toluene and naphthalene. The decomposition of lignin produces gaseous products and char. Yong and Matsumara noticed that the char formation is enhanced in supercritical water. Due this, a major part of lignin forms char and only a small amount of desired compounds, such as aromatic compounds, is achieved. The gaseous products mainly consisted of hydrogen and carbon dioxide, but formation of methane increases under supercritical conditions.

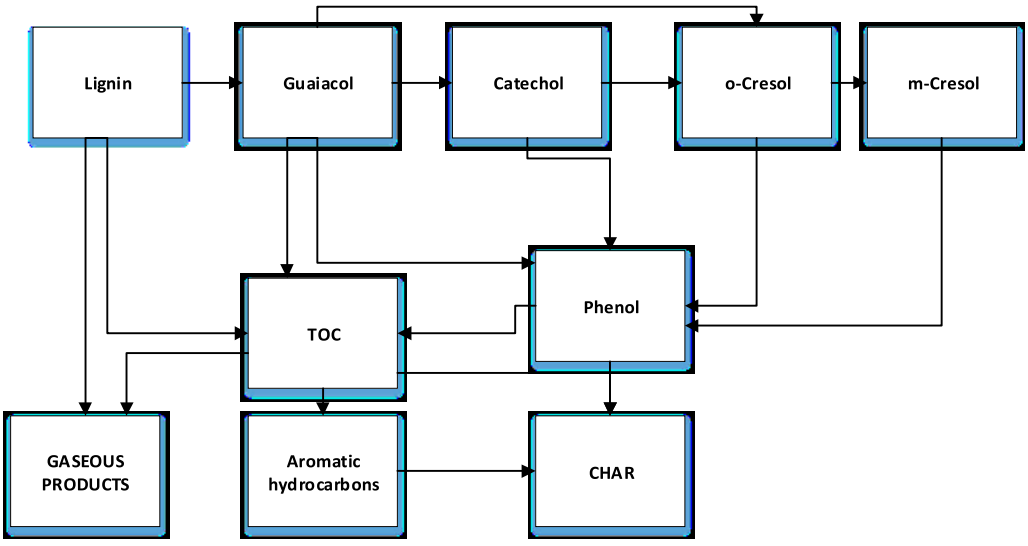

Figure 24 Decomposition of lignin (Adapted from Yong & Matsumura 2012, p. 11984)

Forchheim et al. (2014) carried out hydrothermal liquefaction tests with a lignin rich-residue obtained from ethanol production. They suggested a reaction pathway to degradation of lignin in supercritical water found in Figure 25. The lignin degrades into guaia-

col, phenol, catechol, different intermediate products, char and gaseous products. Intermediates divide into reactive intermediates and partially water-soluble stabile intermediates, but they were not able to define the chemical compounds of these fractions. The char forms from catechol and reactive intermediate fractions. The gaseous products mainly contain carbon dioxide (CO_2), but also a small amount of both methane (CH_4), and carbon monoxide (CO). The carbon monoxide disappears when the residence time increases. At the same time, the methane yield increases. Forchheim et al.(2014) suggested that this is caused by water-gas-shift reaction (Figure 28) and methanation reaction (Figure 29). The composition of gaseous products differs compared with experimental results from Yong and Matsumura (2012), because Forchheim et al.(2014) did not observe hydrogen in gaseous products.

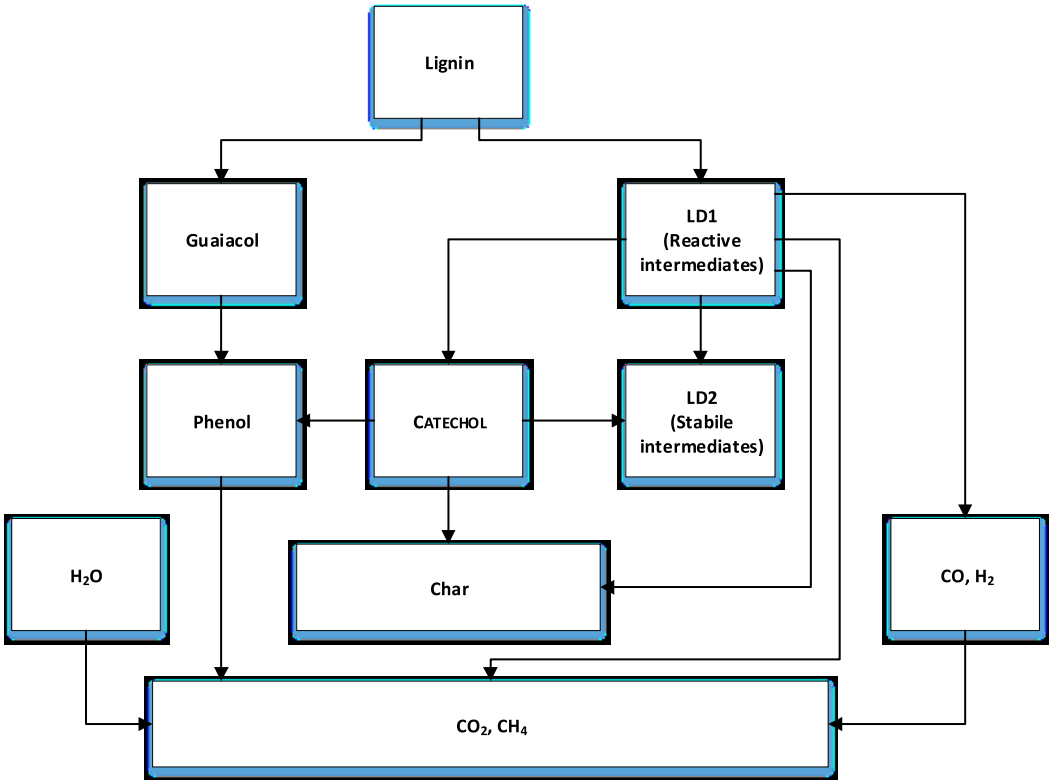

Figure 25 Degradation of lignin (Adapted from Forchheim et al. 2014, p. 988)

Forchheim et al.(2014, pp. 988 & 992) proposed decomposition pathways to guaiacol, catechol and phenol shown in Figure 26. The decomposition of guaiacol occurs via cleavage of the C-O bond and it produces either phenol or catechol. Catechol reacts with carbon monoxide and form phenol further. Phenol reacts into carbon dioxide and methane.

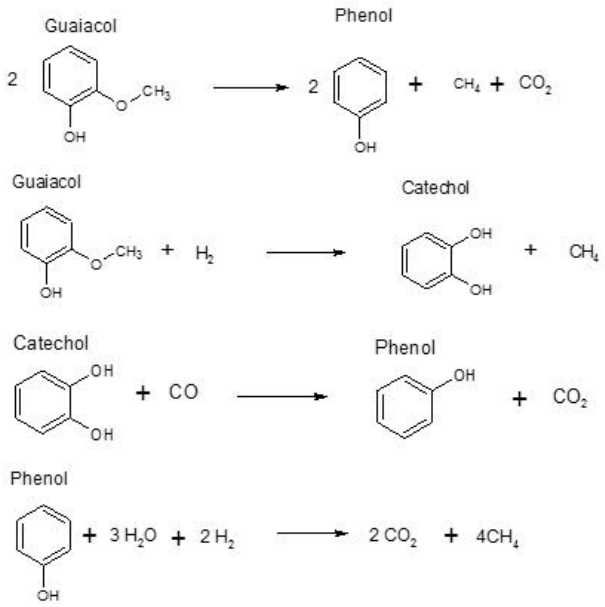

Figure 26 Decomposition of guaiacol, catechol and phenol (Adapted from Forchheim et al. 2014, pp. 988 & 992)

3.4.4 Other reactions in supercritical water

Pedersen et al.(2015) proposed that acetic acid reacts into acetone by decarboxylation and dehydration reactions. Produced acetone reacts into 2-methylcyclopentan-1-one by dehydration reaction. Figure 27 shows the reaction pathways of producing acetone and 2-methylcyclopentaone. This could explain the high concentrations of group of cyclopentaone derivatives in the biocrude.

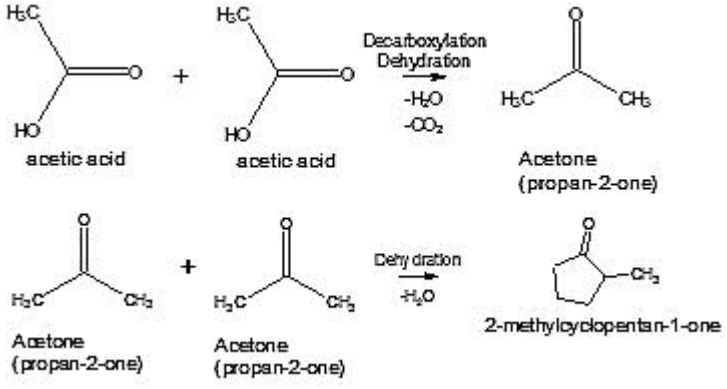

Figure 27 Formation of 2-methylcyclopentan-1-one (Adapted from Pedersen et al. 2015, p. 214)

The lack of carbon monoxide in gaseous product is explained by water-gas-shift reaction (Figure 28) and methanation reactions (Figure 29), in which carbon monoxide reacts with either water or hydrogen (Goodwin & Rorrer 2010, p. 12-13; Pedersen et al. 2015).

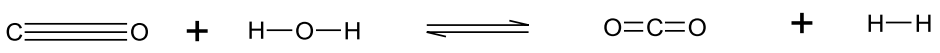

Figure 28 Water-Gas-Shift reaction

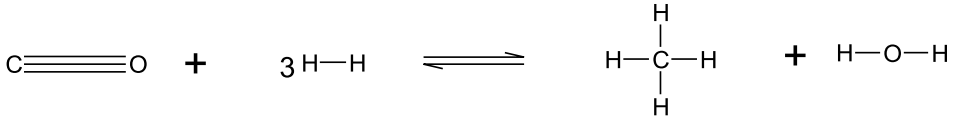

Figure 29 Methanation reaction

The water-gas-shift reaction occurs when carbon monoxide reacts with water to produce hydrogen and carbon dioxide while in the methanation reaction carbon monoxide reacts with hydrogen to produce methane and water.

3.4.5 Reaction kinetic parameters

The reaction kinetics of reactions shown in chapters 3.4.1, 3.4.2, 3.4.3 and 3.4.4 are listed in the appendix C. Depending on the source, the reaction kinetic parameters are shown either with activation energy and pre-exponential factor or with rate constant at specific temperature. Furthermore, all of these reactions have been modelled as first order reactions (Kabyemela et al. 1998; Kabyemela et al. 1999; Yong & Matsumura 2012; Forchheim et al. 2014; Paksung & Matsumura 2015).

3.5 Products of the hydrothermal liquefaction process

Products of the hydrothermal liquefaction process divide into 4 phases, which are oil phase, gas phase, aqueous phase, and solid phase (Fang et al. 2008, p. 3429). The oil phase, known as biocrude, includes non-water-soluble hydrocarbons and aromatic hydrocarbons, such as phenols. The aqueous phase contains hydrocarbons, which are soluble to water, such as aldehydes, alcohols and acids. The gas phase includes light hydrocarbons (C1-C4), carbon monoxide, carbon dioxide and hydrogen. The solid phase includes char and inorganic compounds, such as ash and salts. Fang et al. (2008) concluded that char divides by its structure into phenolic and polyaromatic char. The phenolic char forms when phenols repolymerizes with aldehydes. Polyaromatic char mainly consists of degraded lignin, which has formed eventually linked aromatic compounds. The produced gas consist mainly carbon dioxide and hydrogen, but also methane was discovered in some studies (Goodwin & Rorrer 2010; Forchheim et al. 2014).

Panisko et al. (2015, p. 163) reported carbon yields for different product fractions (Table 4). The results showed that the most of carbon remained in the biocrude and the aqueous fraction. The yields of the different fractions depended on the process conditions and the feedstock.

Table 4 Carbon yields of the hydrothermal liquefaction. (Adapted from Panisko et al. 2015, p. 164, 166).

Feed-stock	Temper-ature ˚C	Pressure Mpa	Catalyt-yst	Oil carbon yield wt-%	Aqueous carbon yield wt-%	Gas carbon yield wt-%	Solid carbon yield wt-%
L. Pine (W14)	355	20.8	Na_2CO_3	60	34	-	-
L. Pine (W16)	347	20.7	Na_2CO_3	50	45	-	-
L. Pine (W18)	350	20.5	Na_2CO_3	64.1	27.7	8.2	0.0
L. Pine (W121)	359	21	Na_2CO_3	43.9	36.1	6	14

Biocrude properties vary depending on feedstock and process conditions (Tekin & Karagöz 2013, p. 494; Dimitriadis & Bezergianni 2017). Typical properties for biocrude are high heating value due to low oxygen and moisture contents, but also it has high viscosity and it is corrosive (Panisko et al. 2015; Dimitriadis & Bezergianni 2017, p. 119). The biocrude contains a variety of different chemical compounds, such as ketones, phenols, nitrogenated compounds and sulfurized compounds (Table 5). Biocrude separates into light and heavy fractions; the light fraction includes mostly ketones and the heavy fractions consist of mostly aromatic compounds, such as phenols (Pedersen et al. 2017a, p. 419). Yu et al. (2017, pp. 837-839) discovered that biocrude contained high amounts of substituted cyclopentenones, substituted phenols and both fatty and palmitic acids.

Table 5 Chemical families found in the biocrude (Adapted from Christensen et al. 2014, p. 164)

Chemical family	Example compounds found in biocrude
Aldehydes	glyceraldehyde, glycoaldehyde
Aliphatics	n-alkenes, cycloalkenes
Fatty acids	carboxylic acids
Ketones	2-methylcyclopentaone, acetone
Nitrogenated aliphatics	amines, amides
Nitrogenated aromatics	indoles, pyrroles
Phenols	o-cresol, catechol, guaiacol
Other	sugars, sulfurized compounds

Separating the aqueous fraction from biocrude is easy, because biocrude is insoluble to water. The aqueous phase contains mainly water, but it also contains dissolved organic compounds (Panisko et al. 2015, p. 163). Panisko et al. (2015, p. 168) determined the composition of two different aqueous fractions obtained from two different biomasses, wood and corn. The samples were processed in four different process conditions (see Table 4). The results of the aqueous fraction produced from wood are shown in Table 6.

The organic compounds of the aqueous fraction included mainly acids, such as glycolic acid, formic acid, acetic acid and propionic acid. Alcohols were present in the aqueous fraction; especially methanol was present in significant amount. Moreover, there were small concentrations of organic compounds, such as phenol, propylene glycol and acetone.

Table 6 Concentrations of organic compounds in the aqueous fractions (Adapted from Panisko et al. 2015, p. 168).

Concentration	W14 mol/dm3	W16 mol/dm3	W18 mol/dm3	W21 mol/dm3
Acetic acid	0.44	0.47	0.50	0.36
Formic acid	0.09	0.05	0.05	0.04
Glycolic acid	1.05	1.50	1.19	0.65
Propionic acid	0.12	0.13	0.13	0.09
Ethanol	0.06	0.05	0.07	0.03
1-Propanol	0.02	0.02	0.02	0.01
Phenol	0.01	0.01	0.01	0.01
2-Methoxyphenol	0.04	0.03	0.03	0.03
Methanol	0.32	0.46	0.40	0.24
4-Ethylphenol	-	-	-	-
Proplyene glycol	0.01	0.02	0.01	0.01
Ethylene glycol	0.09	0.14	0.01	0.02
Acetone	0.05	0.08	0.08	0.03
2-Butanone	0.02	0.02	0.03	0.01
Cyclopentanone	0.02	0.02	0.02	0.01
2-Cyclopenten-1-one	0.01	0.02	0.02	0.01
2-Methyl-cyclopentanone	0.01	BQL	0.01	0.01
2-Methyl-2-cyclopenten-1-one	0.03	0.03	0.03	0.02
3-Methyl-2-cyclopenten-1-one	0.02	0.02	0.02	0.01
2,3-Dimethyl-2-cyclopenten-1-one	0.01	0.01	0.01	0.01
γ-Butyrolactone	0.02	0.04	0.03	0.03
γ-Valerolactone	0.01	0.02	0.02	0.01

The produced biocrude contains too much oxygen and impurities to be used directly as fuel for vehicles. This leads to a need for upgrading the biocrude, before it meets the demands of transport fuel. The upgraded biocrude divides into several fractions, such as biogasoline or biodiesel, in the distillation column (Jena & Das 2011, p. 5481). Using hydrotreating is one way to decrease the amounts of oxygen and nitrogen in the biocrude, where hydrogen gas works as reducing gas (Yu et al. 2017, pp. 839-840). It is possibly to carry out the hydrogen gas production by using catalytic hydrothermal gasification, where the hydrocarbons dissolved in water is gasified into hydrogen gas (Elliott et al. 2015b, pp. 151-152). The decreasing amount of oxygen and nitrogen increases the heating value of the oil and improves its shelf life (Viljava 2011, p. 41; Biller et al. 2015, pp. 197 & 201).

3.6 The scalability of hydrothermal liquefaction process

The scaling reactor from a batch size to an industrial size is a challenging task, and the reaction medium, i.e. supercritical water, makes the scaling even more challenging. This is due to the properties of supercritical water that varies significantly depending on the temperature and the pressure of the system. The aim of scaling the reactor is to increase the production capacity of biocrude from the hydrothermal liquefaction process while keeping the biocrude yield and the composition of the product the same.

Nauman (2008, pp. 107-109) proposed the definition of the scaling factor as:

$$S_X = \frac{X_{full\ scale}}{X_{pilot\ scale}} \tag{3.8}$$

where X means the variable wanted to scale up from pilot size to certain size. However, certain scaling factors depend on the type of the reactor, conditions in the reactor and the type of flow. For example, the radius and the length of the plug flow reactor (PFR) (see 4.5) have their own scaling factors in different cases.

Nauman (2008, p. 113-120) proposed strategies for scaling up the PFR. There are several ways to scale the PFR: by using reactors that are either in parallel or in series or by increasing reactor dimensions without changing geometries. The scaling the reactor by using reactors in parallel means that the increasing the reactor capacity is carried out using several identical reactors in parallel. This design allows using the shell-tube –design, which makes easier to arrange the heat exchange keeping the reaction conditions constant and the basic construct is inexpensive. However, there are some concerns relating this design, such as the distribution of feed in the tubes. Another concern is the differences in the process conditions between the PFR tubes, such as temperatures of tubes or residence times, which may cause differences in yields. The PFR reactors in series mean that adding reactors sequentially, i.e. the same thing as increasing the length of the reactor while the diameter of the reactor is constant. This allows using higher flow rate, if the residence time is constant. However, the higher flow rate leads the higher pressure drop leading to different density of the feed, because higher inlet pressure is used to keep the residence time constant. This leads to higher pumping energy consumption to achieve the required pressure. Furthermore, the design is not suitable for using a heat exchanger. The last one is the increasing the diameter and the length of reactor without changing the ratio of length to radius, which is typically used scaling continuous stirred tank reactors (CSTR).

Donati and Paludetto (1997, pp. 486-488) said that upscaling the reactor needs a skill to develop a qualitative model basing on existing knowledge of experiments, innovative ideas, models and basic knowledge of process (Figure 30). A large amount of experiments and studies has to be done before building the mathematical model used to upscale and to optimize an industrial process. It is more important to understand the influences of different process parameters to reactions and fluid dynamics in the reactor than knowing

the exact chemical reactions and reaction kinetics. The most important fluid dynamics phenomena to know are transport phenomena, dead spaces, bypasses, and mixing, especially in the reactor. All of these phenomena can have a significant influence on the efficiency of the process. However, the model cannot present the exact result of the process due to simplifications in the model, but it can predict with sufficient precision the results of the process, if it is well done.

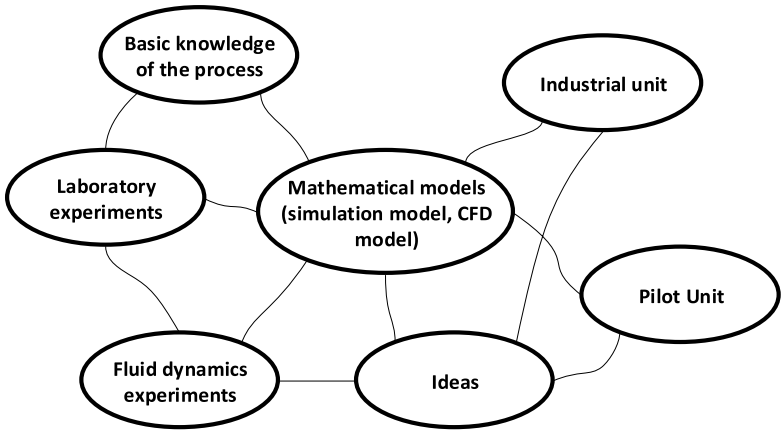

Figure 30 Key elements of upscaling the reactor to industrial size. (Adapted from Donati & Paludetto 1997, pp. 486-488)

Upscaling the HTL process has many uncertainties, which can cause a huge difference between performances in the laboratory scale, the pilot scale and the industrial scale. The uncertainties arise from the feed, reactions in supercritical water, reactor conditions and design of the reactor. The feed, i.e. biomass, is not homogenous and it can include impurities, which may lead to unknown effects. The reactions in the supercritical water are not well known and the reactions in the pilot reactor and in the industrial reactor may differ from each other. The reactor condition influences the reactions and properties of the reaction medium, i.e. water. In the industrial scale, keeping the reaction conditions constant is harder when compared with a pilot reactor or a batch reactor.

The reactor design is a key factor to achieve expected results in the industrial scale. The residence time should be rather short (see 3.3.2), because the gasification reactions decrease the biocrude yield when using longer residence times in supercritical water. For this reason, the other dimensions of the reactor should be dimensioned while keeping the residence time constant. The studying of fluid dynamics in the reactor is an important part of building the computational fluid dynamics (CFD) model, which makes optimizing the flow in the reactor possible. Moreover, it helps to prevent dead spaces and by-pass flows in the reactor. There is no need for heating due the liquefaction reactions are exothermic at high temperatures (Akhtar & Amin 2011, p. 1617), but the need for cooling has to be taken into consideration in the design. The reactor wall as a catalyst did not have a major influence on the yield, so it can be ignored when designing the reactor (see 3.3.3).

4. CALCULATION THEORY

This chapter focuses on the most important calculation theories related to the hydrothermal liquefaction. Thermodynamic properties, such as equation-of-state (EoS), enthalpies and entropies, are the most important properties when studying the hydrothermal liquefaction reactor. The EoS is examined the most accurately, because of it has a significant effect on other thermodynamic properties, such as enthalpy. The Aspen Plus simulation software has a built-in library of different methods that can be used in simulation models, such as Soave-Redlich-Kwong (SRK) EoS, predictive SRK EOS, and UNIFAC method. The UNIFAC method can be used to estimate missing parameters that are required when using predictive SRK EoS.

4.1 Soave-Redlich-Kwong Equation-of-State

SRK EoS defines the vapor-liquid equilibrium in a wide temperature and pressure range (Nasri & Binous 2007, p. 534). The equation 4.1 shows the connection between liquid and vapor phases in the equilibrium

$$f_i^V = f_i^l \,, \tag{4.1}$$

where f_i^v is the fugacity of chemical component in the vapor phase and f_i^l is the fugacity of chemical component in the liquid phase. There are two ways to calculate the fugacity parameters, which are the EoS method and an activity coefficient method. This work focus on the equation-of-state method, because the EoS method is suitable for calculating physical properties in supercritical state.

$$f_i^x = \phi_i^x y_i p \tag{4.2}$$

$$ln\varphi_i^x = -\frac{1}{RT}\int_{\infty}^{V_x}\left[\left(\frac{\vartheta p}{\vartheta n_i}\right)_{T,P,n_{i\neq j}} - \frac{RT}{V}\right]dV - lnZ_m^x \tag{4.3}$$

$$ln\varphi_i^x = -\frac{1}{RT}\int_{\infty}^{P}\left[\left(\frac{\vartheta p}{\vartheta n_i}\right)_{T,V,n_{i\neq j}} - \frac{RT}{P}\right]dP \tag{4.4}$$

where x is the phase of component (liquid or vapor), V is the total volume of the system, n_i is the number of moles of chemical component and φ_i^x is fugacity coefficient factor.

The total pressure, P, is the pressure in the system. The pressure calculation depends on the chosen method. Predictive Soave-Redlich-Kwong equation of state method is EoS

method, which is capable to calculate systems that contain both polar and non-polar components in sub- and supercritical state. The equation of state formula simplifies to the next formula. (Holderbaum & Gmehling 1991; Penttilä 2011; Su 2012)

$$P = \frac{RT}{(V_m - b_m)} - \frac{a_m}{V_m(V_m + b_m)} \tag{4.5}$$

where R is the gas constant and V_m is the molar volume of the system. Formulas 4.6-4.9 show how a_m and b_m calculation occurs (Holderbaum & Gmehling 1991; Su 2012):

$$a_m = \sum_i \sum_j x_i x_j \sqrt{a_i a_j}\,(1 - K_{ij}) or\ \sum_i \sum_j y_i y_j \sqrt{a_i a_j}\,(1 - k_{ij}) \tag{4.6}$$

$$b_m = \sum_i x_i b_i\ \ or\ \sum_i y_i b_i \tag{4.7}$$

$$a_i = 0.42748 \frac{R^2 T_{c,i}^2}{P_{c,i}} \alpha_i(T) \tag{4.8}$$

$$b_i = 0.08664 \frac{R T_{c,i}}{P_{c,i}} \tag{4.9}$$

where $T_{c,i}$ is the critical temperature of chemical component, $P_{c,i}$ is the critical pressure of chemical component and k_{ij} is the binary interaction factor. The equation 4.10 below shows the Alpha function, $\alpha_i(T)$

$$\alpha_i(T) = [1 + (0.48 + 1.574\omega_i - 0.176\omega_i^2)(1 - T_r^{0.5})]^2 \tag{4.10}$$

where ω_i is the empirical acentric factor of chemical component:

$$\omega_i = -\ln\left(\frac{P}{P_{ci}}\right) - 1 \tag{4.11}$$

The equation 4.11 above is calculated when temperature T is 0.7xT_{ci}.

The equation 4.12 shows expanded form of equation 3.4 by equations 3.5-3.8 (Penttilä 2011).

$$Z^3 - Z^2 + Z(A - B - B^2) - AB = 0 \tag{4.12}$$

where Z is compressibility factor and other parameters are (Penttilä 2011):

$$Z = \frac{\nu P}{RT} \tag{4.13}$$

$$A = \frac{a_m P}{R^2 T^2} \tag{4.14}$$

$$B = \frac{b_m P}{R\,T} \tag{4.15}$$

The equation 4.12 is solved by using analytical trigonometric functions. Solving this equation gives three roots; the first root is the compressibility factor of liquid and the third one is the compressibility factor of vapor. The second root does not have a meaning when solving the compressibility factor. However, the equation has only one solution in supercritical conditions, which is logical because only one phase occurs under supercritical conditions

Calculating the fugacity coefficients of pure component and component in the mixture occurs by using equations 4.16 and 4.17.

$$\ln \phi = (Z-1) - \ln(Z - B_m) - \frac{A_i}{B_i}\ln(\frac{Z+B_m}{Z}) \tag{4.16}$$

$$\ln \hat{\phi}_i = \frac{b_i}{b_m}(Z-1) - \ln(Z - B_m) - \frac{A_m}{B_m}\left(\frac{2}{a_m}\sum_j x_j a_{ij} - \frac{b_i}{b_m}\right)\ln(\frac{Z+B_m}{Z}) \tag{4.17}$$

4.2 Predictive Soave-Redlich-Kwong Equation of state method

The predictive Soave-Redlich-Kwong (PSRK) EoS method basis on SRK, but it able to predict the behavior of chemical components without experimental data from vapor-liquid equilibrium. When using PSRK EOS method, the Alpha function depends on both temperature of system and critical temperature of the component. If the temperature is below the critical temperature of component, the calculation occurs by using the formula 4.18. If the temperature is above the critical temperature of component, then the calculation of $\alpha_i(T)$ function occurs by using the formula 4.19. (Holderbaum & Gmehling 1991; Horstmann et al. 2005; Su 2012)

$$\alpha_i(T) = \left[1 + C_{1,i}(1 - T_r^{0.5}) + C_{2,i}(1 - T_r^{0.5})^2 + C_{3,i}(1 - T_r^{0.5})^3\right]^2 \tag{4.18}$$

$$\alpha_i(T) = \left[1 + C_{1,i}(1 - T_r^{0.5})\right]^2 \tag{4.19}$$

$$T_r = \frac{T}{T_C}$$

Where $C_{1,i,}$ $C_{2,i,}$ $C_{3,i}$ are Mathias-Copeman parameters and T is the temperature of the system and T_C is the critical temperature of chemical component. Parameter $C_{1,i,}$ is possible to calculate with acentric factor in which case values for parameters $C_{2,i,}$ and $C_{3,i,}$ (equation 4.20) are zero (Horstmann et al. 2005).

$$C_{1,i} = 0.48 + 1.574\,\omega_i - 0.176\,\omega_i^2 \; and \; C_{2,i} = C_{3,i} = 0 \tag{4.20}$$

However, the alpha function and the parameter b are possible to calculate using modified PSRK mixing rule, which needs parameters a_{ii} (equation 4.8), b_i (equation 3.9), and the excess Gibbs energy at the reference state (Fischer & Gmehling 1996, pp. 186-187; Horstmann et al. 2005).

$$\frac{\alpha_i(T)}{bRT} = \frac{\sum x_i a_{ii}(T)}{b_i RT} + \frac{\frac{g_0^E}{RT} + \sum x_i \ln\frac{b_i}{b}}{\ln\frac{u}{u+1}} \tag{4.21}$$

Where u is constant and b is calculated by applying the linear mixing rule (equation 4.23) (Fischer & Gmehling 1996, p. 187).

$$u = 1.1 \tag{4.22}$$

$$b = \sum x_i \, b_i \tag{4.23}$$

Now the equation 4.6 is replaced with equation 4.24 (Penttilä 2011).

$$\alpha_m = \sum_i x_i \alpha_i + \frac{1}{q_1}\left(\sum_i x_i \, ln \, \gamma_i - \sum_i x_i \ln\frac{b_i}{b_m}\right) \tag{4.24}$$

Where the parameter γ_i is molecular activity coefficient achieved from UNIFAC method (see chapter 4.3) and equations for α_i and q_1 is shown below (equations 4.25 and 4.26)

$$\alpha_i = \frac{a}{bRT} \tag{4.25}$$

$$q_i = -0.64333 \tag{4.26}$$

The fugacity coefficient of certain component in the mixture can be expressed with equation 4.27 (Penttilä 2011).

$$\ln \hat{\phi}_i = \frac{b_i}{b_m}(Z-1) - \ln(Z - B_m) - \overline{\alpha}_i \ln\left(1 + \frac{B_m}{Z}\right) \tag{4.27}$$

where parameter $\overline{\alpha}_i$ is calculated with equation 4.28

$$\overline{\alpha}_i = \alpha_i + \frac{1}{q_1}\left(ln\gamma_i - \ln\frac{b_i}{b_m} + \frac{b_i}{b_m} - 1\right) \tag{4.28}$$

4.3 UNIFAC method

UNIFAC method makes possible to estimate the phase equilibrium data when experimental data is not available for all components. The UNIFAC model estimates the molecular activity coefficient by estimating the value by using existing data from similar components. Calculating the molecular activity coefficient divides into calculating combinatorial and residual contributions. The combinatorial contribution takes account of effects of molecular size and the residual contribution estimates the impacts of molecular interactions. (Reid et al. 1987, pp. 314).

$$ln \, \gamma_i = ln \; \gamma_i^C + ln \, \gamma_i^R \tag{4.29}$$

where $ln\,\gamma_i^C$ is combinatorial contribution and $ln\,\gamma_i^R$ is residual contribution. The equations 4.30 and 4.31 show how combinatorial contribution and residual contribution factors are calculated. (Reid et al. 1987, pp. 315).

$$ln\,\gamma_i^C = \ln\frac{\phi_i}{x_i} + 5q_i ln\frac{\theta_i}{\phi_i} + l_i - \frac{\phi_i}{x_i}\sum_j x_j l_j \tag{4.30}$$

$$ln\,\gamma_i^R = q_i[1 - \ln(\sum_j\ \theta_j\tau_{ji}) - \sum_j \frac{\theta_j\tau_{ij}}{\sum_k \theta_k\tau_{kj}}] \tag{4.31}$$

The binary parameters τ_{ji} and τ_{ij} in equation 4.3.3 are adjustable parameters received from experimental results. Parameters l_i, θ_i, ϕ_i and τ_{ji} are calculated with equations 4.32-4.3.5. (Reid et al. 1987, p. 315).

$$l_i = 5(r_i - q_i) - (r_i - 1) \tag{4.32}$$

$$\theta_i = \frac{q_i x_i}{\sum_j q_j x_j} \tag{4.33}$$

$$\phi_i = \frac{r_i x_i}{\sum_j r_j x_j} \tag{4.34}$$

$$\tau_{ji} = \exp(-\frac{u_{ji} - u_{ii}}{RT}) \tag{4.35}$$

Parameters r_i and q_i are calculated by using equations 4.36 and 4.3.7. (Reid et al. 1987, p. 316).

$$r_i = \sum_k v_k^{(i)} R_k \tag{4.36}$$

$$q_i = \sum_k v_k^{(i)} Q_k \tag{4.37}$$

The parameter $v_k^{(i)}$ is the number of groups of certain structural group *k* in the molecule *i*. R_k and Q_k are group volume and area parameters received from experimental data. The equation 4.38 is possible to replace with equation 4.3.9. (Reid et al. 1987, p. 316)

$$ln\,\gamma_i^R = \sum_k v_{(k)}^i\ (\ln\Gamma_k - \ln\Gamma_k^{(i)}) \tag{4.38}$$

The parameter Γ_k is a group activity coefficient of UNIFAC group k and parameter $\Gamma_k^{(i)}$ is the group activity coefficient of UNIFAC group k in a reference solution containing only certain molecules of type i. The parameter Γ_k is achieved by using the equation 4.39. The parameter $\Gamma_k^{(i)}$ is calculated with the same equation (4.39), but in that case the residual activity coefficient is calculated for the pure component i. (Reid et al. 1987, p. 316)

$$\ln\Gamma_k = Q_k[1 - \ln(\sum_m \theta_m\Psi_{mk}) - \sum_m \frac{\theta_m\Psi_{km}}{\sum_n \theta_n\Psi_{nm}}] \tag{4.39}$$

where θ_m and Ψ_{mk} are calculated with equations 4.40 and 4.41. (Reid et al. 1987, p. 316)

$$\theta_m = \frac{Q_m X_m}{\sum_n Q_n X_n} \tag{4.40}$$

where X_m is the mole fraction of certain UNIFAC group in the examined mixture. Lastly, Ψ_{xy} is the group interaction parameter of between group x and y, and it is calculated with equation 4.3.12. (Reid et al. 1987, pp. 316 & 322)

$$\Psi_{mn} = \exp(-\frac{a_{mn}}{T}) \tag{4.41}$$

The parameter a_{mn} is achieved from experimental results and its unit is in Kelvin. When using the UNIFAC method, it should be noted that the parameters a_{mn} and a_{nm} are not same. (Reid et al. 1987, p. 322)

4.4 Relationship between departure functions and Equation-of-State

Departure functions are used to calculate the departure between real fluid and ideal gas at the same conditions (Yeo 2017, pp. 158-159). The Departure functions allow calculating the real values of enthalpy, entropy and Gibbs energy, because the changes between the ideal gas and the real fluid are the same and the difference between these values can be corrected with the retrieved value from the departure function. Departure functions from equation state of enthalpy, entropy and Gibbs energy are shown in equations 4.43-4.45 (Aspen Technology Inc 2017, pp. 8-9). These equations depend on the EoS (see chapters 4.1 and 4.2) function essentially, because pressure, volume and compressibility factor are related to EoS function.

$$H_m - H_m^{ig} = -\int_\infty^V \left(p - \frac{RT}{V}\right) dV - RTln\left(\frac{V}{V^{ig}}\right) - T\left(S_m - S_m^{ig}\right) + RT(Z-1) \tag{4.42}$$

$$S_m - S_m^{ig} = -\int_\infty^V \left(\frac{\partial p}{\partial T} - \frac{R}{V}\right) dV - Rln\left(\frac{V}{V^{ig}}\right) \tag{4.43}$$

$$G_m - G_m^{ig} = -\int_\infty^V \left(p - \frac{RT}{V}\right) dV - RTln\left(\frac{V}{V^{ig}}\right) + RT(Z-1) \tag{4.44}$$

where *ig* refers to reference state. The vapor enthalpy calculation happens using the equation and 4.46 and the liquid enthalpy calculation occurs using the equation 4.47 (Aspen Technology Inc 2017, p. 9).

$$H_m^v = H_m^{ig} + (H_m^v - H_m^{ig}) \tag{4.45}$$

$$H_m^l = H_m^{ig} + (H_m^l - H_m^{ig}) \tag{4.46}$$

The enthalpy of reference state is calculated by the equation 4.48 (Aspen Technology Inc 2017, p. 9).

$$H_m^{ig} = \sum_i y_i[\Delta_f H_i^{ig} + \int_{T^{ref}}^{T} C_{p,i}^{ig}(T)dT] \quad (4.47)$$

where parameters $C_{p,i}^{ig}$, T^{ref} and H_i^{ig} are ideal gas heat capacity, reference temperature (T = 298.15 K) and standard enthalpy of formation for ideal gas (T = 298.15 K and P = 1.013 bar). The vapor and liquid both entropy and Gibbs energy calculations (equations 4.49-4.52) occur in the same way as enthalpy calculations in the equations 4.46-4.48 (Aspen Technology Inc 2017, p. 9).

$$S_m^v = S_m^{ig} + (S_m^v - S_m^{ig}) \quad (4.48)$$

$$S_m^l = S_m^{ig} + (S_m^l - S_m^{ig}) \quad (4.49)$$

$$G_m^v = G_m^{ig} + (G_m^v - G_m^{ig}) \quad (4.50)$$

$$G_m^l = G_m^{ig} + (G_m^l - G_m^{ig}) \quad (4.51)$$

4.5 Reaction kinetics in plug flow reactor

Chemical reactions used in this study occur in the plug flow reactor (PFR). The product composition depends on the dimensions of PFR, reaction conditions and feed material. The reaction rates depends on the Arrhenius parameters, temperature and concentration of chemical compounds in the reactor. The equations below is based on equations 4.53 and 4.54 (Rosen 2017, pp. 7-8). The formulas below are calculated by assuming that reactions are first order reactions, because the reaction kinetic models found during this thesis work use the first order models (see chapter 3.4.5).

$$aA + bB \leftrightarrow cC + dD \quad (4.52)$$

$$\frac{-r_a}{a} = \frac{-r_b}{b} = \frac{-r_c}{c} = \frac{-r_d}{d} \quad (4.53)$$

Rate constant

For nonreversible reaction a reaction rate is

$$-r_A = k_A C_A^{\alpha} \quad (4.54)$$

where k_X is a reaction rate is constant, C_X is concentration or partial pressure and both α and β are the orders of the reactions (Zumdahl 2009, p. 747; Rosen 2017, p. 8). The partial pressure of component A in the supercritical phase is calculated with EoS (see 4.1 and 4.2). The total reaction order is the sum of the α and β.

For reversible reaction the reaction rate is

$$-r_A = k_A(C_A^{\alpha} - \frac{k_{-A}}{k_A} \; C_B^{\gamma} C_B^{\delta}) \tag{4.55}$$

where k_{-A} is the reaction rate constant of reverse reaction (Zumdahl 2009, p. 741; Rosen 2017, p. 8).

The equilibrium constant is possible to define with equation 4.57 (Zumdahl 2009, p. 741; Rosen 2017, p. 8).

$$K_C = \frac{k_{-A}}{k_A} = \frac{C_{A,eq}^{\alpha} C_{B,eq}^{\beta}}{C_{B,eq}^{\gamma} C_{B,eq}^{\delta}} \tag{4.56}$$

Now, the equation 4.59 is possible to express as

$$-r_A = k_A(C_A^{\alpha} - \frac{C_B^{\gamma} C_B^{\delta}}{K_C}) \tag{4.57}$$

Arrhenius equation

The Arrhenius equation is defined as equation 4.59

$$k(T) = \mathrm{A}e^{-\frac{E}{RT}} \tag{4.58}$$

where *A* is an activation energy and *R* is the universal gas constant (Zumdahl 2009, pp. 749-750). The equation is possible to define as an equation 4.60, if the rate constant at certain temperature (T_0) is known (Rosen 2017, p. 8).

$$k(T) = \mathrm{k}(\mathrm{T_0})e^{[\frac{E}{R}(\frac{1}{T_0} - \frac{1}{T})]} \tag{4.59}$$

Isothermal plug flow reactor

Plug flow reactor is a pipe, where the reactions occur simultaneously as material flows through the reactor (Figure 31). The assumptions for the reactor is that the mixing is complete in all part of the reactor and the mixing happens only in the radial direction, not in the axial direction. Due to complete mixing, the velocity profile is steady. The calculations below basis on materials from both Rodgers (2013, pp. 3-21) and Rosen (Rosen 2017, pp. 4-12).

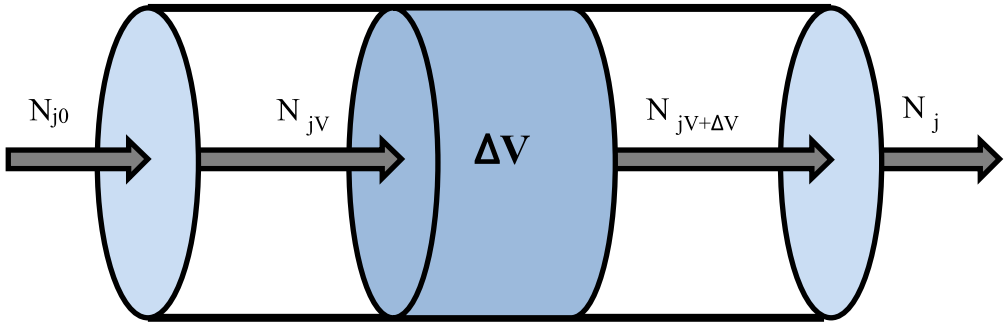

Figure 31 Plug flow reactor

Material balance of the PFR is based on the equation 4.61:

$$\sum m_{in} - \sum m_{out} + \sum m_{generated} = accumulation = \frac{dm}{dt} \tag{4.60}$$

Molar balance is then

$$n_{jV} - n_{jV+\Delta V} + r_j \Delta V = \frac{dn}{dt} \tag{4.61}$$

Shortly, the design equation for the PFR is:

$$\frac{dF_A}{dV} = r_A \tag{4.62}$$

The equation 4.63 is achieved when integrating the equation 4.63

$$F_{A0} \frac{dX}{dV} = -r_A \tag{4.63}$$

The conversion of the component A is also possible to express as equation 4.64

$$\frac{dX}{dt} = -\frac{r_A V}{n_{A0}} \tag{4.64}$$

5. HYDROTHERMAL LIQUEFACTION PILOT FACILITY

The building up the pilot facility is an essential part of studying the hydrothermal liquefaction reactions enabling to study different process conditions and their impact on products. The validation and development of the simulation model will be based on the test results when the pilot facility is completed. This chapter presents the pilot facility and its components.

The main idea of the process is to test hydrothermal liquefaction with a pilot plant, which feeding capacity to the process is 10 liters/hour. The pilot plant is a continuous-flow process, where the premixed biomass-water –slurry is pressurized to 300 bar and then heated up to 400 ˚C (Figure 32). When the condition of the slurry is above the critical point of water, slurry goes to the reactor. Then the biomass begins to hydrolyze to different components, which still react to other products. After the reactor, the products cool down to 80 ˚C in the cooler section and the pressure decreases to atmospheric pressure in the depressurizing pump. The next stage of the process is the extraction of gaseous products from the liquid product. In the last stage, gas goes to condenser, where non-condensable gases go out of the process and the condensable gases remain in a collection container.

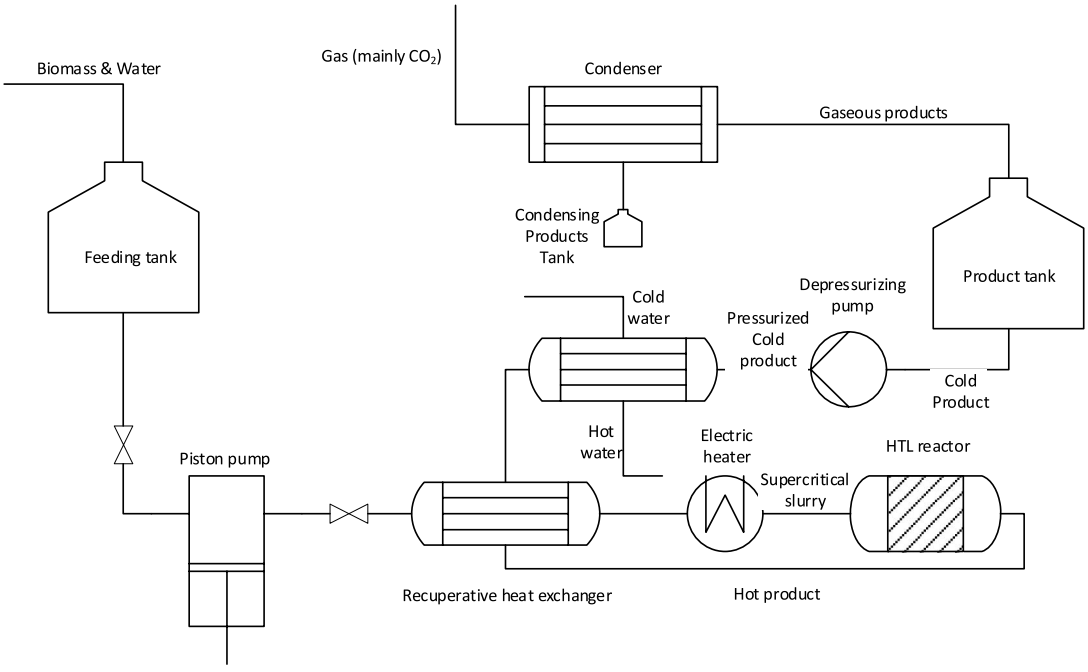

Figure 32 Hydrothermal liquefaction process overview.

5.1 Pretreatment of biomass

Before feeding the biomass into the process, it is ground into small particles whose diameter is 1 mm or less in a grinder. Next, the biomass and water are mixed in mixing tank keeping the mixture homogenous before feeding it into the process. If necessary, other chemicals, such as catalyst chemicals or sodium hydroxide (NaOH), are fed to the mixing thank.

5.2 Pressurizing the slurry

One of the most difficult challenges of hydrothermal liquefaction process is pumping the slurry to the high pressure (Elliott et al. 1989, pp. 23-24; Berglin et al. 2012; Jazrawi et al. 2013). Hong and Spritzer (2002, p. 8) tested pumping of wood dust. The maximum concentration of wood dust in the slurry was between 10 wt-% – 15 wt-%, before pumping problems arise. Another thing that affected pumpability was the size of biomass particles in the slurry (Elliott et al. 1989, pp. 23-24). When the size of biomass particles was above 0.125 inc, i.e. around 0.32 cm, the slurry was no longer pumpable. For this reason, the diameter of the particle should be under 0.3 cm and the concentration of the slurry around 10 wt-% to ensure the pumpability of the slurry.

In this pilot plant, the piston pump pressurizes the slurry to the target pressure. The main idea of a piston pump is presented in Figure 33. Firstly, the suction valve (left) opens while the process valve (right) is closed, and the piston starts to move downwards. Similarly, the slurry begins to flow into a cylinder. At the end of a suction phase, the suction valve closes down and then the piston starts to move upwards. When the pressure on the cylinder achieves the target pressure, the process valve opens and the pressurized slurry goes to the process. The process valve closes at the end of the pressurizing phase. After this, the suction phase begins again.

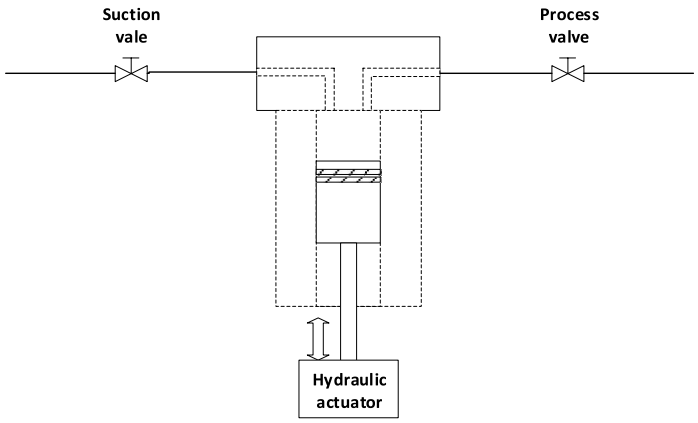

Figure 33 the main idea of piston pump

5.3 Heat exchangers

The slurry goes to the heating sector after lifting the pressure. There are a couple of different ways to increase the temperature of the slurry to the target temperature, which is possible to utilize in this pilot plant. The first one is to use several serial electric heaters until achieving the target temperature. However, this leads to low energy efficiency, because of the heating the slurry causes the most of the energy required in process. The second way is to use a recuperative heat exchanger, which improves the energy efficiency of the process. The recuperative heat exchanger recovers most of the heat energy of hot product to the cold pressurized feed by heating the feed. After the recuperative heat exchanger, an electric heater adjusts the temperature of the slurry to the target temperature.

5.4 Hydrothermal liquefaction reactor

The reactor is the main process component of the HTL process, where the pressurized slurry converts into chemical components of a different kind. However, the biomass starts to convert before the reactor, when the temperature and pressure are favorable for hydrolysis reactions and other reactions, but this is minor in comparison with reactions in the reactor. Figure 34 presents the main idea of the hydrothermal liquefaction reactor. The reactor is a plug flow reactor, where the pressurized slurry enters the reactor at one end and the product comes out from the other end. The reactor design allows using solid catalyst materials to study the effects of different catalyst materials. Another way is to use a homogenous catalyst in which case the catalyst is fed with the slurry to the reactor.

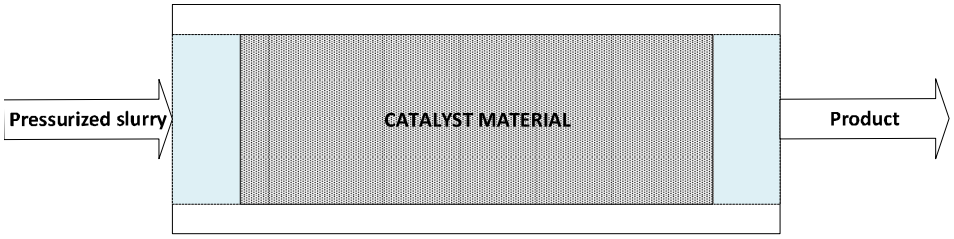

Figure 34 Basic idea of hydrothermal liquefaction reactor

5.5 Cooling

The cooling of the hot product occurs in the recuperative heat exchanger and a cooler. The process is modular so that it is possible to use only the cooler or combination of the recuperative heat exchanger and the cooler to cool down the product to the target temperature. The recuperative heat exchanger transfers heat energy from the hot product to the cold product. After the heat exchanger, there is an additional cooler, where, the hot product cools down to the desired temperature (Figure 35).

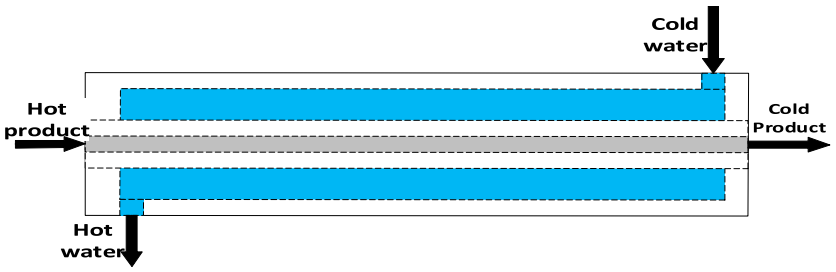

Figure 35 The basic idea of the cooler

5.6 Depressurizing the product

The pilot plant uses the same kind of design like the pump (Figure 33) to decrease the pressure of the cold product to target pressure. In this case, the process side valve opens and the piston starts to move downward from the upright position. When the piston has gone a certain distance down, the process valve closes and the piston continues to go down while reducing the pressure of the product to the desired pressure. Next, the piston starts to move upward and the valve on the product tank side opens and the depressurized product flows to the tank. Finally, the valve on the product tank side closes and the cycle starts again.

5.7 Extraction of gaseous products

The product is at atmospheric pressure after the depressurizing pump and it flows into product tank. However, the gases continue to the condenser, where the gas cools down near to room temperature and the condensable gases condense into a container. The rest of gases, such as carbon dioxide, is conducted outside of the process container.

6. HYDROTHERMAL LIQUEFACTION REACTION SIMULATION MODEL

There are several reasons, why the creating the hydrothermal liquefaction simulation model is an important part of studying the hydrothermal liquefaction. Especially, the importance of the model emphasizes when designing an industrial plant, because it makes possible to study different process variations to optimize the process. The optimization includes both minimizing the energy need for the process and maximizing the biocrude yield. The simulation model allows user to change process conditions, such as the temperature and the mass flows of different components, and to see the effects of change. This chapter contains the study of existing hydrothermal liquefaction simulation models, introduction to simulation software, creating the model and model overview.

6.1 Existing simulation models

There are several existing simulation models of hydrothermal liquefaction, which predict the composition of the product and the energy need for the process. Most of these simulation models use RYield –block to calculate the product composition. The observation below concentrates studying the hydrothermal liquefaction including the pretreatment, heat exchangers, reactor, cooling and the separating of the products. The most important properties of these models have been gathered into Appendix F.

Tews et al.(2014, pp. 17-20) modelled the hydrothermal liquefaction of a wet wood residue using the Aspen Plus software. They used the model to study the feasibility and life cycle assessment of the process compared with a pyrolysis process. The model divides into five parts: pretreatment, hydrothermal liquefaction in subcritical water, a hydrogen plant, hydrotreating, and wastewater treatment (Figure 36). Firstly, biomass is mixed with water in the pretreatment sector. Secondly, biomass-water slurry is pressurised into a target pressure in the pretreatment sector. The slurry goes into a HTL reactor working at temperature of 355 ˚C and pressure of 20.3 MPa. The produced biocrude is treated with hydrogen in the hydrotreating sector, where both the oxygen content of biocrude decreases and the heating value of biocrude increases. The gases produced in both the HTL reactor and the hydrotreating is fed to the hydrogen plant, where hydrogen needed in the hydrotreating is produced. The wastewater produced in the HTL reactor goes into the wastewater treatment.

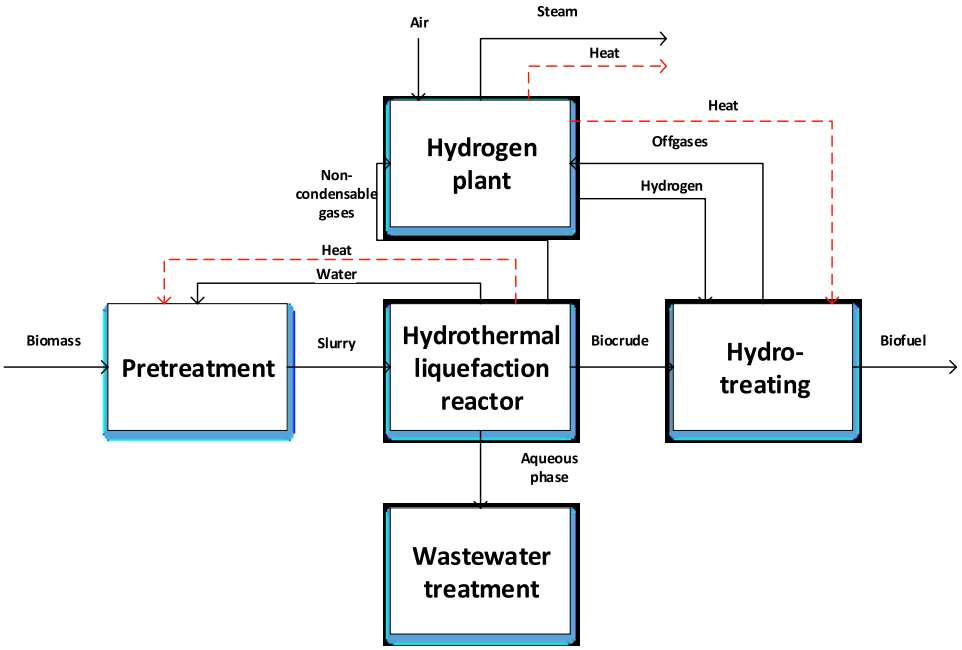

Figure 36 Hydrothermal liquefaction integrated with hydrogen plant and hydrotreating (Adapted from Tews et al. 2014, p. 14)

Tews et al. (2014, pp. 17-20) used the Soave-Redlich-Kwong (SRK) method to determining the thermodynamic properties in the model. The model uses RYield block to calculate the yields of the reactor, which works under subcritical conditions at the temperature of 330 ˚C and the pressure of 25 MPa. The yield of the RYield block is based on the study from Hammerschmidt et al.(2011). They achieved 27 wt-% yield for products from the whole process. The mass flows for gasoline, diesel and heavy oil were 2.9 kg/s, 2.5 kg/s and 0.95 kg/s, when the input flow of a dry forest residue was 23.15 kg/s. The energy efficiency of the whole process was 62.3 %, which was calculated by comparing the energy content of the products with the input energy, i.e. the energy content of the input and the required electrical and thermal energy.

Hoffman et al. (2013, pp. 403-410) used Aspen Plus to model a combination of a biogas process and the hydrothermal liquefaction process (Figure 37). Firstly, the biomass, i.e. animal manure, goes into the biogas plant, where biomass converts into biogas and digestate. The biogas goes into hydrogen production unit, where a part of biomethane separated from biogas converts into hydrogen carbon monoxide. The rest of methane goes into gas grid. The digestate flows into a hydrothermal liquefaction plant, which converts digestate into biocrude and fertilizers. Then the biocrude is treated in the upgrading unit with hydrogen into biofuel. The hydrogen needed in the upgrading unit comes from hydrogen production unit. They used the Soave-Redlich-Kwong (SRK) method to determining the thermodynamic properties in the model. The model uses RYield block to calculate the yields of the reactor, which works under subcritical conditions at the temperature of 330 ˚C and the pressure of 25 MPa. The yield of the RYield block is based on the study from

Hammerschmidt et al.(2011). They modelled two cases; the first one is the low-yield scenario and the second one is the high-yield scenario. The first scenario yielded in for 36.8 kg/h with the feed of a 1000 kg/h substrate slurry and the second scenario yielded in for 30.3 kg/h with the same feed. The energy efficiency of the first and second scenarios were 62 % and 84 %. The upgraded biofuel had a LHV of 43.1 MJ/kg.

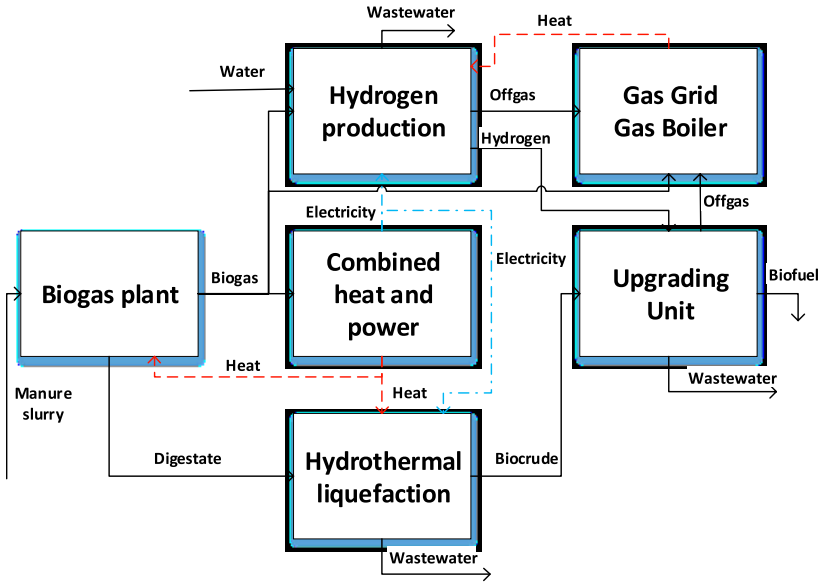

Figure 37 The overall process of combined biogas plant and hydrothermal liquefaction unit (Adapted from Hoffmann et al. 2013, p. 404).

Pedersen et al. (2017b) did a techno-economic analysis from hydrothermal liquefaction process with Aspen Plus studying three different cases. The feed is a mixture of glycerol, Aspen wood and water in Scenario 1. In scenario 2, the portion of glycerol is replaced with water. In the last scenario, scenario 3, the product consists only of saturated hydrocarbons without oxygenated aromatics and the feed is same as in the scenario 2. The yields of different processes are based on the study of Pedersen et al.(2017a). The pressurized and heated slurry goes into the hydrothermal liquefaction process, which works at the temperature of 400 ˚C and the pressure of 30 MPa. The product of the HTL reactor is separated into three phases: biocrude, gas and water phase. A major part of the water phase circulates into the pretreating sector and the rest of it goes to waste water treatment. The biocrude consists of volatile and non-volatile phases; the volatile phase goes to a hydrotreating and the non-volatile fraction gets into a cracker. The non-volatile fraction undergoes the thermal cracker process producing hydrogen and other products. The hydrotreating unit uses the produced hydrogen to upgrade the volatile fraction of biocrude into gasoline products. There is an additional hydrogen feed to the hydrotreating process, because the hydrogen from the cracker is not enough to treat the completely volatile fraction. The yields of the hydrothermal liquefaction process for biocrude, gas and the sum of solids and dissolved organics were 30 wt-%, 13 wt-% and 57 wt-% in scenario 1. The biocrude yield increased into 40 wt-% in scenarios 2 and 3. The thermal cracking efficiency was 70 % and the hydrogen need to upgrade biocrude into the gasoline equivalent

product in hydrotreatment unit were 0.036 $kg_{hydrogen}/kg_{biocrude}$ in scenario 1 and 2 and 0.0482 $kg_{hydrogen}/kg_{biocrude}$ in scenario 3. The yields of hydrotreatment unit were 80.25 wt-% for the gasoline equivalent product and 19.75 wt-% for the water. The gasoline equivalent product consists of a wide range of hydrocarbons, but also a small portion of oxygenated hydrocarbons. The production cost € per liter of gasoline equivalent product. The production cost for biocrude was at its lowest in the scenario 2, where the base cost of production was 0.821 $/liter which varied between 0.56 and 1.16 $/ liter when changing the process parameters and costs of different feeds

Tzanetis et al. (2017) modelled the production of aviation fuel using the hydrothermal liquefaction process with Aspen Plus. They used the model to study the effects of different catalysts, biomass to water ratios and the temperatures of the HTL reactor to the production costs and greenhouse gas emissions. The process divides into a thermochemical conversion of biomass into biocrude and upgrading the biocrude into aviation and transportation fuels in the hydrotreatment unit. The model uses the SRK thermodynamic method in all other components except in the vapor-liquid –equilibrium (VLE) unit, which separates vapor and liquid phases from each other. The used thermodynamic method was the non-random two-liquid (NRTL) method in the VLE unit. The feed is unspecified biomass, which goes to the HTL reactor (Tzanetis et al. 2017). Before the reactor, the pressure of feed increases in the pump and the temperature increases in two heat exchanger. The first one is a recuperative heat exchanger, where hot product releases a large part of its thermal energy to the cold feed. The other heat exchanger uses the hot flue gas from a furnace to warm up the feed to the target temperature. The HTL reactor is modelled as RYield block, which uses experimental data to solve the yields of different components (Sun et al. 2010; Veses et al. 2014). After the reactor, the product goes into a filter, which separates solid products from other streams. The solid products are burned in the furnace and the hot flue gas goes into the heat exchanger, which warms up the biomass feed to the reactor. The rest of the product goes into the recuperative heat exchanger and after that to VLE unit, which separates the gaseous and liquid product from each other. The gas product is burned in the furnace and the liquid product goes into a liquid-liquid equilibrium unit, which separates the oil and water phase.

6.2 Introduction to ASPEN PLUS

The Aspen Plus software is chemical process simulation software, which allows user to simulate complex chemical processes to study the feasibility and the economy of the process (AspenTech Inc.). The Aspen Plus software includes a large databank of different chemicals and theirs properties, such as critical temperatures and miscibility parameters to other chemicals, and both thermodynamic and transport property methods to calculate the properties of real fluids in different conditions. It allows user to add experimental data to improve and validate models to correspond to the experimental results. The software includes a variety of building blocks corresponding to unit processes, such as pumps,

reactors, heat exchangers and distillation columns, but it can also handle solid processes. The simulation allows studying steady state and dynamic models.

The modelling environment divides into two stages: the setting of the properties of the model and building the model with unit process blocks. The setting of properties includes adding the chemical components in the model and the choosing of the physical property method, which is suitable for calculating the thermodynamic and the transport properties. It also allows studying different properties of the components, such as miscibility and phase behavior. The building of the model happens in the simulation environment, where user can connect unit processes to each other and determine the process conditions in each unit. When the necessary data is set, user can run the model and see the results. Studying different kind of process conditions is easy with Aspen Plus, because it includes a variety of model analysis tools, such as sensitivity analysis and optimization tools.

6.3 Creating simulation model

The building up the hydrothermal liquefaction model divided into literature search, building the simulation model, calculating the results of the model and comparing the results with existing results. Figure 38 presents the used procedure of building up the simulation model.

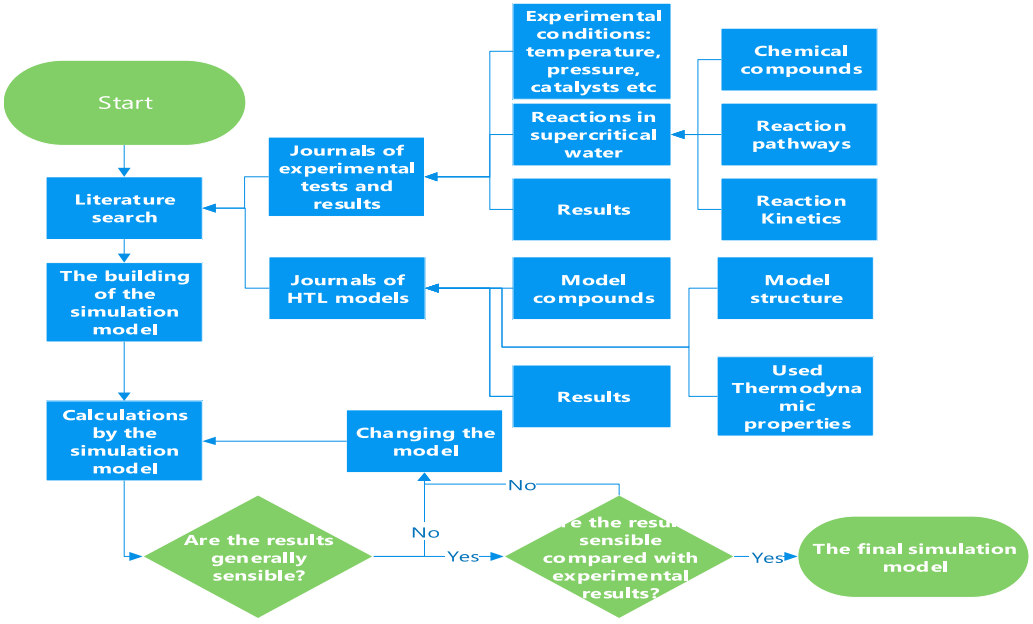

Figure 38 the used procedure to build up the simulation model

The literature search included searching journals concerning on experimental hydrothermal liquefaction including the results and proposed reaction pathways and the existing simulation models including the results of the model. The building of the simulation model included creating the Aspen Plus simulation model and Excel spreadsheet linked

to the simulation model. The calculations in the model included various cases under different process conditions. These results were compared with results from other models and experimental hydrothermal liquefaction results. The model was developed comparing the results of the model with the results of existing models and experimental data. The changes were mainly made by changing the physical method of the simulation and the reaction pathways and kinetics.

6.4 Model overview

The overall view of the hydrothermal liquefaction process, where biomass converts into biocrude and byproducts, is shown in appendix C. The first stage of hydrothermal liquefactions is the pretreatment of biomass, which includes blending the biomass into water in MIXER -block and rising the pressure of slurry to 30 MPa (Figure 39) in PUMP -block. In the next stage, the temperature of slurry increases into 400 ˚C. There are two heat exchanger, which raise the temperature of sludge to the desired temperature. The first heat exchanger, EXH1 -block, is a recuperative heat exchanger whereby the thermal energy of the hot product is recovered to slurry. The second heat exchanger, EXH2 -block, adjust the temperature of the slurry to 400 ˚C.

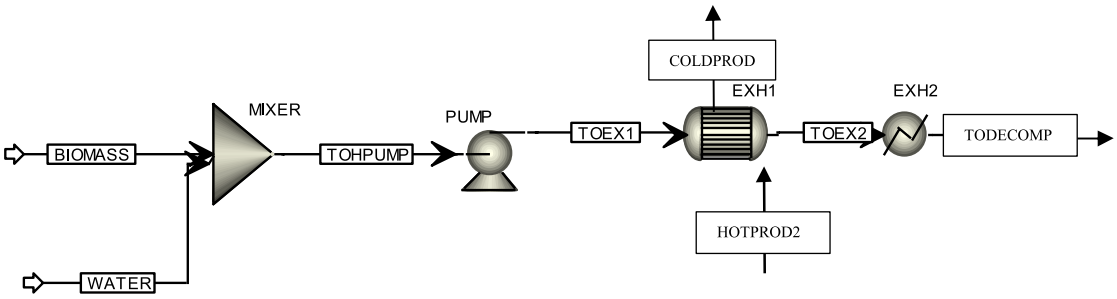

Figure 39 Pretreatment of biomass-water slurry

The next stage is the decomposition of biomass into products, which divides into dividing the biomass into model compounds, mixing the decomposed product with hydrogen, plug flow reactor sector and solid separating sector (Figure 40). The decomposition of biomass occurs in DECOMP –block, which is RYIELD –block. The RYIELD –block divides the feed into ash and model compounds of lignin, cellulose and hemicellulose. Calculator based on Excel specifies the distribution of products using the ultimate analysis of biomass and distribution of hemicellulose, cellulose and lignin content in the biomass. The plug flow reactor, REACTOR, calculates the conversion of model compounds into biocrude model compounds. The reactions occur at the temperature of 400℃ and the pressure of 30 MPa. The hot product flows to the solid separator (SOLIDSEP), which separates the solid products, i.e. char and ash, from the product flow. The SOLIDY block is used to convert char from conventional flow to solid flow.

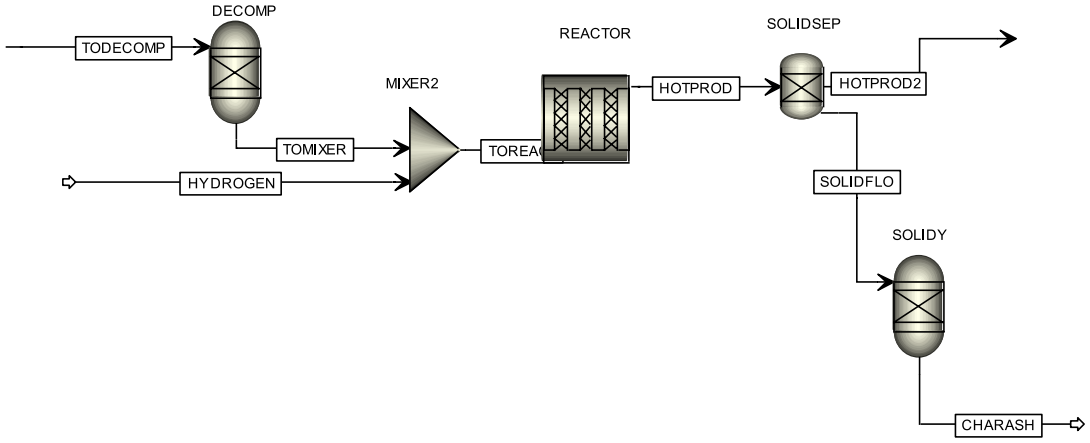

Figure 40 Hydrothermal liquefaction reactor

After solid separation, the product cools down transferring heat energy to feed stream in the recuperative heat exchanger (EXH1) and the rest of cooling required to achieve the target temperature takes place in the cooler (COOLER1). Next, the cold product goes into a depressurizing unit, where the pressure of the product decreases into the atmospheric pressure. The product divides into product gas (PRODGAS), biocrude (BIOCRUDE) and wastewater (WASTEWAT) streams in the vapor-liquid-liquid –equilibrium unit (FLASH1). The Product gas goes into condenser (FLASH12), where condensable gases condense into liquid phase (DISTIL) and non-condensing gases, i.e. EXHAUST, continue out of the process.

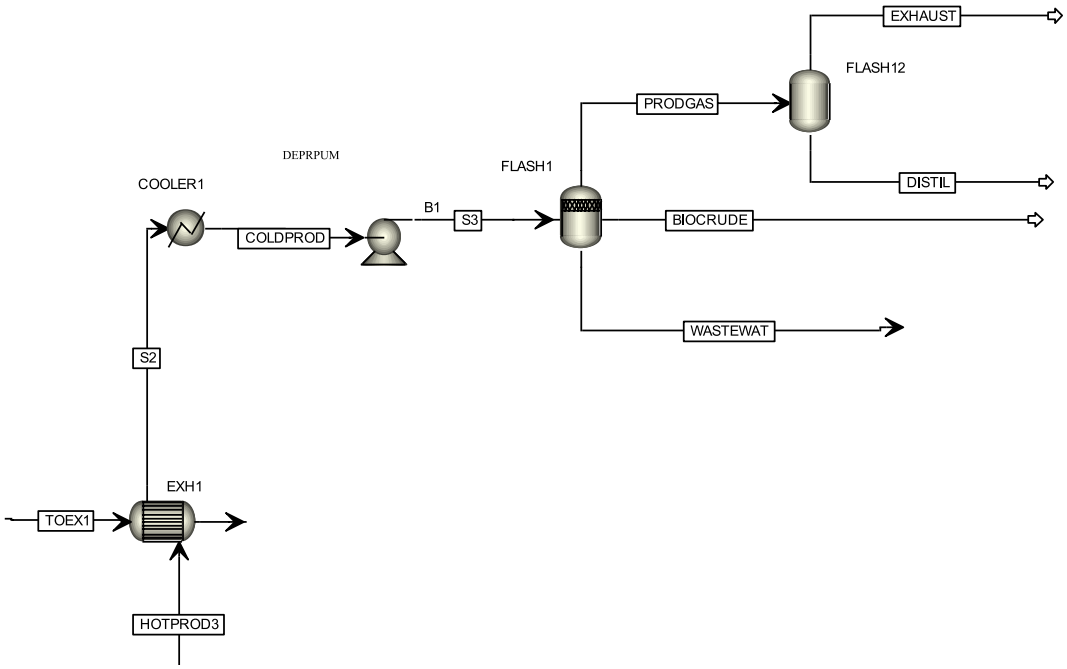

Figure 41 Cooling and depressurizing the product and vapor-liquid-liquid separation

6.4.1 Hydrothermal liquefaction reactions

The reactions and reaction kinetics in supercritical water were discussed in the paragraph 3.4, which are added to the simulation model. The paragraph 3.4 includes two different degradation pathways for lignin. The degradation pathway for lignin proposed by Yong and Matsumura (2012) did not produce reasonable results, because the degradation of lignin was too fast and the yields of biocrude was too low. The degradation pathway proposed by Forccheim et al. (2014) produced reasonable results when comparing the results with experimental results (see Chapter 7.2). For this reason, the degradation pathway proposed by Forccheim et al. (2014) was chosen to represent lignin degradation. Aspen Plus simulation tool calculates other needed data required for reaction modeling, such as fugacities of chemical compounds present in the system. The calculation is based on the selected property method.

6.4.2 Property method

The property method means the calculation method, which solves both the thermodynamic values, and the transport values in Aspen Plus (Aspen Technology Inc 2017). The choice of the right property method enables the getting of the most realistic results from the simulation model. The property method defines how Aspen Plus program calculates different properties for chemical components, such as thermodynamic and transport property methods. The most important properties for this model are vapor-liquid equilibrium (VLE) and enthalpies of different components (see Chapter 4).

The calculation of The VLE occurs via using either an equation-of-state (EoS) method or an activity coefficient method. Other thermodynamic properties depend significantly on the phase equilibrium, which why the right choice of VLE method is important. The activity coefficient method is accurate to non-ideal liquid mixtures at low pressures, which why it does not suitable for calculating supercritical liquefaction process. The EoS method enables calculations in sub- and supercritical regions, which why this type of property method is chosen for this simulation model. EoS methods are capable of calculating accurate results for ideal and nearly ideal systems, but they do not provide accurate results in highly non –ideal systems. In this situation, the predictive equation of state gives much more accurate computation results. There are several calculation methods for EOS computing, such as SRK EoS (see Chapter 4.1), predictive SRK EoS (see Chapter 4.2), and the Peng-Robinson EoS. In this case, the predictive SRK EoS determines the thermodynamic properties and transport properties of the model, because it is capable of predicting interactions between components without an experimental data.

6.4.3 Biomass

The biomass used in this case is Norway spruce. The simulation model needs ultimate analysis and proximate analysis as input to the process. The ultimate analysis needs percentages of the weights of components, i.e. C, H, N, O, S and ASH, basing on dry biomass and the moisture content in wt-%. The weight percentages of volatile matter, fixed carbon and ash are needed input data as weight percentage to the proximate analysis.The ultimate analysis determines heating values of the biomass, i.e. both HHV and LHV, and it is needed to determine the degradation products of the biomass in the supercritical water.

6.5 Model compounds

There are some challenges when modelling the degradation due to the complex structure of the lignocellulosic biomass. The cellulose, hemicellulose and lignin are modelled as cellobiose (Figure 14), xylose (Figure 23) and coniferyl alcohol (Figure 6). The degradation products of cellulose and hemicellulose in supercritical water are shown in chapters 3.4.1 and 3.4.2 and those chemical components are used as model compounds. However, the degradation products are not unambiguous for lignin, because there are undefined intermediate products (3.4.3).

7. SIMULATION MODEL RESULTS AND DISCUSSION

This chapter includes the results of case study achieved from the simulation model, which calculates the mass and energy balances of hydrothermal liquefaction reactions. The results contain a case study, where Norway spruce liquefies into the biocrude. A sensitivity analysis is used to find the optimal size of the reactor to get a high biocrude yield while keeping the reactor size as small as possible. The accuracy of the simulation model was estimated by comparing the simulation results with two experimental tests. These comparison studies used the same feedstock and reaction conditions.

7.1 Results of case study

The study includes a case study, where Norway spruce goes into the hydrothermal liquefaction process and decomposes into biocrude, gas, water-soluble products and char. The optimal reactor size is studied to achieve the high biocrude yield while keeping the reactor size as small as possible. The results include also sensitivity analysis studying the effects of different reactor temperatures on the biocrude yield.

The simulation model simulates the hydrothermal liquefaction of Norway spruce, which ultimate analysis for C, H, O and ash are 48.91 wt-%, 6.02 wt-%, 44.65 wt-% and 0.42 wt-%. The moisture content of biomass was 11.13 %. The used contents of cellulose, hemicellulose and lignin were 41.55 wt-%, 28.55 wt-% and 30.00 wt-%. The hydrothermal liquefaction reactor works at the temperature of 400 ˚C and the pressure of 30 MPa. The biocrude yield was studied with sensitivity analysis, where the yields of biocrude, char, gas and water-soluble hydrocarbons are shown as a function of time (WS) (Figure 42). There was uncertainty with the biocrude yield with short residence times (< 5 min), but after that, the yield stabilized. The yield ranged between 27.5 wt-% and 32.5 wt-% when increasing the residence times. However, increasing residence time resulted in the higher production of char and gas, which are unwanted products. The results presented below are based on the residence time of 15 minutes.

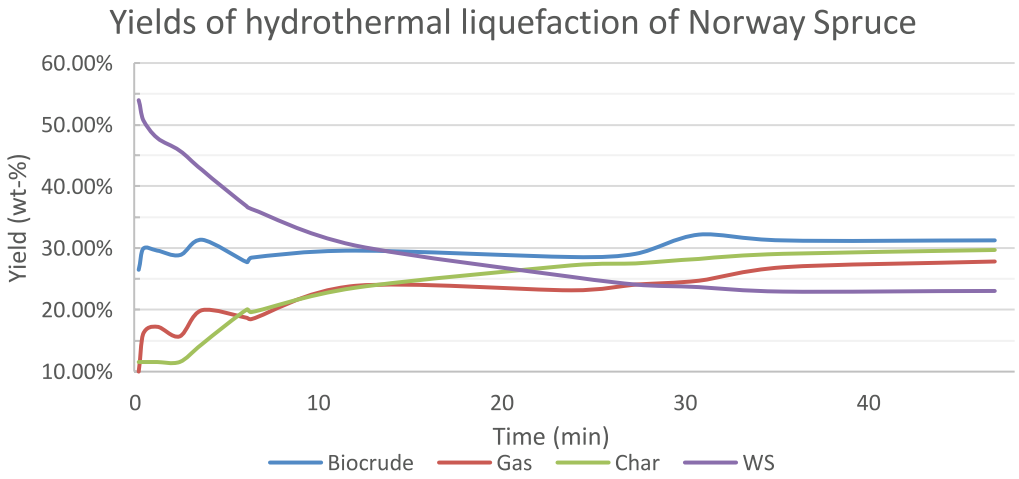

Figure 42 Model yields of hydrothermal liquefaction of Norway spruce with optimal reactor size.

Table 7 shows the simulation results of hydrothermal liquefaction of Norway spruce. The biocrude flow is 0.53 kg/sec corresponding 29.8 wt-% mass yield. The biocrude consist of various hydrocarbons, but it also contains small amounts of water, carbon monoxide and carbon dioxide. The main component in the biocrude is 2-methycyclopentaone (2-METCPE). The char and product gas flows are 0.42 kg/sec and 0.42 kg/sec. The wastewater flow is 18.75 kg/sec containing mainly water, but also small amounts of hydrocarbons and dissolved gases, such as methane and carbon monoxide.

Table 7 Mass flows of optimal reactor size

Component	BIOCRUDE	CHAR+ASH	PRODGAS	WASTEWAT
PYRUV-01	1.26E-04	0	1.38E-04	0.03
WATER	6.24E-03	0	5.95E-03	18.2
CONIFALC	2.00E-04	0	1.62E-15	0.15
FURFURAL	6.64E-09	0	5.21E-11	3.59E-09
GUAIACOL	3.41E-04	0	6.77E-08	5.33E-03
CATECHOL	2.73E-07	0	8.00E-13	7.12E-05
HYDROGEN	6.48E-10	0	1.91E-03	2.33E-07
METHANE	4.30E-06	0	1.08E-03	0.08
CO2	0.01	0	0.41	0.27
CO	5.74E-16	0	8.20E-13	3.61E-14
PHENOL	4.77E-05	0	1.70E-08	3.12E-04
O-CRESOL	6.64E-07	0	1.29E-10	7.91E-07
TOC	3.27E-05	0	5.07E-11	5.94E-03
ACETICAC	4.63E-07	0	1.58E-08	1.39E-05
ACETONE	2.58E-07	0	1.50E-07	6.56E-06
2-METCPE	0.5	0	9.42E-03	7.46E-06
ASH	0	0.42	0	0
Total Flow kg/sec	0.53	0.42	0.42	18.75

Table 8 presents the key values of the same streams as in table 5, such as mole recoveries, heating values and enthalpies. The carbon recovery, hydrogen recovery and oxygen recovery from biomass to biocrude are 44.00 mole-%, 38.12 mole-% and 10.25 mole-%. The energy recovery from biomass to biocrude was 65.63 %.

Table 8 Stream properties

Component	BIOCRUDE	CHAR+ASH	PROD-GAS	WASTEWAT
Temperature K	298.15	298.15	298.15	298.15
Volume Flow cum/sec	5.72E-04	0.00E+00	1.95E-02	1.95E-02
Enthalpy J/kmol	-2.73E+08	-	-2.86E+08	-2.86E+08
Carbon recovery (mole-%)	44.00	12.91	13.60	29.18
Hydrogen recovery mole-%)	38.12	35.85	2.71	23.32
Oxygen recovery (mole-%)	10.25	32.88	30.87	26.00
HHV (MJ/kg)	37.13	12.79	1.64	-
LHV (MJ/kg)	34.97	11.32	1.48	-
Energy recovery (%)	65.63	16.93	2.23	15.21

Table 9 and Table 10 present the results of power usage of different process components, when the biomass feed is 2 kg/sec and water feed is 18 kg/sec and the HTL reactor working at the temperature of 400 ˚C and the pressure of 30 MPa. Table 9 presents the results of case study, where the recuperative heat exchanger is used to improving the thermal efficiency. Table 10 includes the results of case study, where the recuperative heat exchanger is not used. The power consumption increases 28.24 MW without the recuperative heat exchanger significantly increasing operating costs. Similarly, the need for cooling increases the same amount as the power need.

Table 9 Power usage with the recuperative heat exchanger

Block	Description	Power need	Unit
COOLER1	Heater	-5.07	MW
DECOMP	RYield	0.31	MW
DEPPUMP	Pump	-0.72	MW
EXH1	HeatX	0.00	MW
EXH2	Heater	12.49	MW
FLASH1	Flash3	-3.85	MW
FLASH12	Flash2	-1.94E-04	MW
MIXER	Mixer	0.00	MW
MIXER2	Mixer	0.00	MW
PUMP	Pump	0.79	MW
REACTOR	RPlug	-4.44	MW
SOLIDSEP	Sep	-0.15	MW
SOLIDY	RYield	-2.44	MW
	Total need		
Electricity		13.59	MW
Cooling		-16.68	MW

Table 10 Power usage without the recuperative heat exchanger

Block	Description	Power need	Unit
COOLER1	Heater	-33.31	MW
DECOMP	RYield	0.31	MW
DUPLICER	Dupl	-0.72	MW
EXH1	HeatX	0.00	MW
EXH2	Heater	40.73	MW
FLASH1	Flash3	-3.85	MW
FLASH12	Flash2	-1.94E-04	MW
MIXER	Mixer	0.00	MW
MIXER2	Mixer	0.00	MW
PUMP	Pump	0.79	MW
REACTOR	RPlug	-4.44	MW
SOLIDSEP	Sep	-0.15	MW
SOLIDY	RYield	-2.44	MW
	Total need		
Electricity		41.83	MW
Cooling		-44.91	MW

The temperature of the system has a great influence on the biocrude yield. Figure 43 includes biocrude yields as a function of time with four different temperatures: 380 ˚C, 390 ˚C, 400 ˚C and 410 ˚C. The sensitivity analysis shows that increasing the temperature to 410 ˚C decreases the needed time to achieve the maximum biocrude yield, but prolonging the reaction time radically reduces the yield. Decreasing the temperature from 400 ˚C to 390 ˚C increases the needed time to achieve the maximum yield. However, the maximum yield is much lower when using the temperature of 380 ˚C. The reaction rates depend on the temperature of the system; increasing the temperature increases the reaction rates and decreasing the temperature decreases the reaction rates. A rapid yield decline can be explained with gasification reaction at the temperature of 410 ˚C, because the higher the temperature the higher the reaction rates of gasification reactions.

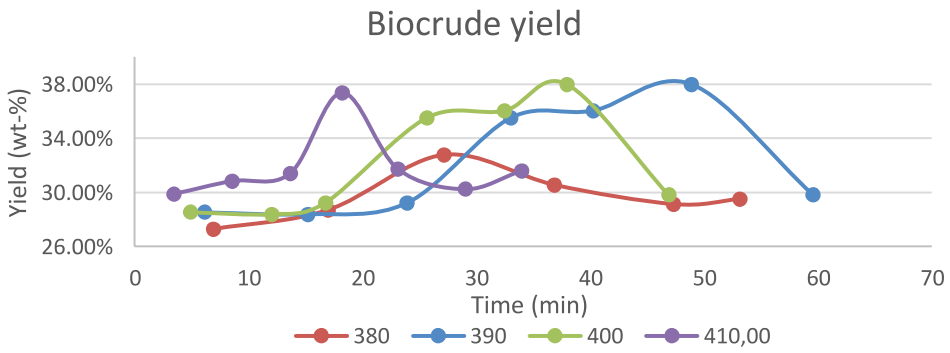

Figure 43 Biocrude yield as a function of time with four different temperatures

In conclusion, the simulation model results showed that rather short residence time, i.e. under 15 minutes, should be used with HTL reactor to achieve the optimal biocrude yield while keeping the reactor size small. Changing the reactor temperature showed that increasing the reactor temperature shortens needed time to achieve the optimal biocrude

yield. However, the yield decreases rapidly when increasing the residence time. Furthermore, there was some inaccuracy with the model results

7.2 Simulation model results comparison with experimental results

To analyze the reliability of the simulation model and needs for development, the model results are compared with existing experimental results. There are several studies related to hydrothermal liquefaction, but most of these tests have been carried out under the different conditions, i.e. subcritical water, or with catalysts.

Chan et al. (2015) studied the effects of different circumstances for the hydrothermal liquefaction of different materials. The tested materials were raw empty fruit bunch (EFB), palm mesocarp fiber (PMF) and palm kernel shell (PKS). The experimental results of different residence times of hydrothermal liquefaction of empty fruit bunch and palm kernel shell are compared with the model results (Figure 44). In experimental tests, the hydrothermal liquefaction of EFB achieved its maximum at the point of 120 min, but in the model reached the maximum after 60 min. With prolonged residence time, the biocrude yield decreased in both cases. When comparing the results of hydrothermal liquefaction of palm kernel shell with both the experiments and the model gave a better yield when the residence time was extended. However, the experimental tests achieved higher biocrude yield than the model predicted in both cases. The biocrude yield is nearly same with short residence times when testing the hydrothermal liquefaction of EFB, but with longer residence time the difference between yields increases. When studying the hydrothermal liquefaction of PKS, the difference between results obtained from experimental and model are larger compared with the EFB case. The comparison results showed that the longer residence time the higher the difference between model and experimental results when using the PKS as the feedstock to the process.

The differences in yields may be due contents of hemicellulose, lignin and extractives in the feed. The model has reaction pathways for lignin, hemicellulose and lignin, but it does not have data for hydrothermal liquefaction of extractives. This combined with the extractives content, i.e. 27.9 wt-% in the EFB and 22.9 wt-% in the PKS, lead to lower biocrude yield. The other thing, which may cause the difference in the yields, is the lignin content and its reaction pathway and reaction kinetics. The lignin contents in EFB and PKS are 18.6 wt-% and 33.5 wt-% and the difference between yields is smaller with EFB. Based on this information, the high extractives content and high lignin content increased the inaccuracy when predicting the yields of hydrothermal liquefaction of biomass.

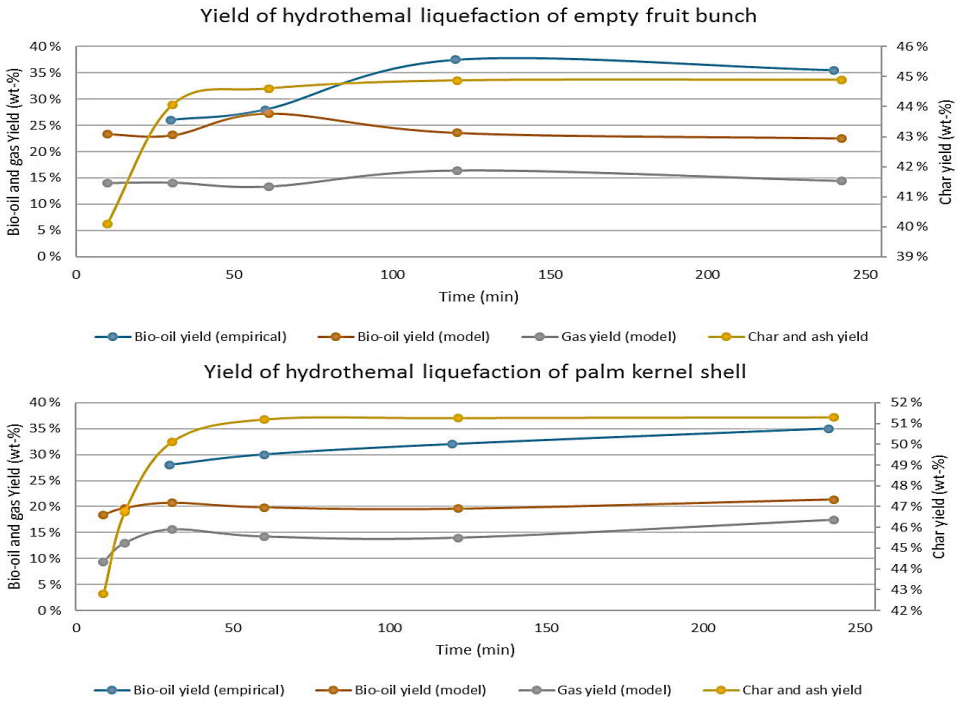

Figure 44 Experimental results of hydrothermal liquefaction of empty fruit bunch and palm kernel shell compared with model results. The empirical data is adapted from Chan et al. (2015, p. 184)

The comparison study is made in the transition region of hydrothermal liquefaction and hydrothermal gasification, i.e. slightly above the supercritical point of water. For this reason, a significant part of the input goes to product gas when using prolonged residence times. Castello et al. (2017) performed experimental tests with biomass in supercritical water. They used a variety of feed materials, such as beech sawdust and malt spent grains, in the batch reactor with long residence time (16 h) in the temperature of 400 ˚C and the pressure of 300 bar. Table 11 includes experimental results for three different reactors and model results.

Table 11 Experimental and model results of hydrothermal gasification test in the temperature of 400 ˚C and the pressure of 300 bar. The feed to process is beech sawdust. (The experimental test results are adopted from Castello et al. 2017, p. 4, 9)

	Reactor material			Model
	Inconel	Stainless steel	Ceramics	-
Gas yield (%)	32.10	33.30	34.20	20.56
Solid yield (%)	26.10	22.00	21.30	35.46
Liquid yield (%)[a]	41.40	44.70	44.50	19.28[b] 10.77[c]
Product gas HHV (MJ/kg)	8.10	8.20	10.90	7.72
Energy recovery (%)	14.50	15.05	20.50	8.61

[a] Liquid yield include both the yield water-soluble hydrocarbons and the biocrude yield
[b] the biocrude yield
[c] yield of water-soluble hydrocarbons.

The model results are achieved at the same temperature and pressure, but the residence time was shorter, max six hours, due to problems with longer residence times. However, the model yield stabilized after two hours and there were no significant changes in the yields of liquid, gas and char product. Therefore, it can be assumed that the results are almost the same although the residence time is six hours instead of 16 hours. The model predicts the char yield too high and both yields of liquid and gas too low. However, the higher heating value of produced gas is at the same level. The differences may be due to different contents of lignin, cellulose and hemicellulose, because the article did not have information on the contents of these components.

7.3 Discussion

The results included the simulation results of hydrothermal liquefaction of biomass and comparison results comparing simulation results with experimental results. The used biomass was Norway spruce. The optimal biocrude yield was studied by changing the residence time and studying its effect on biocrude yield. The temperature effect on the biocrude yield was also studied by changing the reactor temperature. The simulation model predicted biocrude yield to be around 30 wt-% when the residence time is longer than 10 minutes and the biocrude yield achieved its maximum, i.e. around 32.5 wt-%, after 30 minutes. The sensitivity study showed that increasing the temperature accelerates the reactions and the biocrude yield achieves its maximum with a shorter residence time. Decreasing temperature will prolong the required residence time to achieve the maximum biocrude yield. The needs of electricity and cooling were studied with and without the recuperative heat exchanger. It is obvious that using the recuperative heat exchanger decreases both the electric power need and the cooling need around 28 MW corresponding to a 67.5% reduction in energy demand and a 62.9% reduction in cooling demand. For this reason, it is important part of the hydrothermal liquefaction process to make it feasible. Comparing the simulation results with experimental results showed that the simulation model predicts the yields of biocrude and gas too low. However, the simulation model predicted the char formation too high.

The accuracy of the model was studied by comparing the model results with two different experimental results. The first experimental test included tests where empty fruit bunch and palm kernel shell were liquefied with various temperatures and residence times. The results of comparison showed that the model is accurate with short residence times, i.e. under 30 minutes, where the biocrude yield was nearly the same. Increasing the residence time increased the difference between the model and experimental test. The difference compared the experimental yield with model results were around 56 % with empty fruit bunch and around 85 % with palm kernel shell at its maximum. The second comparison included hydrothermal gasification experimental tests and its results, where gasification was made with beech sawdust with the residence time of 6 hours. It showed that the model

predicts the yields of biocrude and gas too low and on the contrary, the solid yield was too high. When comparing the yields of gas, solid and liquid between experimental results and model results showed that, the differences were 61.5%, -37.8% and 44.1%.

The reaction pathways and kinetics have a great influence on the yields of different products. There are several problems with the used reactions pathways. The degradation of cellulose does not take account for gasification reactions, which decreases the biocrude yield with longer residence times. The degradation studies of cellulose and hemicellulose used rather short residence times ranging from 0 to 2 seconds for cellulose and from 0 to 6 seconds for hemicellulose (Kabyemela et al. 1998; Kabyemela et al. 1999; Paksung & Matsumura 2015). Hydrothermal liquefaction reactions are rather complex, which why the proposed reaction pathways are simplified in comparison with real reactions in subcritical and supercritical water (Kabyemela et al. 1998; Kabyemela et al. 1999; Forchheim et al. 2014; Paksung & Matsumura 2015). For this reason, all of these models use model chemical compounds that represent a group of similar chemical compounds, such as total organic carbon (TOC) and aromatic hydrocarbons. Moreover, these studies had difficulties in identifying all chemical compounds found in different products; especially identifying water-soluble hydrocarbons caused problem.

The last thing, which has an effect on the biocrude yield, is the used thermodynamic calculation model. Especially the EoS (see chapters 4.1 and 4.2) influences to the different phase separation, because it determines both the separation of the component into liquid or gas and the component dissolution into polar liquid or non-polar liquid. The EoS calculation depends on the chemical compounds present in the system. As mentioned above, some of the reactions are modelled by using model compounds, which represent a group of chemical compounds. This makes it hard to determine the parameters needed to calculate the EoS. This causes inaccuracy when calculating the distribution of components to different products.

When studying the results, it is obvious that the model requires adjustment to predict the yields of different products more accurately, especially when using long residence time. Further studies should focus on making experimental tests of hydrothermal liquefaction of biomass with various residence times. These tests should include various different reaction conditions, such as pressures, temperatures and catalyst materials. Identifying the chemical compounds in products is important to provide data for reaction pathway and kinetics modelling. Another way to predict the biocrude yield is to use RYield –block in Aspen Plus, which predicts the product composition based on the experimental results. The use of RYield block should be investigated if the reaction kinetics models do not produce sufficient results.

8. CONCLUSIONS

The study shows that hydrothermal liquefaction is a promising way to convert biomass into liquid biofuel with high energy and material efficiency. The need for developing new renewable transportation fuels makes the hydrothermal liquefaction interesting technology, because the biocrude is rather similar with a fossil crude. The degradation of biomass takes place through numerous of intermediate stages, which have been studied in recent decades. However, there are still a lot of unknown quantities with reactions in sub- the supercritical water and process variables. Additionally, the biocrude cannot be directly fed into refinery process due to both high oxygen content and impurities in the biocrude.

During the study, the simulation model of hydrothermal liquefaction reactions was built with Aspen Plus –simulation program, which is controlled by an Excel spreadsheet that serves as a user interface. The user interface enables user to change different process variables, such as input material and reactor size, and to study the effects of the changes on the results. The accuracy of the model was studied by comparing the model results with experimental tests. The comparison showed that predicted yields are inaccurate, especially with longer residence times. The hydrothermal liquefaction of Norway spruce was tested with the simulation model. The case study showed that the optimal biocrude yield compared with the reactor size was obtained with the residence time of 15 minutes. In that case, the mass yield was 29.8 wt-% and the energy recovery was 65.6 %. The study showed that using the recuperative heat exchanger reduces energy requirement by 67.5 % and need for cooling by 62.9 % in comparison with the case without recuperative heat exchanger.

The first research question was “The hydrothermal liquefaction has been studied for several decades. However, the knowledge of the existing reaction pathways and kinetics are limited. How well the current knowledge can be applied to the Aspen Plus simulation software?” The literature research showed that the most existing kinetic models used simple power law models for modelling the degradation reactions of biomass in sub- and supercritical models. The adding of power law type reactions to the Aspen Plus Simulation software is rather easy, but problem arises from the reactions used in the model. The used reaction pathways are simplified versions of the real reaction pathways in sub- and supercritical water. Due this, these reaction pathways and kinetics uses model compounds to present a group of similar chemical compounds. This makes modelling chemical reactions difficult with Aspen Plus simulation software, because the simulation software needs exact reactions to model the degradation of the studied component. This problem was solved by using a chemical compound that acted on the reaction path as a so-called model component, which represents one or more chemical compounds. For example, the

model compound *Aromatic Hydrocarbon* was modelled as Benzene, but in reality, it represents several compounds, such as benzene and naphthalene. Another problem arises with the phase separation, i.e. product separation, where the gaseous products, biocrude and wastewater are separated from each other. The separation is based on the EoS, which calculates the phase separation based on the chemicals present in the phase-separation unit. The use of model compound causes inaccuracy in phase separation, because the chemical compounds in the system do not correspond to reality.

The second question was "Are there enough data related to the reaction pathways and kinetics of the hydrothermal liquefaction process available?" There are many studies relating to reactions in the sub- and the supercritical water, where the hydrothermal liquefaction of different compounds is tested in several different temperatures and pressures (Kabyemela et al. 1998; Kabyemela et al. 1999; Yong & Matsumura 2012; Forchheim et al. 2014; Paksung & Matsumura 2015). However, these studies are made by studying the decomposition of different chemical compounds separated from other chemical compounds. In this case, the interactions between other compounds remain unobserved. This leads to problem that reactions in a real process may take place differently than in these experiments. Another problem with the degradation pathways of cellulose and hemicellulose was that the used residence times were significant short, which could cause inaccuracy when using a longer residence time in the simulation model. For lignin, the complexity of its structure and decomposition are problem leading to inaccuracy in the presented lignin reaction pathways (Yong & Matsumura 2012; Forchheim et al. 2014). Overall, the existing reaction pathways are inaccurate, and they only work in a limited temperature and pressure range.

The third question was "Does the model give reasonable calculation results?" The results showed that the model predicts the biocrude yield accurate when using short residence time. Using longer residence times in the simulation model (>30 min) showed that the biocrude yield was significant low and the solid yield was excessively high in comparison with experimental results. Moreover, the model is not suitable for predicting the exact composition of biocrude, because the chemical reactions are modelled with model compounds. The concentration of the model compound is the sum of the concentrations of the chemical compounds in the chemical group, which the model compound represents.

The last question was "What issues should take account for when scaling the reactor from pilot plant size to industrial plant size?" When studying the scaling of chemical reactors showed several issues which must be taken into account when designing the reactor. The residence time is one of the most important factor when scaling the reactor, because too short or too long residence time leads to the lower biocrude yield. There are two solutions to increase the production capacity while keeping the reactor size constant. The first one is to scale the reactor dimensions and to increase the mass flow while keeping the residence time constant. The other way is to increase the mass flow and use parallel reactors. The endothermic or exothermic nature of reactions can cause changes in the temperature,

which influences into reaction rates. In this case, the changing temperature can have a significant influence on both biocrude and its composition. Using the parallel reactors makes possible to use a shell-tube design, where the reacting slurry flows in the tube and the thermal fluid flows in the shell side keeping the reaction conditions constant. However, the flow rate distribution of the flow rate across the pipes may be different resulting in a different product than desired. Creating a CFD model for the reactor is also an important part to prevent unwanted flows, such as by-bass flow and dead-spaces, and to enable steady flow in the reactor.

This study shows that the simulation model requires further research, which should include both batch tests and continuous tests. The batch tests should include experimental tests using different reaction conditions and residence times to gather the data of reactions in the sub- and the supercritical water. The results of continuous experiments can be used to develop the simulation model and to validate the simulation model. Especially, the lignin degradation is one of the most important topics for further research, because the existing degradation pathways are inaccurate. The last thing to do in further research is to validate the model when the continuous test facility is ready to use. In conclusion, the study shows that a model can be built on the basis of current knowledge. However, the model gives reliable results in conditions where the reaction kinetics have been tested.

REFERENCES

Aida, T.M., Sato, Y., Watanabe, M., Tajima, K., Nonaka, T., Hattori, H. & Arai, K. (2007). Dehydration of d-glucose in high temperature water at pressures up to 80MPa, The Journal of Supercritical Fluids, Vol. 40(3), pp. 381-388. http://www.sciencedirect.com/science/article/pii/S0896844606002117.

Akhtar, J. & Amin, N.A.S. (2011). A review on process conditions for optimum bio-oil yield in hydrothermal liquefaction of biomass, Renewable and Sustainable Energy Reviews, Vol. 15(3), pp. 1615-1624. http://www.sciencedirect.com/science/article/pii/S1364032110004235.

Alen, R., Moilanen, A. & Nieminen, M. (2002). Chapter 5: Polttoaineiden ominaisuudet ja luokittelu, in: Anonymous (ed.), Poltto ja palaminen, Teknistieteelliset akatemiat,

Anikeev, V. & Fan, M. (2014). Supercritical Fluid Technology for Energy and Environmental Applications, Elsevier, NL,

Appell, H.R., Friedman, S., Fu, Y.C., Wender, I. & Yavorsky, P.M. (1971). Converting organic wastes to oil : a replenishable energy source, USA, Available: http://hdl.handle.net/2027/mdp.39015078478008.

Aro, E. (2016). From first generation biofuels to advanced solar biofuels, Ambio, Vol. 45(Suppl 1), pp. 24-31. https://www.ncbi.nlm.nih.gov/pmc/articles/PMC4678123/.

Aspen Technology Inc (2017). Aspen Physical Property System. Physical Property Methods., Aspen Technology Inc, USA,

AspenTech Inc. Aspentechhttps://www.aspentech.com/.

Baiker, A. (1999). Supercritical fluids in heterogeneous catalysis, Chemical Reviews, Vol. 99(2), pp. 453-474. https://search.proquest.com/docview/224671902.

Bajpai, P. (2016). Structure of Lignocellulosic biomass, in: Anonymous (ed.), Pretreatment of Lignocellulosic Biomass for Biofuel Production, pp. 7-12.

Basu, P. (2013). Chapter 4 - Torrefaction, in: Anonymous (ed.), Biomass Gasification, Pyrolysis and Torrefaction (Second Edition), Academic Press, Boston, pp. 87-145.

Bazaev, A., Abdulagatov, I., Bazaev, E. & Abdurashidova, A. (2007). PVT Measurements for Pure Ethanol in the Near-Critical and Supercritical Regions, International Journal of Thermophysics, Vol. 28(1), pp. 194-219. https://link.springer.com/article/10.1007/s10765-007-0158-2.

Belgiorno, V., De Feo, G., Della Rocca, C. & Napoli, R.M.A. (2003). Energy from gasification of solid wastes, Waste Management, Vol. 23(1), pp. 1-15. http://www.sciencedirect.com/science/article/pii/S0956053X02001496.

Bell, R.P. acid–base reactionhttps://academic.eb.com/levels/collegiate/article/acidbase-reaction/110110#49255.toc.

Berge, N.D., Ro, K.S., Mao, J., Flora, J.R.V., Chappell, M.A. & Bae, S. (2011). Hydrothermal carbonization of municipal waste streams, Environmental science & technology, Vol. 45(13), pp. 5696. http://www.ncbi.nlm.nih.gov/pubmed/21671644.

Berglin, E.J., Enderlin, C.W. & Schmidt, A.J. (2012). Review and Assessment of Commercial Vendors/Options for Feeding and Pumping Biomass Slurries for Hydrothermal Liquefaction, USDOE, United States, Available: http://www.osti.gov/scitech/biblio/1056168.

Bermejo, M. & Cocero, M. (2006). Supercritical water oxidation: A technical review, American Institute of Chemical Engineers. AIChE Journal, Vol. 52(11), pp. 3933-3951. https://search.proquest.com/docview/199464097.

Berni, M., Dorileo, I., Prado, J., Forster-Carneiro, F. & Meireles, M. (2014). Advances in Biofuel Production, in: Babu, V., Thapliyal, A. & Patel, G. (ed.), Biofuels Production,

Bhaskar, T., Sera, A., Muto, A. & Sakata, Y. (2008). Hydrothermal upgrading of wood biomass: Influence of the addition of K2CO3 and cellulose/lignin ratio, Fuel, Vol. 87(10), pp. 2236-2242. http://www.sciencedirect.com/science/article/pii/S0016236107004577.

Biller, P., Sharma, B.K., Kunwar, B. & Ross, A.B. (2015). Hydroprocessing of bio-crude from continuous hydrothermal liquefaction of microalgae, Fuel, Vol. 159 pp. 197-205. http://www.sciencedirect.com/science/article/pii/S0016236115006572.

Blackwood Technology FlashTorhttp://www.blackwood-technology.com/technology/flashtor/.

Britannica Academic Izomerizationhttps://academic.eb.com/levels/collegiate/article/isomerization/42955.

Brownsort, P. (2009). Biomass Pyrolysis Processes: Review of Scope, control and variability, UK Biochar Research Centre, UK, Available: https://www.biochar.ac.uk/download.php?id=14.

Brunner, G. (2010). Applications of Supercritical Fluids, Annual Review of Chemical and Biomolecular Engineering, Vol. 1(1), pp. 321-342. http://www.ncbi.nlm.nih.gov/pubmed/22432584.

BTG Torrefactionhttp://www.btgworld.com/en/rtd/technologies/torrefaction.

Castello, D., Rolli, B., Kruse, A. & Fiori, L. (2017). Supercritical Water Gasification of Biomass in a Ceramic Reactor: Long-Time Batch Experiments, Energies, Vol. 10(11), pp. 1734. http://www.mdpi.com/1996-1073/10/11/1734.

Chan, Y.H., Yusup, S., Quitain, A.T., Tan, R.R., Sasaki, M., Lam, H.L. & Uemura, Y. (2015). Effect of process parameters on hydrothermal liquefaction of oil palm biomass for bio-oil production and its life cycle assessment, Energy Conversion and Management, Vol. 104 pp. 180-188. http://www.sciencedirect.com/science/article/pii/S0196890415002939.

Chemistry LibreTexts 11.6: Critical Temperature and Pressurehttps://chem.libretexts.org/Textbook_Maps/General_Chemistry_Textbook_Maps/Map%3A_Chemistry_(Averill_and_Eldredge)/11%3A_Liquids/11.6%3A_Critical_Temperature_and_Pressure.

Chen, H. (2014). Chemical Composition and Structure of Natural Lignocellulose, in: Anonymous (ed.), Biotechnology of Lignocellulose, Springer, Dordrecht, pp. 25-71.

Chen, W. & Kuo, P. (2011). Torrefaction and co-torrefaction characterization of hemicellulose, cellulose and lignin as well as torrefaction of some basic constituents in biomass, Energy, Vol. 36(2), pp. 803-811. http://www.sciencedirect.com/science/article/pii/S0360544210007267.

Chen, W., Peng, J. & Bi, X.T. (2015). A state-of-the-art review of biomass torrefaction, densification and applications, Renewable and Sustainable Energy Reviews, Vol. 44(Supplement C), pp. 847-866. http://www.sciencedirect.com/science/article/pii/S1364032114010910.

Cheng, X. & Schulenberg, T. (2001). Heat transfer at supercritical pressures, Als Ms gedr. ed. Forschungszentrum Karlsruhe, Karlsruhe,

Child, M. (2014). INDUSTRIAL-SCALE HYDROTHERMAL CARBONIZATION OF WASTE SLUDGE MATERIALS FOR FUEL PRODUCTION, Lappeenranta University of Technology,

Christensen, P.R., Mørup, A.J., Mamakhel, A., Glasius, M., Becker, J. & Iversen, B.B. (2014). Effects of heterogeneous catalyst in hydrothermal liquefaction of dried distillers grains with solubles, Fuel, Vol. 123 pp. 158-166. http://www.sciencedirect.com/science/article/pii/S0016236114000477.

Chumpoo, J. & Prasassarakich, P. (2010). Bio-Oil from Hydro-Liquefaction of Bagasse in Supercritical Ethanol, Energy & Fuels, Vol. 24(3), pp. 2071-2077. https://doi.org/10.1021/ef901241e.

Climate Action Tracker EU. Country Summary https://climateactiontracker.org/countries/eu/.

Cortright, R.D., Dumesic, J.A. & Davda, R.R. (2002). Hydrogen from catalytic reforming of biomass-derived hydrocarbons in liquid water, Nature, Vol. 418(6901), pp. 964-967. http://dx.doi.org/10.1038/nature01009.

Creager, S. (2007). Chapter 3: Solvents and Supporting Electrolytes, in: Zoski, C.G. (ed.), Handbook of Electrochemistry, pp. 57-72.

Crocker, M. & Andrews, R. (2010). The Rationale for Biofuels, in: Anonymous (ed.), Thermochemical Conversion of Biomass to Liquid Fuels and Chemicals, Royal Society of Chemistry, pp. 1.

Danilo Alberto Cantero Sposetti (2014). Intensification of Cellulose Hydrolysis Process by Supercritical Water. Obtaining of Added Value Products, Available: http://uva-doc.uva.es:80/handle/10324/5374.

Davda, R.R., Shabaker, J.W., Huber, G.W., Cortright, R.D. & Dumesic, J.A. (2005). A review of catalytic issues and process conditions for renewable hydrogen and alkanes by aqueous-phase reforming of oxygenated hydrocarbons over supported metal catalysts, Applied Catalysis B, Environmental, Vol. 56(1), pp. 171-186. https://www.sciencedirect.com/science/article/pii/S0926337304005077.

de Caprariis, B., De Filippis, P., Petrullo, A. & Scarsella, M. (2017). Hydrothermal liquefaction of biomass: Influence of temperature and biomass composition on the bio-oil production, Fuel, Vol. 208 pp. 618-625. http://www.sciencedirect.com/science/article/pii/S0016236117309092.

Demirbaş, A. (2009). Biofuels, Springer, London,

Demirbaş, A. (2001). Biomass resource facilities and biomass conversion processing for fuels and chemicals, Energy Conversion and Management, Vol. 42(11), pp. 1357-1378. http://www.sciencedirect.com/science/article/pii/S0196890400001370.

Dimitriadis, A. & Bezergianni, S. (2017). Hydrothermal liquefaction of various biomass and waste feedstocks for biocrude production: A state of the art review, Renewable and Sustainable Energy Reviews, Vol. 68(Part 1), pp. 113-125. http://www.sciencedirect.com/science/article/pii/S1364032116306347.

Doherty, W.O.S., Mousavioun, P. & Fellows, C.M. (2011). Value-adding to cellulosic ethanol: Lignin polymers, Industrial Crops and Products, Vol. 33(2), pp. 259-276. http://www.sciencedirect.com/science/article/pii/S0926669010002670.

Donati, G. & Paludetto, R. (1997). Scale up of chemical reactors, Catalysis Today, Vol. 34(3), pp. 483-533. http://www.sciencedirect.com/science/article/pii/S0920586196000697.

Dutta, A. & Leon, M.A. (2011). PROS AND CONS OF TORREFACTION OF WOODY BIOMASS
, https://www.agrireseau.net/references/32/presentations_guelph/2torrefaction%20-%20pros%20and%20cons%20by%20mathias%20leon%20uog.pdf.

Ebringerová, A., Hromádková, Z. & Heinze, T. (2005). Hemicellulose, in: Heinze, T. (ed.), Polysaccharides I, Springer, Berlin, Heidelberg, pp. 1-67.

Elliott, D.C., Sealock, L.J.J., Butner, R.S., Baker, E.G. & Neuenschwander, G.G. (1989). Low-temperature conversion of high-moisture biomass: Continuous reactor system results, DOE/CE, United States, Available: http://www.osti.gov/scitech/biblio/5657956.

Elliott, D.C. (2011). Hydrothermal Processing, in: Brown, R.C. (ed.), Thermochemical Processing of Biomass: Conversion into Fuels, Chemicals and Power, USDOE, United States,

Elliott, D.C., Biller, P., Ross, A.B., Schmidt, A.J. & Jones, S.B. (2015a). Hydrothermal liquefaction of biomass: Developments from batch to continuous process, Bioresource Technology, Vol. 178 pp. 147-156. http://www.sciencedirect.com/science/article/pii/S0960852414013911.

Elliott, D.C., Biller, P., Ross, A.B., Schmidt, A.J. & Jones, S.B. (2015b). Hydrothermal liquefaction of biomass: Developments from batch to continuous process, Bioresource Technology, Vol. 178 pp. 147-156. http://www.sciencedirect.com/science/article/pii/S0960852414013911.

European Commission (2016a). 2030 climate & energy framework, Climate Action - European Commission, https://ec.europa.eu/clima/policies/strategies/2030_en.

European Commission (2017a). Biomass
, European Commission, https://ec.europa.eu/energy/en/topics/renewable-energy/biomass.

European Commission (2016b). Clean Energy for All Europeans, Energy, /energy/en/topics/energy-strategy-and-energy-union/clean-energy-all-europeans.

European Commission (2017b). Developing a European energy grid - Energy - European Commission, Energy, /energy/en/topics/infrastructure/developing-european-energy-grid.

European Commission (2015). Paris Agreement
, European Commission, https://ec.europa.eu/clima/policies/international/negotiations/paris_en.

European Commission (2017c). Renewable energy. Moving towards a low carbon economy, European Commission, https://ec.europa.eu/energy/en/topics/renewable-energy.

European Commission (2011). White paper 2011 - Mobility and Transport - European Commission, Mobility and Transport, /transport/themes/strategies/2011_white_paper_en.

European Environment Agency (2017). Annex 1 — Progress towards greenhouse gas emission targets: data and methodology, European Environment Agency, https://www.eea.europa.eu/themes/climate/trends-and-projections-in-europe/trends-and-projections-in-europe-2017/annexes/annex-1.

Eurostat (2018). Complete energy balances - annual data
, http://appsso.eurostat.ec.europa.eu/.

Faeth, J.L., Valdez, P.J. & Savage, P.E. (2013). Fast Hydrothermal Liquefaction of Nannochloropsis sp. To Produce Biocrude, Energy & Fuels, Vol. 27(3), pp. 1398. https://doi.org/10.1021/ef301925d.

Fang, Z., Sato, T., Smith, R.L., Inomata, H., Arai, K. & Kozinski, J.A. (2008). Reaction chemistry and phase behavior of lignin in high-temperature and supercritical water, Bioresource Technology, Vol. 99(9), pp. 3424-3430. http://www.sciencedirect.com/science/article/pii/S0960852407006311.

Fischer, K. & Gmehling, J. (1996). Further development, status and results of the PSRK method for the prediction of vapor-liquid equilibria and gas solubilities, Fluid Phase Equilibria, Vol. 121(1), pp. 185-206. https://www.sciencedirect.com/science/article/pii/0378381295027920.

Forchheim, D., Hornung, U., Kruse, A. & Sutter, T. (2014). Kinetic Modelling of Hydrothermal Lignin Depolymerisation, Waste and Biomass Valorization, Vol. 5(6), pp. 985-994. https://link.springer.com/article/10.1007/s12649-014-9307-6.

Fortum Fortum's bio-oil plant commissioned in Joensuu - first of its kind in the worldhttps://www3.fortum.com/media/2013/11/fortums-bio-oil-plant-commissioned-joensuu-first-its-kind-world.

Gallina, G., Biasi, P., Piqueras, C.M. & García-Serna, J. (2017). Chapter 6:Processing of Lignocellulosic Biomass Derived Monomers using High-pressure CO2 and CO2–H2O Mixtures, in: Anonymous (ed.), High Pressure Technologies in Biomass Conversion, pp. 115-136.

GoBiGas GoBiGashttps://gobigas.goteborgenergi.se/English_version/Start.

Gollakota, A.R.K., Reddy, M., Subramanyam, M.D. & Kishore, N. (2016). A review on the upgradation techniques of pyrolysis oil, Renewable and Sustainable Energy Reviews, Vol. 58 pp. 1543-1568. http://www.sciencedirect.com/science/article/pii/S1364032115015634.

Gomes, F N D C, Pereira, L.R., Ribeiro, N.F.P. & Souza, M M V M (2015). PRODUCTION OF 5-HYDROXYMETHYLFURFURAL (HMF) VIA FRUCTOSE DEHYDRATION: EFFECT OF SOLVENT AND SALTING-OUT, Brazilian Journal of Chemical Engineering, Vol. 32(1), pp. 119-126. http://www.scielo.br/scielo.php?script=sci_abstract&pid=S0104-66322015000100119&lng=en&nrm=iso&tlng=en.

Goodwin, A.K. & Rorrer, G.L. (2010). Reaction rates for supercritical water gasification of xylose in a micro-tubular reactor, Chemical Engineering Journal, Vol. 163(1), pp. 10-21. http://www.sciencedirect.com/science/article/pii/S1385894710006133.

Hall, D.O. & Rao, K.K. (1999). Photosynthesis
, Sixth Edition ed. Cambridge University Press, United Kingdom,

Halstead, S.J. & Masters, A.J. (2010). A classical molecular dynamics study of the anomalous ionic product in near-critical and supercritical water, Molecular Physics, Vol. 108(2), pp. 193-203.
http://www.tandfonline.com/doi/abs/10.1080/00268971003604591.

Hammerschmidt, A., Boukis, N., Hauer, E., Galla, U., Dinjus, E., Hitzmann, B., Larsen, T. & Nygaard, S.D. (2011). Catalytic conversion of waste biomass by hydrothermal

treatment, Fuel, Vol. 90(2), pp. 555-562. http://www.sciencedirect.com/science/article/pii/S0016236110005338.

Hart, H., Craine, L.E. & Hart, D. (2002). Organic chemistry a short course
, Houghton Miffling Company, United States of America,

He, C., Chen, C., Giannis, A., Yang, Y. & Wang, J. (2014). Hydrothermal gasification of sewage sludge and model compounds for renewable hydrogen production: A review, Renewable and Sustainable Energy Reviews, Vol. 39 pp. 1127-1142.

Heiskanen, J. (2013). From concept to demonstation. Developing an advanced biofuel project.
, Fortum,

Helmenstine, A.M. Definition of Dehydration Reactionhttps://www.thoughtco.com/definition-of-dehydration-reaction-605001.

Higman, C. & van der Burgt, M. (2008). Chapter 2 - The Thermodynamics of Gasification, in: Anonymous (ed.), Gasification (Second Edition), Gulf Professional Publishing, Burlington, pp. 11-31.

Hoekman, K., Broch, A. & Robbins, C. (2011). Hydrothermal carbonization (HTC) of lignocellulosic biomass, Energy Fuels, Vol. 25 (4) pp. 1802–1810. http://pubs.acs.org/doi/abs/10.1021/ef101745n.

Hoffmann, J., Rudra, S., Toor, S.S., Holm-Nielsen, J.B. & Rosendahl, L.A. (2013). Conceptual design of an integrated hydrothermal liquefaction and biogas plant for sustainable bioenergy production, Bioresource Technology, Vol. 129 pp. 402-410. http://www.sciencedirect.com/science/article/pii/S0960852412017348.

Holderbaum, T. & Gmehling, J. (1991). PSRK: A Group Contribution Equation of State Based on UNIFAC, Fluid Phase Equilibria, Vol. 70(2), pp. 251-265. https://www.sciencedirect.com/science/article/pii/037838129185038V.

Hong, G.T. & Spritzer, M.H. (2002). Supercritical water partial oxidation
, National Renewable Energy Laboratory, USA, Available: https://www.nrel.gov/docs/fy02osti/32405a12.pdf.

Honma, T. & Inomata, H. (2014). Density functional theory study of glyceraldehyde conversion in supercritical water, The Journal of Supercritical Fluids, Vol. 90(Supplement C), pp. 1-7. http://www.sciencedirect.com/science/article/pii/S0896844614000680.

Hoogwijk, M., Faaij, A., Eickhout, B., de Vries, B. & Turkenburg, W. (2005). Potential of biomass energy out to 2100, for four IPCC SRES land-use scenarios, Biomass and Bioenergy, Vol. 29(4), pp. 225-257. https://www.sciencedirect.com/science/article/pii/S0961953405000759.

Horstmann, S., Jabłoniec, A., Krafczyk, J., Fischer, K. & Gmehling, J. (2005). PSRK group contribution equation of state: comprehensive revision and extension IV, including critical constants and α-function parameters for 1000 components, Fluid Phase Equilibria, Vol. 227(2), pp. 157-164. http://www.sciencedirect.com/science/article/pii/S0378381204005072.

Hrnčič, M.K., Kravanja, G. & Knez, Ž (2016). Hydrothermal treatment of biomass for energy and chemicals, Energy, Vol. 116(Part 2), pp. 1312-1322. http://www.sciencedirect.com/science/article/pii/S0360544216309380.

Hwang, H., Lee, J.H., Choi, I. & Choi, J.W. (ed.). 2018. Comprehensive characterization of hydrothermal liquefaction products obtained from woody biomass under various alkali catalyst concentrations. Taylor & Francis. 1-11 p.

IEA (2017). Key World Energy Statistics 2017, International Energy Agency, Key World Energy Statistics Available: http://dx.doi.org/10.1787/key_energ_stat-2016-en.

Jazrawi, C., Biller, P., Ross, A.B., Montoya, A., Maschmeyer, T. & Haynes, B.S. (2013). Pilot plant testing of continuous hydrothermal liquefaction of microalgae, Algal Research, Vol. 2(3), pp. 268-277. http://www.sciencedirect.com/science/article/pii/S2211926413000532.

Jena, U. & Das, K.C. (2011). Comparative Evaluation of Thermochemical Liquefaction and Pyrolysis for Bio-Oil Production from Microalgae, Energy & Fuels, Vol. 25(11), pp. 5482. http://dx.doi.org/10.1021/ef201373m.

Jindal, M. & Jha, M. (2015). Effect of process conditions on hydrothermal liquefaction of biomass, IJCBS Research Paper, Vol. 2(8), pp. 8-18.

Jordan, D.B., Bowman, M.J., Braker, J.D., Dien, B.S., Hector, R.E., Lee, C.C., Mertens, J.A. & Wagschal, K. (2012). Plant cell walls to ethanol, The Biochemical Journal, Vol. 442(2), pp. 241-252.

Kabyemela, B.M., Takigawa, M., Adschiri, T., Malaluan, R.M. & Arai, K. (1998). Mechanism and Kinetics of Cellobiose Decomposition in Sub- and Supercritical Water, Industrial & Engineering Chemistry Research, Vol. 37(2), pp. 357-361. http://dx.doi.org/10.1021/ie9704408.

Kabyemela, B.M., Adschiri, T., Malaluan, R.M. & Arai, K. (1999). Glucose and Fructose Decomposition in Subcritical and Supercritical Water: Detailed Reaction Pathway, Mechanisms, and Kinetics, Industrial & Engineering Chemistry Research, Vol. 38(8), pp. 2888-2895. http://dx.doi.org/10.1021/ie9806390.

Karlbrink, M. (2015). An evaluation of the Perrformance of the GoBiGas Gasification Process, Chaermelrs University of Technology,

Kim, K.H., Brown, R.C., Kieffer, M. & Bai, X. (2014). Hydrogen-Donor-Assisted Solvent Liquefaction of Lignin to Short-Chain Alkylphenols Using a Micro Reactor/Gas Chromatography System, 28, USDOE, United States, 6429-6437 p. Available: http://www.osti.gov/scitech/biblio/1158726.

Krevelen, D.W.v. (1993). Coal--typology, chemistry, physics, constitution, Netherlands,

Kruse, A. (2009). Hydrothermal biomass gasification, The Journal of Supercritical Fluids, Vol. 47(3), pp. 391-399. http://www.sciencedirect.com/science/article/pii/S0896844608003501.

Kruse, A. & Dahmen, N. (2015). Water – A magic solvent for biomass conversion, The Journal of Supercritical Fluids, Vol. 96(Supplement C), pp. 36-45. http://www.sciencedirect.com/science/article/pii/S0896844614003271.

Loudon, M. (2009). Organic Chemistry, Fifth ed.

Lu, Y., Guo, L., Zhang, X. & Yan, Q. (2007). Thermodynamic modeling and analysis of biomass gasification for hydrogen production in supercritical water, Chemical Engineering Journal, Vol. 131(1), pp. 233-244. http://www.sciencedirect.com/science/article/pii/S1385894706005079.

Matubayasi, N., Wakai, C. & Nakahara, M. (1997). Structural study of supercritical water. I. Nuclear magnetic resonance spectroscopy, The Journal of Chemical Physics, Vol. 107(21), pp. 9133-9140. http://aip.scitation.org/doi/abs/10.1063/1.478728.

McKendry, P. (2002a). Energy production from biomass (part 1): overview of biomass, Bioresource Technology, Vol. 83(1), pp. 37-46. http://www.sciencedirect.com/science/article/pii/S0960852401001183.

McKendry, P. (2002b). Energy production from biomass (part 3): gasification technologies, Bioresource Technology, Vol. 83(1), pp. 55-63. http://www.sciencedirect.com/science/article/pii/S0960852401001201.

Murti, G.W. (2017). The effect of ethanol/water on lignocellulosic biomass and cellulose liquefaction
, Universiteit Twente,

Mussatto, S.I. (2016). Biomass Pretreatment with Acids, in: Mussatto, S.I. (ed.), Biomass Fractionation Technologies for a Lignocellulosic Feedstock Based Biorefinery, Elsevier, pp. 1.

Möller, M., Nilges, P., Harnisch, F. & Schröder, U. (2011). Subcritical Water as reaction Environment: Fundamentals of Hydrothermal Biomass Transformation
, ChemSusChem, Vol. 4(5), https://onlinelibrary.wiley.com/doi/full/10.1002/cssc.201000341.

Nasri, Z. & Binous, H. (2007). Applications of the Soave–Redlich–Kwong Equation of State Using Matematica, Journal of Chemical Engineering of Japan - J CHEM ENG JPN, Vol. 40 pp. 538.

Nauman, E.B. (2008). Chemical reactor design, optimization, and scaleup, 2. ed. ed. Wiley, Hoboken, NJ,

Nazari, L., Yuan, Z., Souzanchi, S., Ray, M.B. & Xu, C.(. (2015). Hydrothermal liquefaction of woody biomass in hot-compressed water: Catalyst screening and comprehensive characterization of bio-crude oils, Fuel, Vol. 162 pp. 74-83. http://www.sciencedirect.com/science/article/pii/S0016236115008649.

Neste Oil Plc NESTE OIL's NExBTL DIESEL, Neste Oil Plc, Available: corresponding to 22.5% of total energy consumption.

NIIR Project Consultancy Services (2015). The Complete Book On Biomass Based Products (biochemicals, Biofuels, Activated Carbon) by Npcs Board Of Consultants & Engineers,

NIST (2017a). Ethane, NIST Chemisry WebBook, SRD 69, https://webbook.nist.gov/cgi/cbook.cgi?ID=C74840&Mask=4.

NIST (2017b). Methane, NIST Chemistry WebBook, SRD 69, https://webbook.nist.gov/cgi/cbook.cgi?ID=C74828&Mask=4.

NIST (2017c). Water
, NIST Chemistry WebBook, SRD 69, https://webbook.nist.gov/cgi/cbook.cgi?ID=C7732185&Mask=4.

Nunes, L.J., Matias, Joao Carlos De Oliveira & Catalao, Joao Paulo Da Silva (2017). Torrefaction of Biomass for Energy Applications : From Fundamentals to Industrial Scale, Elsevier Science, Saint Louis, 136 p.

Oasmaa, A. & Czernik, S. (1999). Fuel oil quality of biomass pyrolysis oils - state of the art for the end users, Energy and Fuels, Vol. 13(4), pp. 914-921.

Paksung, N. & Matsumura, Y. (2015). Decomposition of Xylose in Sub- and Supercritical Water, Industrial & Engineering Chemistry Research, Vol. 54(31), pp. 7604-7613. http://dx.doi.org/10.1021/acs.iecr.5b01623.

Panisko, E., Wietsma, T., Lemmon, T., Albrecht, K. & Howe, D. (2015). Characterization of the aqueous fractions from hydrotreatment and hydrothermal liquefaction of lignocellulosic feedstocks, Biomass and Bioenergy, Vol. 74 pp. 162-171. https://www.sciencedirect.com/science/article/pii/S0961953415000124.

Pedersen, T.H., Jensen, C.U., Sandström, L. & Rosendahl, L.A. (2017a). Full characterization of compounds obtained from fractional distillation and upgrading of a HTL biocrude, Applied Energy, Vol. 202 pp. 408-419. https://www.sciencedirect.com/science/article/pii/S030626191730733X.

Pedersen, T.H. (2016). HydroThermal Liquefaction of Biomass and Model Compounds, http://vbn.aau.dk/en/publications/hydrothermal-liquefaction-of-biomass-and-model-compounds(d11becba-5f60-4a8a-a38d-d16cbece0e6b).html.

Pedersen, T.H., Hansen, N.H., Pérez, O.M., Cabezas, D.E.V. & Rosendahl, L.A. (2017b). Renewable hydrocarbon fuels from hydrothermal liquefaction: A techno-economic analysis, Biofuels, Bioproducts and Biorefining, pp. n/a. http://onlinelibrary.wiley.com/doi/10.1002/bbb.1831/abstract.

Pedersen, T.H., Jasiūnas, L., Casamassima, L., Singh, S., Jensen, T. & Rosendahl, L.A. (2015). Synergetic hydrothermal co-liquefaction of crude glycerol and aspen wood, Energy Conversion and Management, Vol. 106 pp. 886-891. http://www.sciencedirect.com/science/article/pii/S0196890415009395.

Pedersen, T.H. & Rosendahl, L.A. (2015). Production of fuel range oxygenates by supercritical hydrothermal liquefaction of lignocellulosic model systems, Biomass and Bioenergy, Vol. 83 pp. 206-215. http://www.sciencedirect.com/science/article/pii/S0961953415301045.

Penttilä, K. (2011). EOS/GCM Models With ChemSheet
, Equations-of-State models in ChemApp/ChemSheet, a Fluent-KilnSimulink, and a metallurgical process simulation tool based on SimuSage,

Peterson, A.A., Vogel, F., Lachance, R.P., Fröling, M., Antal, J., Michael J & Tester, J.W. (2008). Thermochemical biofuel production in hydrothermal media: A review of sub- and supercritical water technologies, Energy & Environmental Science, Vol. 1(1), pp. 32-65. http://publications.lib.chalmers.se/publication/72770-thermochemical-biofuel-production-in-hydrothermal-media-a-review-of-sub-and-supercritical-water-tech.

Pioro, I. & Mokry, S. (2011). Thermophysical Properties at Critical and Supercritical Conditions, in: Anonymous (ed.), Heat Transfer - Theoretical Analysis, Experimental Investigations and Industrial Systems, pp. 573-592.

Puig-Arnavat, M., Bruno, J.C. & Coronas, A. (2010). Review and analysis of biomass gasification models, Renewable and Sustainable Energy Reviews, Vol. 14(9), pp. 2841-2851. http://www.sciencedirect.com/science/article/pii/S1364032110002108.

Qian, Y., Zuo, C., Tan, J. & He, J. (2007). Structural analysis of bio-oils from sub-and supercritical water liquefaction of woody biomass, Energy, Vol. 32(3), pp. 196-202. http://www.sciencedirect.com/science/article/pii/S0360544206000946.

Qu, Y., Wei, X. & Zhong, C. (2003). Experimental study on the direct liquefaction of Cunninghamia lanceolata in water, Energy, Vol. 28(7), pp. 597-606. http://www.sciencedirect.com/science/article/pii/S0360544202001780.

Reid, R., Praushnitz, J. & Poling, B. (ed.). 1987. The properties of Gases & Liquids. Fourth Edition ed. The United State of America, McGraw-Hill Inc.

Reimer, J., Peng, G., Viereck, S., De Boni, E., Breinl, J. & Vogel, F. (2016). A novel salt separator for the supercritical water gasification of biomass, The Journal of Supercritical Fluids, Vol. 117 pp. 113-121. http://www.sciencedirect.com/science/article/pii/S0896844616301747.

Rodgers, T. (2013). Chemical Reaction Engineering, UK,

Rosen, A. (2017). Reactor Design,

Sasaki, M., Adschiri, T. & Arai, K. (2004). Kinetics of cellulose conversion at 25 MPa in sub- and supercritical water, AIChE Journal, Vol. 50(1), pp. 192-202. http://onlinelibrary.wiley.com/doi/10.1002/aic.10018/abstract.

Sasaki, M., Fang, Z., Fukushima, Y., Adschiri, T. & Arai, K. (2000). Dissolution and Hydrolysis of Cellulose in Subcritical and Supercritical Water, Industrial & Engineering Chemistry Research, Vol. 39(8), pp. 2883-2890. http://dx.doi.org/10.1021/ie990690j.

Sasaki, M., Furukawa, M., Minami, K., Adschiri, T. & Arai, K. (2002). Kinetics and Mechanism of Cellobiose Hydrolysis and Retro-Aldol Condensation in Subcritical and Supercritical Water, Industrial & Engineering Chemistry Research, Vol. 41(26), pp. 6642-6649. http://dx.doi.org/10.1021/ie020326b.

Sasaki, M., Goto, M. & Wahyudiono (2008). Recovery of phenolic compounds through the decomposition of lignin in near and supercritical water, Chemical Engineering and Processing: Process Intensification, Vol. 47(9), pp. 1609-1619. http://www.sciencedirect.com/science/article/pii/S0255270107002905.

Sato, T., Sekiguchi, G., Saisu, M., Watanabe, M., Adschiri, T. & Arai, K. (2002). Dealkylation and Rearrangement Kinetics of 2-Isopropylphenol in Supercritical Water, Industrial & Engineering Chemistry Research, Vol. 41(13), pp. 3124-3130. https://doi.org/10.1021/ie010763a.

Schmieder, H., Abeln, J., Boukis, N., Dinjus, E., Kruse, A., Kluth, M., Petrich, G., Sadri, E. & Schacht, M. (2000). Hydrothermal gasification of biomass and organic wastes, The Journal of Supercritical Fluids, Vol. 17(2), pp. 145-153. https://www.sciencedirect.com/science/article/pii/S0896844699000510.

Schubert, M., Regler, J.W. & Vogel, F. (2010). Continuous salt precipitation and separation from supercritical water. Part 1: Type 1 salts, The Journal of Supercritical Fluids, Vol. 52(1), pp. 99-112. http://www.sciencedirect.com/science/article/pii/S0896844609003246.

Shuna Cheng, Ian D'cruz, Mingcun Wang, Mathew Leitch & Chunbao (Charles) Xu (2010). Highly Efficient Liquefaction of Woody Biomass in Hot-Compressed Alcohol−Water Co-solvents, Energy & Fuels, Vol. 24(9), pp. 4659-4667. https://doi.org/10.1021/ef901218w.

Singh, A., Olsen, S.I. & Nigam, P.S. (2011). A viable technology to generate third-generation biofuel, Journal of Chemical Technology & Biotechnology, Vol. 86(11), pp. 1349-1353. http://onlinelibrary.wiley.com/doi/10.1002/jctb.2666/abstract.

Soderber, T. 13.3: Aldol reactionshttps://chem.libretexts.org/Textbook_Maps/Organic_Chemistry_Textbook_Maps/Map%3A_Organic_Chemistry_with_a_Biological_Emphasis_(Soderberg)/13%3A_Reactions_with_stabilized_carbanion_intermediates_I/13.3%3A_Aldol_reactions.

Su, C. (2012). Prediction of volumetric properties of carbon dioxide-expanded organic solvents using the Predictive Soave–Redlich–Kwong (PSRK) equation of state, The Journal of Supercritical Fluids, Vol. 72(Supplement C), pp. 223-231. http://www.sciencedirect.com/science/article/pii/S089684461200294X.

Suehiro, Y., Nakajima, M., Yamada, K. & Uematsu, M. (1996). Critical parameters of {xCO2 +(1−x)CHF3} for x=(1.0000, 0.7496, 0.5013, and 0.2522), J. Chem. Thermodynamics, (28), pp. 1153-1164. https://ac.els-cdn.com/S0021961496901019/1-s2.0-S0021961496901019-main.pdf?_tid=c1625a34-ccad-45b3-9b2b-10e1b83d6a82&acdnat=1521787993_bee79144c25db92400c6dfb1d4cb707a.

Sun, P., Heng, M., Sun, S. & Chen, J. (2010). Direct liquefaction of paulownia in hot compressed water: Influence of catalysts, Energy, Vol. 35(12), pp. 5421-5429. http://www.sciencedirect.com/science/article/pii/S0360544210003695.

Susastriawan, A.A.P. & Saptoadi, H. (2017). Small-scale downdraft gasifiers for biomass gasification: A review, Renewable and Sustainable Energy Reviews, Vol. 76(Supplement C), pp. 989-1003. http://www.sciencedirect.com/science/article/pii/S1364032117304471.

Tekin, K. & Karagöz, S. (2013). Non-catalytic and catalytic hydrothermal liquefaction of biomass, Research on Chemical Intermediates, Vol. 39(2), pp. 485-498. https://link.springer.com/article/10.1007/s11164-012-0572-3.

Tews, I.J., Zhu, Y., Drennan, C., Elliott, D.C., Snowden-Swan, L.J., Onarheim, K., Solantausta, Y. & Beckman, D. (2014). Biomass Direct Liquefaction Options. TechnoEconomic and Life Cycle Assessment, USDOE, United States, Available: http://www.osti.gov/scitech/biblio/1184983.

Tolonen, L. (2016). Subcritical and Supercritical Water as a Cellulose Solvent , Aalto University,

Toor, S.S., Rosendahl, L. & Rudolf, A. (2011). Hydrothermal liquefaction of biomass: A review of subcritical water technologies, Energy, Vol. 36(5), pp. 2328-2342. http://www.sciencedirect.com/science/article/pii/S0360544211001691.

Tran, K., Klemsdal, A.J., Zhang, W., Sandquist, J., Wang, L. & Skreiberg, Ø (2017). Fast Hydrothermal Liquefaction of Native and Torrefied Wood, Energy Procedia, Vol. 105 pp. 218-223. http://www.sciencedirect.com/science/article/pii/S1876610217303399.

Tran, K., Trinh, T.N. & Bach, Q. (2016). Development of a biomass torrefaction process integrated with oxy-fuel combustion, Bioresource Technology, Vol. 199(Supplement C), pp. 408-413. http://www.sciencedirect.com/science/article/pii/S0960852415012122.

Tsou, Y.M., Trachtenberg, I., Johnston, K.P., Bard, A.J. & Flarsheim, W.M. (1986). ELECTROCHEMISTRY IN NEAR-CRITICAL AND SUPERCRITICAL FLUIDS .3. STUDIES OF BR-, I-, AND HYDROQUINONE IN AQUEOUS-SOLUTIONS, Journal of Physical Chemistry, Vol. 90 pp. 3857-3862.

Tzanetis, K.F., Posada, J.A. & Ramirez, A. (2017). Analysis of biomass hydrothermal liquefaction and biocrude-oil upgrading for renewable jet fuel production: The impact of reaction conditions on production costs and GHG emissions performance, Renewable Energy, Vol. 113 pp. 1388-1398. http://www.sciencedirect.com/science/article/pii/S0960148117306080.

Valle, L.D., Passamani, G., Rada, E.C., Torretta, V. & Ciudin, R. (2017). Unconventional Reducing Gases Monitoring in Everyday Places, Energy Procedia, Vol. 119 pp. 3-9. http://www.sciencedirect.com/science/article/pii/S187661021732581X.

Vanholme, R., Demedts, B., Morreel, K., Ralph, J. & Boerjan, W. (2010). Lignin Biosynthesis and Structure, Plant Physiology, Vol. 153(3), pp. 895-905. http://www.jstor.org/stable/25704925.

Vardon, D.R., Sharma, B.K., Scott, J., Yu, G., Wang, Z., Schideman, L., Zhang, Y. & Strathmann, T.J. (2011). Chemical properties of biocrude oil from the hydrothermal liquefaction of Spirulina algae, swine manure, and digested anaerobic sludge, Bioresource Technology, Vol. 102(17), pp. 8295-8303. http://www.sciencedirect.com/science/article/pii/S0960852411008686.

Veses, A., Aznar, M., Martínez, I., Martínez, J.D., López, J.M., Navarro, M.V., Callén, M.S., Murillo, R. & García, T. (2014). Catalytic pyrolysis of wood biomass in an auger reactor using calcium-based catalysts, Bioresource Technology, Vol. 162 pp. 250-258. http://www.sciencedirect.com/science/article/pii/S0960852414004519.

Viljava, T. (2011). FROM BIOMASS TO FUELS: HYDROTREATING OF OXYGEN- CONTAINING FEEDS ON A CoMo/Al2O3 HYDRODESULFURIZATION CATALYST, Helsinki University of Technology, Available: https://aalto-doc.aalto.fi:443/handle/123456789/2367.

Warnecke, R. (2000). Gasification of biomass: comparison of fixed bed and fluidized bed gasifier, Biomass and Bioenergy, Vol. 18(6), pp. 489-497. http://www.sciencedirect.com/science/article/pii/S096195340000009X.

World Energy Council (2016). World Energy Resources. Bioenergy 2016 , World Energy Council, Available: https://www.worldenergy.org/wp-content/uploads/2017/03/WEResources_Bioenergy_2016.pdf.

Xiu, S. & Shahbazi, A. (2012). Bio-oil production and upgrading research: A review, Renewable and Sustainable Energy Reviews, Vol. 16(7), pp. 4406-4414.

Xu, C. & Etcheverry, T. (2008). Hydro-liquefaction of woody biomass in sub- and super-critical ethanol with iron-based catalysts, Fuel, Vol. 87(3), pp. 335-345. http://www.sciencedirect.com/science/article/pii/S0016236107002268.

Yakaboylu, O., Harinck, J., Smit, K.G. & Jong, W. (2015). Supercritical Water Gasification of Biomass: A Literature and Technology Overview, Energies, Vol. 8 pp. 859-894.

Yakaboylu, O., Yapar, G., Recalde, M., Hanrinck, J., Smit, K.G., Martelli, E. & de Jong, W. (2015). Supercritical Water Gasification of Biomass: An Integrated Kinetic Model For the Prediction of Product Compounds, Industrial & Engineering Chemistry Research, Vol. 54 pp. 150818120455002.

Yaman, S. (2004). Pyrolysis of biomass to produce fuels and chemical feedstocks, Energy Conversion and Management, Vol. 45(5), pp. 651-671. http://www.sciencedirect.com/science/article/pii/S0196890403001778.

Yeo, Y.K. (2017). Chemical Engineering Computation with MATLAB®, CRC Press, Milton, UNITED KINGDOM,

Yin, S., Dolan, R., Harris, M. & Tan, Z. (2010). Subcritical hydrothermal liquefaction of cattle manure to bio-oil: Effects of conversion parameters on bio-oil yield and characterization of bio-oil, Bioresource Technology, Vol. 101(10), pp. 3657-3664. http://www.sciencedirect.com/science/article/pii/S0960852409017234.

Yong, T.L. & Matsumura, Y. (2012). Reaction Kinetics of the Lignin Conversion in Supercritical Water, Industrial & Engineering Chemistry Research, Vol. 51(37), pp. 11975-11988. http://dx.doi.org/10.1021/ie300921d.

Yu, J., Biller, P., Mamahkel, A., Klemmer, M., Becker, J., Glasius, M. & Brummerstedt Iversen, B. (2017). Catalytic hydrotreatment of bio-crude produced from the hydrothermal liquefaction of aspen wood: a catalyst screening and parameter optimization study, Sustainable Energy & Fuels, Vol. 1(4), pp. 832-841. http://pubs.rsc.org/en/Content/ArticleLanding/2017/SE/C7SE00090A.

Zakzeski, J., Bruijnincx, P., L Jongerius, A. & Weckhuysen, B. (2010). The Catalytic Valorization of Lignin for the Production of Renewable Chemicals, 99 p.

Zhang, B., von Keitz, M. & Valentas, K. (2009). Thermochemical liquefaction of high-diversity grassland perennials, Journal of Analytical and Applied Pyrolysis, Vol. 84(1), pp. 18-24. http://www.sciencedirect.com/science/article/pii/S016523700800123X.

Zhong, C. & Wei, X. (2004). A comparative experimental study on the liquefaction of wood, Energy, Vol. 29(11), pp. 1731-1741. http://www.sciencedirect.com/science/article/pii/S0360544204001768.

Zhu, Z., Rosendahl, L.A., Toor, S.S. & Chen, G. (2018). Optimizing the conditions for hydrothermal liquefaction of barley straw for bio-crude oil production using response surface methodology, Science of the Total Environment, http://vbn.aau.dk/en/publications/optimizing-the-conditions-for-hydrothermal-liquefaction-of-barley-straw-for-biocrude-oil-production-using-response-surface-methodology(f7c11298-8ecb-4f3a-84e7-f00b6f63b3c3).html.

Zumdahl, S. (2009). Chemical Kinetics
, in: Anonymous (ed.), Chemical principles, Sixth Edition ed., Brooks/Cole, United States of America, pp. 714-776.

APPENDIX A: STRUCTURES OF HEMICELLULOSE

The structures are adapted from Jordan et al. (2012, p. 242).

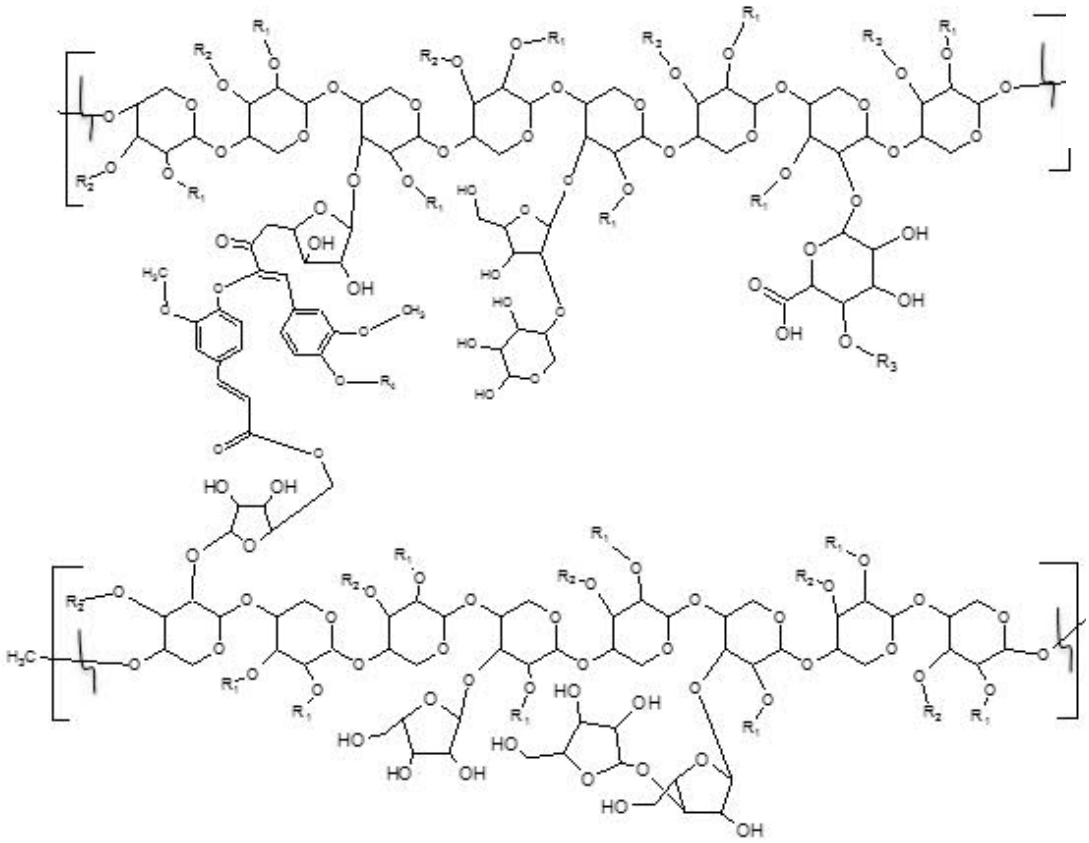

Xylan (beta1,4-Xyl)
R1 = H-, alpha-GlcA (4-Me)-, alpha-Ara or Ac-
R2 = H-, alpha-Ara or Ac-
R3 = (4-O-Me)GlcAp-alpha-(1,2)-Xylp or
(4-OH)GlcAp-alpha-(1,2)-Xylp
R4 = Lignin

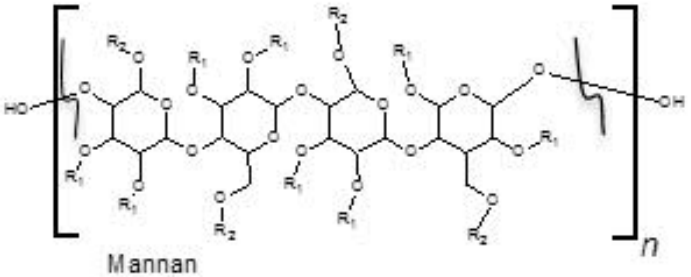

Mannan
(beta1,4-Man)
R1 = H- or Ac-
R2 = H- or alpha-Gal

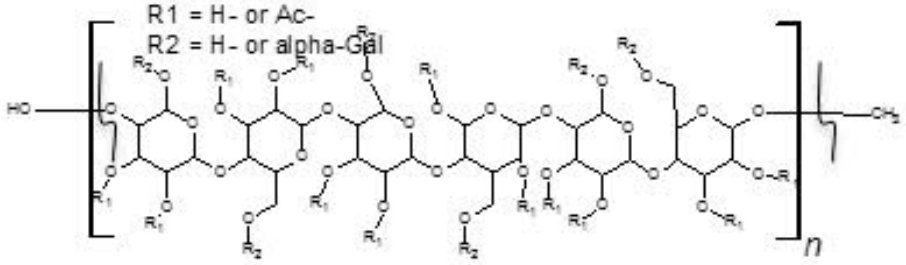

Glucomannan
(beta1,4-Man-beta1,4
-Glc)
R1 = H- or Ac-
R2 = H- or alpha-Gal

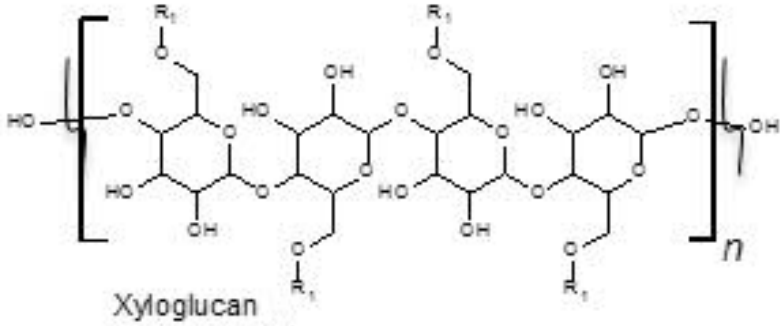

Xyloglucan
(beta-1,4-Glc)
R1 = H- or alpha-Xyl

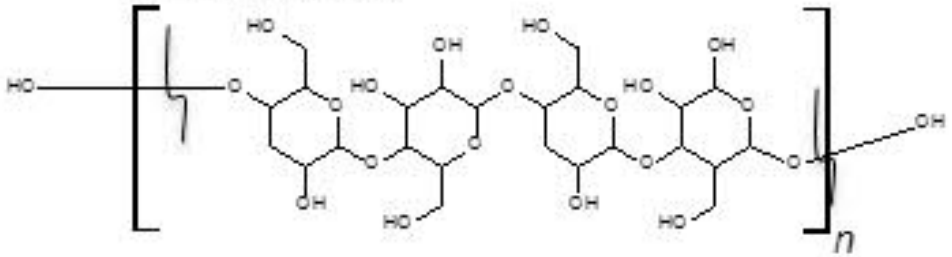

Mixed-linkake
beta-Gucan
(beta1,4-beta-1,3-Glc)

APPENDIX B: STRUCTURE OF LIGNIN

The structure of lignin is adapted from Zakzeski et al. (2010, p. 3555)

Softwood

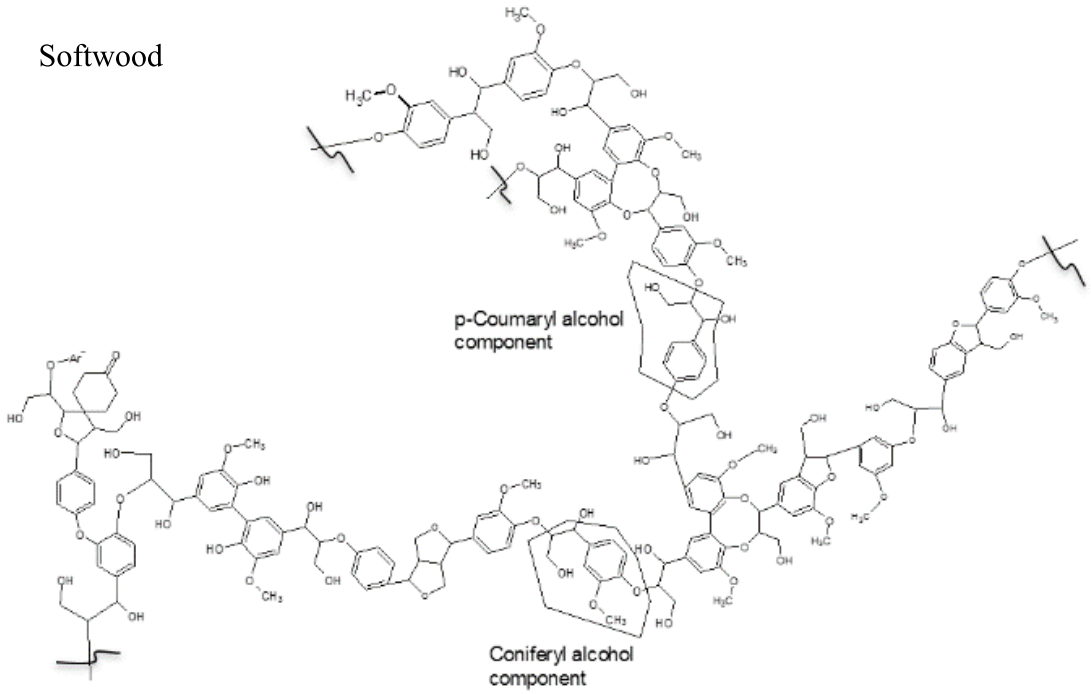

Hardwood

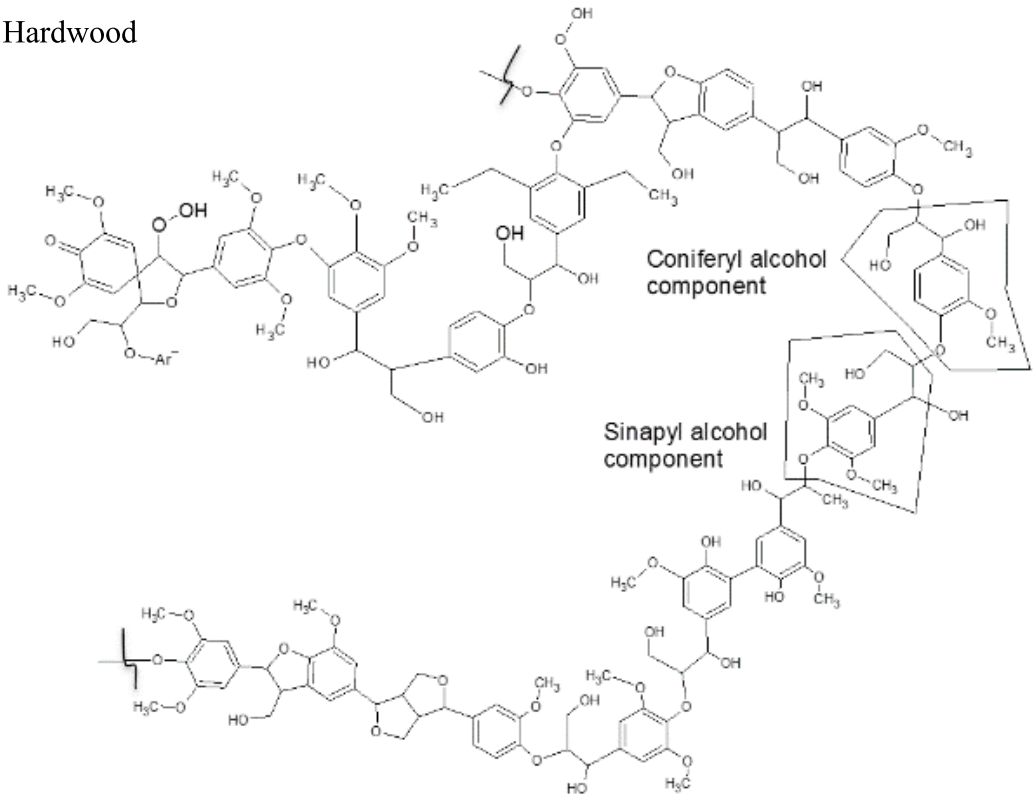

APPENDIX C: THE PROCESS FLOW CHART

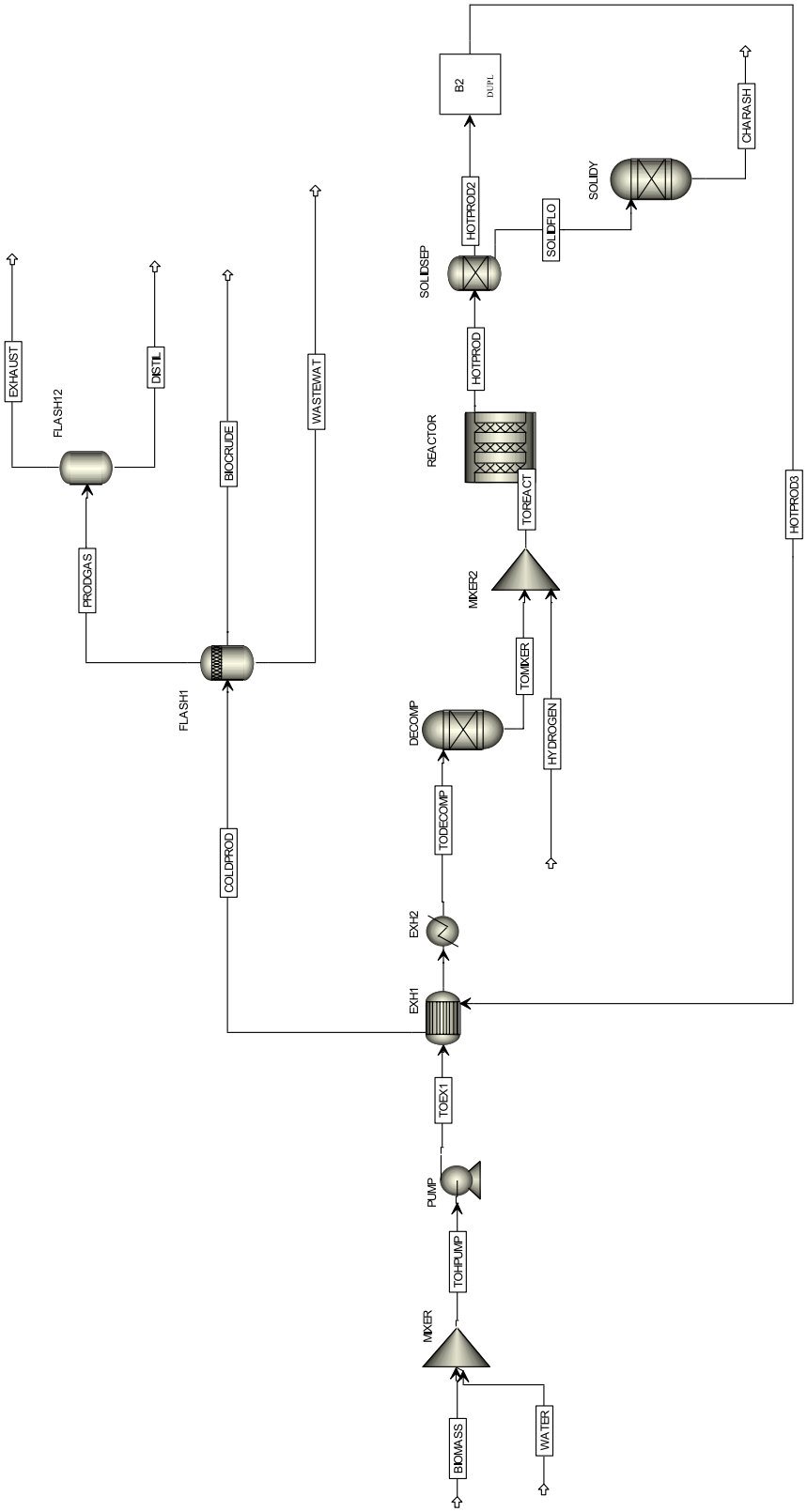

APPENDIX D: STREAM RESULTS OF THE MODEL

Component	BIOCRUDE	BIOMASS	CHARASH	COLDPROD	DISTIL	EXHAUST	HOTPROD	HOTPROD2	HOTPROD3	HOTPRODT	HYDROGEN	PRODGAS	S1	S3	SOLIDFIO	TODECOMP	TOEX1	TOEX2	TOHPUMP	TOMIXER	TOREACT	WASTEWAT	WATER
CELLOBIO	0	0	0	0	0	0	0	0	0	0	0	0	0	0	0	0	0	0	0	0,7	0,7	0	0
GLUCOSE	0	0	0	0	0	0	0	0	0	0	0	0	0	0	0	0	0	0	0	0	0	0	0
FRUCTOSE	0	0	0	0	0	0	0	0	0	0	0	0	0	0	0	0	0	0	0	0	0	0	0
GLYCOALD	0	0	0	0	0	0	0	0	0	0	0	0	0	0	0	0	0	0	0	0	0	0	0
GLUCERYT	0	0	0	0	0	0	0	0	0	0	0	0	0	0	0	0	0	0	0	0	0	0	0
GLUCGLYC	0	0	0	0	0	0	0	0	0	0	0	0	0	0	0	0	0	0	0	0	0	0	0
ERYTHROS	0	0	0	0	0	0	0	0	0	0	0	0	0	0	0	0	0	0	0	0	0	0	0
1,6-ANHY	0	0	0	0	0	0	0	0	0	0	0	0	0	0	0	0	0	0	0	0	0	0	0
PYRUV-01	1,26E-04	0	0	0,03	0	1,38E-04	0,03	0,03	0,03	0,03	0	1,38E-04	0,03	0,03	0	0	0	0	0	0	0	0,03	0
DIHYDACE	0	0	0	0	0	0	0	0	0	0	0	0	0	0	0	0	0	0	0	0	0	0	0
WATER	6,24E-03	0	0	18,2	0	5,95E-03	18,2	18,2	18,2	18,2	0	5,95E-03	18,2	18,2	0	18,0	18,0	18,0	18,0	18,0	18,0	18,2	18,0
XYLOSE	0	0	0	0	0	0	0	0	0	0	0	0	0	0	0	0	0	0	0	0,5	0,5	0	0
CONIFALC	2,00E-04	0	0	0,1	0	0	0,1	0,1	0,1	0,1	0	1,62E-15	0,1	0,1	0	0	0	0	0	0,5	0,5	0,1	0
CLYCALDE	0	0	0	0	0	0	0	0	0	0	0	0	0	0	0	0	0	0	0	0	0	0	0
XYLULOSE	0	0	0	0	0	0	0	0	0	0	0	0	0	0	0	0	0	0	0	0	0	0	0
FURFURAL	6,64E-09	0	0	1,03E-08	0	5,21E-11	1,03E-08	1,03E-08	1,03E-08	1,03E-08	0	5,21E-11	1,03E-08	1,03E-08	0	0	0	0	0	0	0	3,59E-09	0
FORMALDE	0	0	0	0	0	0	0	0	0	0	0	0	0	0	0	0	0	0	0	0	0	0	0
GUAIACOL	3,41E-04	0	0	5,67E-03	0	6,77E-08	5,67E-03	5,67E-03	5,67E-03	5,67E-03	0	6,77E-08	5,67E-03	5,67E-03	0	0	0	0	0	0	0	5,33E-03	0
CATECHOL	2,73E-07	0	0	7,15E-05	0	8,00E-13	7,15E-05	7,15E-05	7,15E-05	7,15E-05	0	8,00E-13	7,15E-05	7,15E-05	0	0	0	0	0	0	0	7,12E-05	0
HYDROGEN	6,48E-10	0	0	1,91E-03	0	1,91E-03	1,91E-03	1,91E-03	1,91E-03	1,91E-03	1,01E-03	1,91E-03	1,91E-03	1,91E-03	0	0	0	0	0	0	1,01E-03	2,33E-07	0
METHANE	4,30E-06	0	0	0,08	0	1,08E-03	0,08	0,08	0,08	0,08	0	1,08E-03	0,08	0,08	0	0	0	0	0	0	0	0,08	0
CO2	0,01	0	0	0,7	0	0,4	0,7	0,7	0,7	0,7	0	0,4	0,7	0,7	0	0	0	0	0	0	0	0,3	0
CO	5,74E-16	0	0	8,57E-13	0	8,20E-13	8,57E-13	8,57E-13	8,57E-13	8,57E-13	0	8,20E-13	8,57E-13	8,57E-13	0	0	0	0	0	0	0	3,61E-14	0
PHENOL	4,77E-05	0	0	3,60E-04	0	1,70E-08	3,60E-04	3,60E-04	3,60E-04	3,60E-04	0	1,70E-08	3,60E-04	3,60E-04	0	0	0	0	0	0	0	3,12E-04	0
O-CRESOL	6,64E-07	0	0	1,46E-06	0	1,29E-10	1,46E-06	1,46E-06	1,46E-06	1,46E-06	0	1,29E-10	1,46E-06	1,46E-06	0	0	0	0	0	0	0	7,91E-07	0
M-CRESOL	0	0	0	0	0	0	0	0	0	0	0	0	0	0	0	0	0	0	0	0	0	0	0
TOC	3,27E-05	0	0	5,97E-03	0	5,07E-11	5,97E-03	5,97E-03	5,97E-03	5,97E-03	0	5,07E-11	5,97E-03	5,97E-03	0	0	0	0	0	0	0	5,94E-03	0
AROMHYDC	0	0	0	0	0	0	0	0	0	0	0	0	0	0	0	0	0	0	0	0	0	0	0
C2H2	0	0	0	0	0	0	0	0	0	0	0	0	0	0	0	0	0	0	0	0	0	0	0
C2H4	0	0	0	0	0	0	0	0	0	0	0	0	0	0	0	0	0	0	0	0	0	0	0
C2H6	0	0	0	0	0	0	0	0	0	0	0	0	0	0	0	0	0	0	0	0	0	0	0
METHANOL	0	0	0	0	0	0	0	0	0	0	0	0	0	0	0	0	0	0	0	0	0	0	0
CHARUG	0	0	0	0	0	0	0	0	0	0	0	0	0	0	0	0	0	0	0	0	0	0	0
CHARAROM	0	0	0	0	0	0	0	0	0	0	0	0	0	0	0	0	0	0	0	0	0	0	0
CHARPHEN	0	0	0	0	0	0	0	0	0	0	0	0	0	0	0	0	0	0	0	0	0	0	0
CHARTOC	0	0	0	0	0	0	0	0	0	0	0	0	0	0	0	0	0	0	0	0	0	0	0
ACETICAC	4,63E-07	0	0	1,44E-05	0	1,58E-08	1,44E-05	1,44E-05	1,44E-05	1,44E-05	0	1,58E-08	1,44E-05	1,44E-05	0	0	0	0	0	0	0	1,39E-05	0
LACTICAC	0	0	0	0	0	0	0	0	0	0	0	0	0	0	0	0	0	0	0	0	0	0	0
ACETONE	2,58E-07	0	0	6,96E-06	0	1,50E-07	6,96E-06	6,96E-06	6,96E-06	6,96E-06	0	1,50E-07	6,96E-06	6,96E-06	0	0	0	0	0	0	0	6,56E-06	0
2-METCPE	0,5	0	0	0,5	0	9,42E-03	0,5	0,5	0,5	0,5	0	9,42E-03	0,5	0,5	0	0	0	0	0	0	0	7,46E-06	0
CHAR	0	0	0	0	0	0	0	0	0	0	0	0	0	0	0	0	0	0	0	0	0	0	0
MIBK	0	0	0	0	0	0	2,21E-03	0	0	0	0	0	0	0	2,21E-03	0	0	0	0	0	0	0	0
CHARCATE	0	0	0	0	0	0	0,2	0	0	0	0	0	0	0	0,2	0	0	0	0	0	0	0	0
BIOMASS	0	2,0	0	0	0	0	0	0	0	0	0	0	0	0	0	2,0	2,0	2,0	2,0	0	0	0	0
ASH	0	0	0,4	0	0	0	0,2	0	0	0	0	0	0	0	0,2	0	0	0	0	0,2	0,2	0	0
otal Flow kg/se	0,53	2,00	0,42	19,70	0,00	0,42	20,12	19,70	19,70	19,70	1,01E-03	0,42	19,70	19,70	0,42	20,00	20,00	20,00	20,00	20,00	20,00	18,75	18,00
Temperature K	298,15			353,15		298,15	672,91	654,44	654,44	654,44	673,15	298,15	654,44	351,12	654,44	673,15	300,96	625,47	298,15	673,15	672,91	298,15	298,15
Pressure N/sqm	101300	101300	101300	30000000	101300	101300	30000000	30000000	30000000	30000000	30000000	101300	30000000	101300	30000000	30000000	30000000	30000000	101300	30000000	30000000	101300	101300
lume Flow cum/	5,72E-04	0,00E+00	0,00E+00	2,71E-02	0,00E+00	2,59E-01	5,56E-02	6,57E-02	6,57E-02	6,57E-02	1,02E-04	2,60E-01	6,57E-02	2,70E-02	2,93E-04	7,22E-02	2,38E-02	2,82E-02	2,39E-02	7,24E-02	7,24E-02	1,95E-02	2,39E-02
Enthalpy J/kmol	-2,73E+08			-2,82E+08		-3,50E+08	-2,49E+08	-2,50E+08	-2,50E+08	-2,50E+08	1,15E+07	-3,50E+08	-2,50E+08	-2,82E+08	-9,88E+07	-2,46E+08	-2,85E+08	-2,58E+08	-2,86E+08	-2,53E+08	-2,53E+08	-2,86E+08	-2,86E+08

cellulose decomposition reactions

Reaction	Pre-exponential factor	Activation energy kJ/mol	Rate constant	Temperature ˚C	Pressure Mpa	Reference
Cellobiose -> Glucose + Fructose	-	108.6	4.300	400	30	Kabyemela et al. 1998, p. 359
Cellobiose -> Glucosyl-erythrose + Glycoaldehyde	-	30.4	0.250	400	30	Kabyemela et al. 1998, p. 359
Cellobiose -> Glucosyl-glycoaldehyde + Erythrose	-	69.3	0.350	400	30	Kabyemela et al. 1998, p. 359
Glucosyl-erythrose -> Glucose + Erythrose	-	106.1	3.700	400	30	Kabyemela et al. 1998, p. 359
Glucosyl-glycoaldehyde -> Glucose + Glycoaldehyde	-	110.5	1.100	400	30	Kabyemela et al. 1998, p. 359
Glucose -> Fructose	-	-	7.000 ± 0.630	400	30	Kabyemela et al. 1999, p. 2891
Glucose -> 1,6-anhydroglucose	-	-	0.080 ± 0.007	400	30	Kabyemela et al. 1999, p. 2891
Glucose -> Erythrose + Glycoaldehyde	-	-	18.100 ± 1.629	400	30	Kabyemela et al. 1999, p. 2891
Glucose -> Glyceraldehyde	-	-	1.000 ± 0.090	400	30	Kabyemela et al. 1999, p. 2891
Fructose -> Erythrose + Glycoaldehyde	-	-	8.000 ± 0.720	400	30	Kabyemela et al. 1999, p. 2891
Fructose -> Dihydroxyacetone	-	-	6.500 ± 0.585	400	30	Kabyemela et al. 1999, p. 2891
1,6 Anhydroglucose -> Acetic acid	-	-	0.310 ± 0.028	400	30	Kabyemela et al. 1999, p. 2891
Erythrose -> Acetic Acid	-	-	5.000 ± 0.450	400	30	Kabyemela et al. 1999, p. 2891
Glyceraldehyde -> Dihydroxyacetone	-	-	7.150 ± 0.630	400	30	Kabyemela et al. 1999, p. 2891
Dihydroxyacetone -> Glyceraldehyde	-	-	1.040 ± 0.094	400	30	Kabyemela et al. 1999, p. 2891
Glyceraldehyde -> Pyruvaldehyde	-	-	4.600 ± 0.414	400	30	Kabyemela et al. 1999, p. 2891
Dihydroxyacetone -> Pyruvaldehyde	-	-	1.200 ± 0.108	400	30	Kabyemela et al. 1999, p. 2891
Pyruvaldehyde -> Acetic acid	-	-	-	400	30	Kabyemela et al. 1999, p. 2891
Fructose -> Acetic acid	-	-	10.400 ± 0.936	400	30	Kabyemela et al. 1999, p. 2891

Reaction	Pre-exponential factor	Activation energy kJ/mol	Rate constant	Temperature ˚C	Pressure Mpa	Reference
Xylose -> Xylulose	-	-	0.239	400	25	Paksung & Matsumura 2015, p. 7606-7611
Xylulose -> Xylose	-	-	4.99×10^{-3}	400	25	Paksung & Matsumura 2015, p. 7606-7611
Xylose -> Furfural	-	-	0.651	400	25	Paksung & Matsumura 2015, p. 7606-7611
Xylose -> Glycoaldehyde + Glyceralhdeyde	2.069×10^{7}	86.64	-	400	25	Paksung & Matsumura 2015, p. 7606-7611
Xylulose -> Glycoaldehyde + Dihydroxyacetone	3.001×10^{3}	56.40	-	400	25	Paksung & Matsumura 2015, p. 7606-7611
Dihydroxyacetone -> Clyceraldehyde	-	-	1.950	400	25	Paksung & Matsumura 2015, p. 7606-7611
Clyceraldehyde -> Dihydroxyacetone	-	-	2.860	400	25	Paksung & Matsumura 2015, p. 7606-7611
Clyceraldehyde -> Clycoaldehyde + Formaldehyde	2.328×10^{3}	35.83	-	400	25	Paksung & Matsumura 2015, p. 7606-7611
Xylose -> TOC	2.162×10^{5}	65.53	-			Paksung & Matsumura 2015, p. 7606-7611
Dihydroxyacetone -> TOC	-	-	0.000	400	25	Paksung & Matsumura 2015, p. 7606-7611
Glyceraldehyde -> TOC	-	-	0.000	400	25	Paksung & Matsumura 2015, p. 7606-7611
Glycoaldehyde -> TOC	4.491×10^{3}	55.25	-	400	25	Paksung & Matsumura 2015, p. 7606-7611
Furfural -> TOC	-	-	-	400	25	Paksung & Matsumura 2015, p. 7606-7611
TOC -> GAS	1.347×10^{1}	31.52	-	400	25	Paksung & Matsumura 2015, p. 7606-7611
Formaldehyde -> GAS	-	-	0.000	400	25	Paksung & Matsumura 2015, p. 7606-7611

Reaction	Pre-exponential factor	Activation energy kJ/mol	Rate constant	Temperature ˚C	Pressure Mpa	Reference
Lignin -> Guaiacol	-	-	0.324	400	25	Yong & Matsumura 2012, p. 11985
Lignin -> TOC	-	-	1.018	400	25	Yong & Matsumura 2012, p. 11985
Lignin -> Char	-	-	3.186	400	25	Yong & Matsumura 2012, p. 11985
Lignin -> Gas	-	-	0.346	400	25	Yong & Matsumura 2012, p. 11985
Guaiacol -> Catechol	-	-	0.333	400	25	Yong & Matsumura 2012, p. 11985
Guaiacol -> o-Cresol	-	-	1.180	400	25	Yong & Matsumura 2012, p. 11985
Guaiacol -> Phenol	-	-	0.700	400	25	Yong & Matsumura 2012, p. 11985
Catechol -> o-Cresol	-	-	0.043	400	25	Yong & Matsumura 2012, p. 11985
Catechol -> Phenol	-	-	0.000	400	25	Yong & Matsumura 2012, p. 11985
Catechol -> TOC	-	-	0.050	400	25	Yong & Matsumura 2012, p. 11985
o-Cresol -> TOC	-	-	0.050	400	25	Yong & Matsumura 2012, p. 11985
o-Cresol -> m-Cresol	-	-	0.650	400	25	Yong & Matsumura 2012, p. 11985
m-Cresol -> TOC	-	-	0.560	400	25	Yong & Matsumura 2012, p. 11985
Phenol -> TOC	-	-	0.000	400	25	Yong & Matsumura 2012, p. 11985
Phenol -> Char	-	-	2.450	400	25	Yong & Matsumura 2012, p. 11985
TOC -> GAS	-	-	0.030	400	25	Yong & Matsumura 2012, p. 11985
TOC -> Aromatic Hydrocarbons	-	-	0.170	400	25	Yong & Matsumura 2012, p. 11985
TOC -> Char	-	-	0.050	400	25	Yong & Matsumura 2012, p. 11985

Reaction	Pre-exponential factor	Activation energy kJ/mol	Rate constant	Temperature ˚C	Pressure Mpa	Reference
Lignin -> Guaiacol	0	58	-	320 - 380		Forchheim et al. 2014, p. 991
Guaiacol -> Catechol	0	101	-	320 - 380		Forchheim et al. 2014, p. 991
Guaiacol -> Phenol	0	94	-	320 - 380		Forchheim et al. 2014, p. 991
Catechol->Phenol	0	55	-	320 - 380		Forchheim et al. 2014, p. 991
Catechol->Char	0	3037	-	320 - 380		Forchheim et al. 2014, p. 991
Phenol->CO2+CH4	0	66	-	320 - 380		Forchheim et al. 2014, p. 991
Lignin -> LD1	0	32	-	320 - 380		Forchheim et al. 2014, p. 991
LD1 -> LD2	0	81	-	320 - 380		Forchheim et al. 2014, p. 991
LD1 -> Char	0	58	-	320 - 380		Forchheim et al. 2014, p. 991
LD1 -> Catechol	0	72	-	320 - 380		Forchheim et al. 2014, p. 991
LD1 -> CO2 + CH4	0	75	-	320 - 380		Forchheim et al. 2014, p. 991
Catechol -> LD2	0	296	-	320 - 380		Forchheim et al. 2014, p. 991
LD1 -> CO + H2	0	69	-	320 - 380		Forchheim et al. 2014, p. 991

Other reactions						
Reaction	**Pre-exponential factor**	**Activation energy kJ/mol**	**Rate constant**	**Temperature ˚C**	**Pressure Mpa**	**Reference**
H2O + CO -> CO2 + H2	0	48	-	320 - 380		Forchheim et al. 2014, p. 991
CO + H2 -> CH4 + CO2	0	42	-	320 - 380		Forchheim et al. 2014, p. 991
$CO + H_2O \rightarrow CO_2 + H_2$	7.943×10^3	98	-	380 - 460	10 -30	Sato et al. 2004, p. 2004
Acetic acid -> Acetone	?	?	?	-	-	Adapted from Pedersen et al. 2015, p. 214
Acetone -> 2-Methylcyclopentanone	?	?	?	-	-	Adapted from Pedersen et al. 2015, p. 214

Biomass	Process	EoS	HTL reactor conditions			Products	Yields	Energy efficiency (%)*	Reference
			Catalysts	Temperature (°C)	Pressure (MPa)				
Forest residue wood	HTL, Hydrogen plant, hydrotreating	SRK	-	355	20.3	Gasoline, Diesel, Heavy hydrocarbon	27 wt-% 52.4 Carbon-%	62.3	Tews et al. 2014
Organic waste streams	Biogas plant, HTL, hydrogen production unit, upgrading unit	SRK	-	330	25	Biogas, Biocrude, upgraded biofuel	30.3-36.8 kg/h (with a substrate slurry feed of 1000 kg/h)	62-84	Hoffman et al. 2013
Lignocellulosic biomass	HTL, Hydrotreating	SRK KD**		400	30	Gasoline equivalent biofuel	30-40 wt-%	-	Pedersen et al. 2017b
Lignocellulosic biomass	HTL + upgrading and integrated hydrogen generation	SRK, NRTL***	-	280	15	Biocrude	24.7 wt-%	58	Tzanetis et al. 2017
Lignocellulosic biomass	HTL + upgrading and integrated hydrogen generation	SRK, NRTL***	-	300	15	Biocrude	28.6 wt-%	69	Tzanetis et al. 2017
Lignocellulosic biomass	HTL + upgrading and integrated hydrogen generation	SRK, NRTL***	Na_2CO_3 (aq.)	280	15	Biocrude	30.5 wt-%	71	Tzanetis et al. 2017
Lignocellulosic biomass	HTL + upgrading and integrated hydrogen generation	SRK, NRTL***	Na_2CO_3 (aq.)	300	15	Biocrude	34.5 wt-%	79	Tzanetis et al. 2017
Lignocellulosic biomass	HTL + upgrading and integrated hydrogen generation	SRK, NRTL***	Fe (aq.)	280	15	Biocrude	30.6 wt-%	71	Tzanetis et al. 2017
Lignocellulosic biomass	HTL + upgrading and integrated hydrogen generation	SRK, NRTL***	Fe (aq.)	300	15	Biocrude	37.5 wt-%	89	Tzanetis et al. 2017

* Energy efficiency is calculated by dividing the energy content of the produced biofuels by the amount of energy input
* SRK KD is used in the hydrotreating sector
*** NRTL is used in phase separation unit